ELECTRIC THERMAL STORAGE IN ISOLATED WIND DIESEL POWER SYSTEMS: USE OF DISTRIBUTED SECONDARY LOADS FOR FREQUENCY REGULATION

By

Nicholas T. Janssen

A Dissertation Submitted in Partial Fulfillment of the Requirement for the Degree of

Doctor of Philosophy

in

Engineering

University of Alaska Fairbanks

August 2017

APPROVED:

Richard W. Wies, Committee Co-chair
Rorik A. Peterson, Committee Co-chair
Marc Mueller-Stoffells, Committee Member
Yujiang Xiang, Committee Member
Rorik A. Peterson, Chair
Department of Mechanical Engineering
Doug Goering, Dean
College of Engineering and Mines
Michael Castellini, *Dean of the Graduate School*

Abstract

Isolated coastal utilities in arctic villages commonly use a mix of diesel and wind power to provide electrical service to their consumers. It is common for such communities to experience periods of high wind generation for which no immediate demand exists and either waste, curtail, or poorly utilize the surplus. The objective of the present work is to explore (through mathematical and numerical modelling) the technical feasibility of and optimization strategies for distributing this excess wind energy as domestic space heat for use as a cleaner, more economical alternative to fossil fuels. Autonomously controlled Electric Thermal Storage (ETS) devices are considered as a solution to decouple the supply of excess wind power with domestic heat demand without the need for communication infrastructure or a second distribution circuit. First, using numerical heat transfer analysis, it is shown that the performance of an ETS heater core can be generalized and expressed in terms of its physical properties and simple geometric dimensions in such a way as to inform system sizing and economic performance studies for prospective applications. Furthermore, a collection of autonomous ETS units is shown (using a full-scale lab-validated mathematical model) to possess the ability to assume the role of partial and/or sole frequency regulator on a hybrid wind-diesel system. Several design changes are proposed, which render the commercially-available units more amenable to frequency regulation. Ultimately, ETS is shown to be a promising alternative means of utilizing excess renewable energy for domestic space heat while providing additional stability to the electrical grid.

Table of Contents

Page

List of Figures

Page

List of Tables

Page

Chapter 1. Introduction

Isolated communities in the arctic predominantly rely upon diesel electric generators to supply electric power to the consumer. However, diesel fuel is expensive and difficult to transport [1], as isolated communities are inaccessible to the major road systems. Additionally, the burning of such fossil fuels contributes negatively to air pollution and global climate change [2]. Many communities are looking to renewable energy technologies, such as wind, to offset the high cost of electricity and minimize their impact on the environment. Since many of these remote villages lie in coastal wind regimes, they have access to good wind resources [3]. However, the technical and operational challenges of integrating dynamic wind power into existing diesel-powered grids are prevalent and well-documented in the literature [4-9, 11-26]. Primarily, these challenges stem from the relatively low ratio of rotating synchronous inertia to the amplitude of the swings seen in dynamic renewable generation.

The primary goal of this dissertation is to address the specific challenge of secondary load utilization to optimize control of system voltage and frequency dynamics in isolated wind-diesel grids through the application of electric thermal storage (ETS). This goal is pursued through the following objectives:

1. Model and generalize the heat flow within an ETS heater core for future economic and performance modeling,
2. Model and understand the electro-dynamic effects of a family of autonomous ETS heaters on an isolated grid, and
3. Demonstrate a method of using ETS to autonomously regulate frequency on a high penetration wind-diesel grid in diesel-off (wind only) mode.

Ultimately, the goal is to increase the value of wind power normally consumed by plant-located secondary loads on isolated wind-diesel electric grids through the use of autonomous, distributed ETS devices.

1.1 Hybrid Wind-Diesel Systems

An electric power system that utilizes both wind and diesel power as its generation source is considered a hybrid wind-diesel (HWD) system [4]. Wind power availability cannot be relied upon, but its power is clean and economically competitive. The fraction of wind power that satisfies the primary load is referred to as the wind power *penetration*. Higher penetration levels are economically favorable, but bring with them substantial technical challenges. Many of these challenges are being addressed within a specific body of research [7-9] surrounding the operation of "microgrids."

The US Department of Energy (DOE) defines a microgrid as "a group of interconnected loads and distributed energy resources within clearly defined electrical boundaries that acts as a single controllable entity with respect to the grid." A defining feature of a microgrid, per the DOE, is its ability to connect to or disconnect from a larger grid and operate in "islanded" mode. Other definitions have been offered as well, including [10], whereby a microgrid is defined as "a small energy system capable of balancing captive supply and demand resources to maintain stable service within a defined boundary." For the present work, the term "microgrid" is generally used in this fashion, but is taken to be an isolated grid that behaves like an islanded DOE-defined-microgrid.

In their simplest form, HWD systems consist of at least one diesel electric generator (DEG), at least one wind turbine generator (WTG), a primary load, and a distribution system

(generally 60 Hz, 3-phase, 480V). The DEG is comprised of a diesel engine and speed governor affixed to a synchronous generator (often referred to as a synchronous *machine*). The WTG consists of a rotor, gearbox, and some type of generator. Generally, they can be of the permanent magnet, induction, or direct current (DC) type, and with power electronics HWD systems may also utilize additional energy sources, storage technologies, or secondary loads [4].

In isolated arctic communities, every system is unique. Such uniqueness leads to a plethora of literature case studies and publications dedicated to sizing components, optimizing dispatch, and analyzing the economic performance of such systems. In [11-19], examples including case studies of these isolated HWD systems are shown. These studies are commonly conducted on a mid-range time scale; greater than one second to no more than an hour. The focus of the present work is largely electromechanical in nature and on a much shorter time scale (milliseconds). Some research has been conducted modeling the electromechanical interactions of wind-diesel systems [20-26]. This is not the thesis of the present work, but a precursor. Before the work is introduced, a cursory background in the electromechanics and dynamics of power systems is prudent.

1.2 Frequency Regulation

The frequency in a 60 Hz electrical grid is defined by the speed of the synchronous generator and the number of poles in the machine:

$$f = \frac{N \cdot P}{120} \tag{1.1}$$

where N is the angular velocity of the synchronous generator (in RPM) and p is the number of poles per phase [27].

An instantaneous balance of real power must flow from the generation sources to the loads for frequency to remain constant. If a surplus of generation is present, it will tend to increase the frequency of the grid (and vice versa). The rate at which this occurs is a function of the total rotational inertia in the system, as described by the swing equation

$$\frac{d\omega}{dt} = \frac{1}{2H} \cdot \left(T_e - T_m - F\omega\right) \tag{1.2}$$

where t is time, ω is the angular frequency of the machine, H is the inertia coefficient, T_e, is the electrical torque (opposed by the load), T_m is the mechanical torque (applied by the machine), and F is the friction factor [28]. The control strategy for the DEG is to ensure that the angular velocity (ω), and hence the grid frequency, remains constant by continuous adjustment of its output torque.

HWD systems are small and generally low in rotational inertia as compared to the large interconnected grids in the continental United States. Variations in wind power generation or consumer load can more easily perturb the frequency of an isolated grid. The HWD system must be capable of matching controlled generation sources (and sinks) with the instantaneous demands of the grid in the presence of the unpredictable generation of the wind farm.

1.3 Voltage Regulation

As frequency regulation is a task of balancing real power in an electrical system, similarly, voltage regulation is a task of balancing reactive power. In diesel powered grids, voltage regulation is the responsibility of the Automatic Voltage Regulator (AVR) on the diesel engine's synchronous generator [28]. Reactive power can flow into or out of any of the loads or generation sources, but generally it is supplied by the synchronous generator and consumed by the load. Reactive power

flow into or out of a synchronous machine (Q) is related to the terminal voltage of the synchronous machine (V_t) through the following equation [29].

$$Q = \frac{V_t E_f \cos(\delta) - V_t^2}{X_s} \tag{1.3}$$

where E_f is the field voltage, δ is the power angle, and X_s is the so called "synchronous reactance."

The relative balance of real power (P) and reactive power (Q) flowing into or out of a system is described by the power factor.

$$\cos(\theta) = \frac{P}{\sqrt{P^2 + Q^2}} \tag{1.4}$$

where cos (θ) is the power factor [26]. If the reactive power is flowing into the load, Q is positive and the power factor is said to be "lagging". (The power factor is "leading" in the reverse case.)

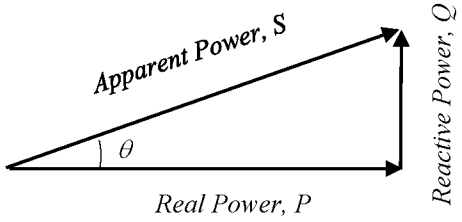

Figure 1.1. Power triangle, illustrating the definition of the power factor. Q is positive and thus the power factor is "lagging."

The power factor says much about the nature of the load. Inductive loads, such as the rotation of large motors, are indicated by lagging power factors. Leading power factors indicate a capacitive load, as seen in the charging of transmission lines [27].

The AVR on the DEG controls the output voltage by measurement and appropriate correction of the field winding current (often called the "excitation"). This DC current is supplied

to the rotor of the synchronous machine by some external source through a set of slip rings or brushes [26]. Brushless exciters also exist, which utilize a second, smaller AC generator directly mounted on the shaft of the primary generator. The output from the exciter stator (stationary winding) is rectified to DC and supplied to the armature (rotary winding) of the primary generator. In either case, the induced voltage in the stator can be calculated as

$$E_A = K\phi\omega \tag{1.5}$$

where K is a constant that describes the structure of the machine, ϕ is the flux from the magnetic field, and ω is the angular velocity [27]. Thus, stable output voltage is dependent upon stable control of frequency. An effective HWD system will be able to control both frequency and voltage in the presence of varying real and reactive power flows.

1.4 Energy Storage

HWD systems may also make use of energy storage technologies, such as flywheels [30-31], compressed air [32], ultra-capacitors [33], super-conducting magnets [34], hydrogen [35], or (most commonly) battery banks [36-41]. Energy storage allows for a momentary decoupling of the wind generation and consumer load signals which do not necessarily align in time. Wind power can be generated in excess and stored for later consumption when demand is higher and/or wind power is lower.

Nearly all storage technologies today rely on the conversion of AC electrical power to DC through the use of fast-switching power electronics [42-46]. AC power is generated and converted to DC through rectification and filtering, stored, and then fed back into the grid (at a later time) as AC power, through an inverter. Installation of such technology can go a long way towards enabling

diesel-off HWD systems. A modern battery bank and inverter system can not only source and sink electrical power, it can often assume the role of frequency and/or voltage controller when the DEG has been disconnected.

Though battery technology continues to drop in cost (thanks, in part, to the development of hybrid vehicle technology [47]), the associated power electronics add a layer of complexity. Technical resources in isolated communities are often very limited. Like a certain subset of "no-storage" HWD research in [48-50], the present work does not consider traditional energy storage.

1.5 Secondary Loads

As stated in 1.2, it is important for an electrical system to maintain a consistent balance of real power generation and real power consumption, or frequency regulation will suffer. This has been the focus of a large body of wind-diesel research in [51-61]. For isolated power systems with a large capacity of wind power generation and no energy storage, there are two general strategies for dealing with this problem: (1) supply side management and (2) demand side management.

Managing power on the *supply* side [62-66] is continuously performed in any HWD system, as the diesel's contribution is consequently reduced when wind supply increases and vice versa. However, there comes a point when the diesel can no longer reduce its output (under high wind or low load) and the wind power itself must be curtailed. If the system lacks energy storage, this is a missed opportunity to extract available energy out of the wind.

Moreover, real power generation and consumption can be balanced on the *demand* side as well. A deficit of wind is not generally a control problem, since the diesel is present to step in and supply the primary load. However, an unmanaged surplus of wind necessitates the use of either secondary loads or some alternative demand side management strategies [67-78].

Secondary loads are common components of HWD systems and are used by the plant to match generation with consumption. Secondary loads may also be referred to as "dump loads". Dump loads that are to participate in frequency regulation must be fast-switching (sub cycle). Most commonly, the devices are co-located in the plant and directly activated by the system supervisory controller. The device may be a resistive load bank, where electricity is simply converted to thermal energy and then cooled by the air. Also common is the electric boiler, used for generating useful steam. Other options exist, but the device cannot count on available electricity for operation, as it is a slave to the energy balance of the grid. Economically, there is limited benefit from such arrangements, since the resulting steam or hot water cannot be affordably delivered very far from the plant. To address this constraint, the concept of distributed secondary loads has been proposed [79].

1.6 Electric Thermal Storage

The research presented herein focuses on the application of a particularly useful form of distributed secondary load for Alaska: Electric Thermal Storage (ETS). ETS units are simple masonry stoves with resistive heating elements that store thermal energy for domestic space heating applications. These devices are common, available commercially, and pair well with wind-powered grids in cold climates as a demand-side management strategy [80-82].

Figure 1.2. Inside view of a Steffes 2102 room unit—a common electric thermal storage device.

ETS devices are a practical way of converting clean, excess wind power to stored thermal energy for domestic heat. However, from a thermodynamic standpoint, they generate a significant amount of entropy. These devices can be considered 100% *first law* efficient, in that any heat generated by them ultimately makes its way into the residence as space heat. However, they may also be considered 0% *second law* efficient, as they destroy all work potential of the highly ordered electrical energy. From a heating standpoint, it would be far better to be able to run a heat pump between the residence and the outdoors with this energy. However, it is the ability to store heat within the media that renders these devices highly useful in wind-diesel microgrid applications.

There is some mature literature [83-84] focused on the behavior of ETS on larger grids and a wave of more recent research as well [85-92]. However, very little study has been conducted on the use of ETS devices as distributed secondary loads on wind-diesel microgrids.

1.7 Summary and Organization of Subsequent Chapters

This dissertation has been written in manuscript form. Chapters 1 and 8 describe the general introduction and overall conclusions of the dissertation, respectively. A discussion of modeling and measurement methodologies is presented in Chapter 2 to provide the reader with a summary of the strategies used in the following body of the work, which begins in Chapter 3. Chapter 3 is a heat transfer focused journal paper that is currently published in the ASME Journal of Thermal Science and Engineering Applications. Chapter 4 is a peer-reviewed conference paper that was presented and published in the proceedings of the ASME Power Conference in 2014. This chapter is included for valuable background on the development of the model used to drive the research in Chapters 5 and 6, which form the core body of work. The journal paper that forms Chapter 5 is published in IEEE Transactions on Sustainable Energy. Chapter 6 is an unpublished manuscript based on a conference proceedings from the 2017 IEEE PES general meeting [93], but with additional content. The authors intend to submit this manuscript for review and possible publication in the IEEE Transactions on Sustainable Energy.

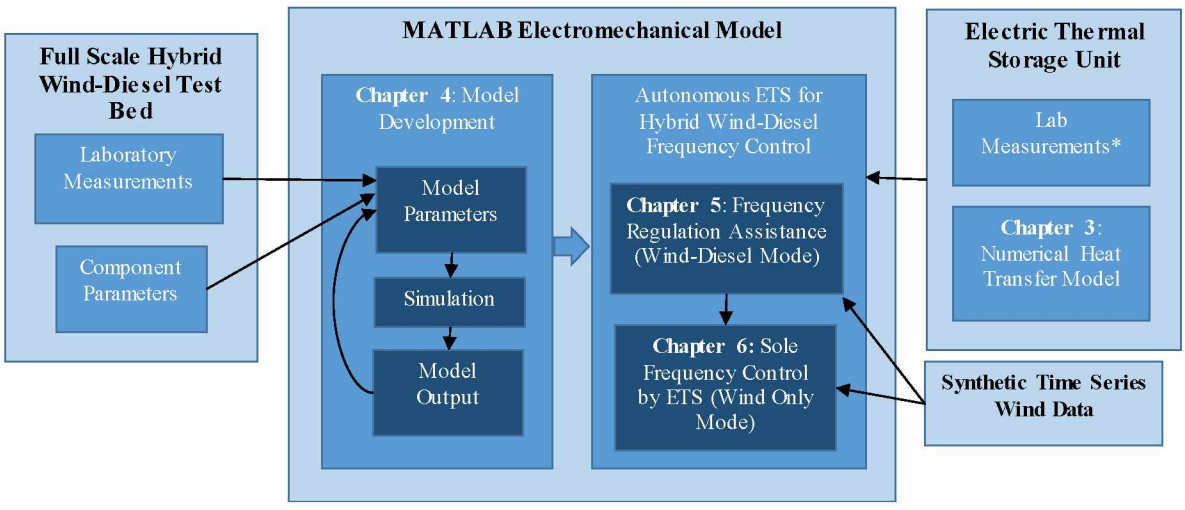

Figure 1.3. Research flow and thesis organization.

As stated earlier, the objective of this dissertation is to explore the technical feasibility of distributing excess wind energy as domestic space heat on islanded wind-diesel microgrids. Before this is established, performance and capacity restrictions of the ETS heater core must first be understood. The flow of heat within a core subject to wind-driven charge and demand-driven discharge cycles is not adequately understood as evidenced by the lack of literature on the topic. Chapter 3 begins the body of this study with the development of a generalized charge/discharge model of an ETS heater core (see Figure 1.3). A numerical finite element model of the heat transfer within the core is conducted for a wide range of parameters, including core material, core geometry, and air flow/discharge rates. The results are generalized into both a one-parameter model and a two-parameter model, which allow one to predict the performance of a single electric thermal storage heater core under realistic conditions.

With this knowledge, a family of distributed ETS units is now considered. However, in order to fully understand how a family of distributed ETS heaters could work in concert to regulate frequency on a hybrid wind-diesel system, a working mathematical model is needed. Moreover, the accuracy of such a model is predicated upon its ability to fully describe the electrodynamics of the following:

1. A realistic hybrid wind-diesel system (a full-scale laboratory, in this case)
2. An ETS heater equipped with a frequency-response controller

Modeling of the first is pursued in Chapter 4, which explains the development and validation of an electromechanical MATLAB® SIMULINK® model for the Alaska Center for Energy and Power (ACEP) hybrid wind-diesel test bed. A series of disturbances were introduced to the test bed and the resulting changes in frequency and voltage were measured at various locations. This data was processed and mapped onto the results predicted by the computer model.

Numerous parameter sweeps and some fine tuning allowed for validation of the computer model under a particular set of circumstances; generally small steps in load at high diesel outputs.

Next, development of the ETS heater model is pursued in Chapter 5 with validating field measurements in [90]. Here, ETS units are considered as distributed secondary loads. Proportional unit controllers are set to respond to changes in the frequency of the grid autonomously, with no instruction from the central plant controller. A family of such ETS units are modelled (electrically) and placed onto a hypothetical wind-diesel microgrid. The electromechanical model is given a synthetic wind speed signal and a varying primary load for adequate perturbation. Variables such as unit relay switching time, unit coordination, controller gain, and number of heating elements are considered. It can be shown that, with proper design, these units can be used to assist with grid frequency regulation while providing stored domestic space heat for village residences. Subsequent voltage fluctuations are minimized by ensuring units are staggered between relay switching events to avoid simultaneous steps in load.

In Chapter 6, all components are put together to simulate an isolated hybrid wind-diesel power system that is capable of wind-only (diesel-off) mode of operation using a family of autonomous distributed ETS heaters to perform exclusive frequency regulation. The diesel is given the ability to disconnect from the synchronous machine and allow the autonomous ETS units to measure and respond to change in grid frequency to ensure steady regulation across a full range of potential conditions. The result is a system that makes economic use of surplus wind energy, is fully capable of "diesel-off", and does not require the use of a central communication infrastructure. Again, the electro-mechanical computer model is used to validate the concept and show steady operation across a full range of wind power penetration levels.

1.8 Nomenclature

f	Frequency	Hz, pu
p	Number of poles	-
t	Time	Sec
E_A	Stator voltage	V
F	Friction coefficient	-
H	Inertia coefficient	-
K	Machine constant	-
N	Angular velocity	RPM
P	Real power	W
Q	Reactive power	VAR
T_e	Electrical torque	Nm
T_m	Mechanical torque	Nm
ϕ	Magnetic flux	Weber
θ	Power factor angle	Rad
ω	Angular velocity	rad/sec

1.9 References

[1] Alaska Energy Authority. *2012 Alaska Energy Statistics Final Report.* Available <http://www.akenergyauthority.org/Portals/0/Publications/2012AlaskaEnergyStatistics FinalReport.pdf?ver=2016-10-05-133221-547>.

[2] Meinshausen, M. et al. "Greenhouse-gas emission targets for limiting global warming to 2 C." *Nature* 458.7242 (2009): 1158-1162.

[3] Elliott, D. L. and M. N. Schwartz. "Wind energy potential in the United States." *Pacific Northwest Laboratory PNL-SA-23109* (1993).

[4] Hunter, R., and G. Elliot. "Wind-diesel systems: a guide to the technology and its implementation." Cambridge University Press (1994). Print.

[5] Drouilhet, S. M., and M. Shirazi. "Wales, Alaska high-penetration wind-diesel hybrid power system: theory of operation." (2002).

[6] Sedaghat, B., A. Jalilvand, and R. Noroozian. "Design of a multilevel control strategy for integration of stand-alone wind/diesel system." *International Journal of Electrical Power & Energy Systems* 35.1 (2012): 123-137.

[7] Lopes, J.A. Peças, C. L. Moreira, and A. G. Madureira. "Defining control strategies for microgrids islanded operation." *IEEE Transactions on Power Systems* 21.2 (2006): 916-924.

[8] Hafez, O., and K. Bhattacharya. "Optimal planning and design of a renewable energy based supply system for microgrids." *Renewable Energy* 45 (2012): 7-15.

[9] Mariam, L., M. Basu, and M. F. Conlon. "A review of existing microgrid architectures." *Journal of Engineering* (2013).

[10] "Microgrid Institute: About Microgrids (Definition)" *About Microgrids*. Microgrid Institute (2014). Available < http://www.microgridinstitute.org/>

[11] Katiraei, F., and C. Abbey. "Diesel plant sizing and performance analysis of a remote wind-diesel microgrid." *2007 IEEE Power and Energy Society General Meeting (2007 PESGM)*. IEEE, 2007.

[12] Deshmukh, M. K., and S. S. Deshmukh. "Modeling of hybrid renewable energy systems." *Renewable and Sustainable Energy Reviews* 12.1 (2008): 235-249.

[13] Bernal-Agustín, J. L., and R. Dufo-López. "Simulation and optimization of stand-alone hybrid renewable energy systems." *Renewable and Sustainable Energy Reviews* 13.8 (2009): 2111-2118.

[14] Su, W., Z. Yuan, and M-.Y. Chow. "Microgrid planning and operation: Solar energy and wind energy." *2010 IEEE Power and Energy Society General Meeting (2010 PESGM)*. IEEE, 2010.

[15] Vafaei, M. and M. Kazerani. "Optimal unit-sizing of a wind-hydrogen-diesel microgrid system for a remote community." *2011 IEEE PowerTech. Trondheim* (2011): 1-7.

[16] Dufo-López, R., et al. "Multi-objective optimization minimizing cost and life cycle emissions of stand-alone PV–wind–diesel systems with batteries storage." *Applied Energy* 88.11 (2011): 4033-4041.

[17] Hong, Y. and R. C. Lian. "Optimal sizing of hybrid wind/PV/diesel generation in a stand-alone power system using Markov-based genetic algorithm." *IEEE Transactions on Power Delivery* 27.2 (2012): 640-647.

[18] Kazem, H. A., and T. Khatib. "A novel numerical algorithm for optimal sizing of a photovoltaic/wind/diesel generator/battery microgrid using loss of load probability index." *International Journal of Photoenergy* (2013).

[19] Merei, G., C. Berger, and D. U. Sauer. "Optimization of an off-grid hybrid PV–Wind–Diesel system with different battery technologies using genetic algorithm." *Solar Energy* 97 (2013): 460-473.

[20] Stavrakakis, G. S. and G. N. Kariniotakis. "A general simulation algorithm for the accurate assessment of isolated diesel-wind turbines systems interaction. I. A general multimachine power system model." *IEEE Transactions on Energy Conversion* 10.3 (1995): 577-583.

[21] Bhatti, T. S., A. A. F. Al-Ademi, and N. K. Bansal. "Load-frequency control of isolated wind-diesel-microhydro hybrid power systems (WDMHPS)." *Energy* 22.5 (1997): 461-470.

[22] Rajendiran, K., W. W. Keerthipala, and C. V. Nayar. "PSCAD/EMTDC based simulation of a wind-diesel conversion scheme." *IEEE 2000 Power Engineering Society Winter Meeting*. IEEE, 2000.

[23] Kaldellis, J. K. "An integrated model for performance simulation of hybrid wind–diesel systems." *Renewable Energy* 32.9 (2007): 1544-1564.

[24] Friedel, V. "Modeling and Simulation of a Hybrid Wind-Diesel Microgrid." Master of Science Thesis in Electric Power Systems, Royal Institute of Technology, Stockhold, Sweden, June 2009.

[25] Arulampalam, A., et al. "Micro-grid control of PV-Wind-Diesel hybrid system with islanded and grid connected operations." *2010 IEEE International Conference on Sustainable Energy Technologies (ICSET 2010)*. IEEE, 2010.

[26] Karim, Md. and M. Ul. "Dynamic modeling of a wind-diesel-hydrogen hybrid power system." Master of Engineering Thesis, Memorial University of Newfoundland, July 2010.

[27] Chapman, S. *Electric Machinery Fundamentals*. Tata McGraw-Hill Education, 2005.

[28] Glover, J. D., M. S. Sarma, and T. Overbye. *Power System Analysis & Design, SI Version*. Cengage Learning (2012).

[29] Bergen, A. R. and V. Vittal. *Power Systems Analysis: 2nd Edition*. Pearson, 1999.

[30] Iglesias, I. J., et al. "Design and simulation of a stand-alone wind-diesel generator with a flywheel energy storage system to supply the required active and reactive power." *IEEE 2000 Power Electronics Specialists Conference (PESC 2000)*. IEEE, 2000.

[31] Sebastián, R., and R. Peña-Alzola. "Control and simulation of a flywheel energy storage for a wind diesel power system." *International Journal of Electrical Power & Energy Systems* 64 (2015): 1049-1056.

[32] Ibrahim, H., et al. "Study and design of a hybrid wind–diesel-compressed air energy storage system for remote areas." *Applied Energy* 87.5 (2010): 1749-1762.

[33] Tankari, M. A. et al. "Use of ultracapacitors and batteries for efficient energy management in wind–diesel hybrid system." *IEEE Transactions on Sustainable Energy* 4.2 (2013): 414-424.

[34] Tripathy, S. C. "Dynamic simulation of hybrid wind-diesel power generation system with superconducting magnetic energy storage." *Energy Conversion and Management* 38.9 (1997): 919-930.

[35] Mufti, M., R. Balasubramanian, and S. C. Tripathy. "Simultaneous frequency and voltage control of wind-diesel power systems using energy storage." *International Journal of Energy Research* 22.3 (1998): 221-235.

[36] Garcia, R. S., and D. Weisser. "A wind–diesel system with hydrogen storage: joint optimisation of design and dispatch." *Renewable Energy* 31.14 (2006): 2296-2320.

[37] El Mokadem, M., et al. "Maximum wind power control using torque characteristic in a wind diesel system with battery storage." *Recent Developments of Electrical Drives* (2006): 385-396.

[38] Sebastián, R. "Smooth transition from wind only to wind diesel mode in an autonomous wind diesel system with a battery-based energy storage system." *Renewable Energy* 33.3 (2008): 454-466.

[39] Sebastian, R. "Modelling and simulation of a high penetration wind diesel system with battery energy storage." *International Journal of Electrical Power & Energy Systems* 33.3 (2011): 767-774.

[40] Sebastian, R., R. Pena-Alzola, and J. Quesada. "Peak shaving simulation in a wind diesel power system with battery energy storage." *IEEE 2013 Annual Conference of the Industrial Electronics Society (IECON 2013)*. IEEE, 2013.

[41] Sebastián, R. "Application of a battery energy storage for frequency regulation and peak shaving in a wind diesel power system." *IET Generation, Transmission & Distribution* 10.3 (2016): 764-770.

[42] Isherwood, W., et al. "Remote power systems with advanced storage technologies for Alaskan villages." *Energy* 25.10 (2000): 1005-1020.

[43] Kim, J. Y., S. K. Kim, and J. H. Park. "Contribution of an energy storage system for stabilizing a microgrid during islanded operation." *Journal of Electrical Engineering and Technology* 4.2 (2009): 194-200.

[44] Abbey, C., and G. Joós. "A stochastic optimization approach to rating of energy storage systems in wind-diesel isolated grids." *IEEE Transactions on Power Systems* 24.1 (2009): 418-426.

[45] Abbey, C., W. Li, and G. Joós. "An online control algorithm for application of a hybrid ESS to a wind–diesel system." *IEEE Transactions on Industrial Electronics* 57.12 (2010): 3896-3904.

[46] Ross, M. et al. "Energy storage system scheduling for an isolated microgrid." *IET Renewable Power Generation* 5.2 (2011): 117-123.

[47] Nykvist, B., and Nilsson, Mans. "Rapidly falling costs of battery packs for electric vehicles." *Nature Climate Change* 5 (2015): 329-332.

[48] Jeffries, W. Q. "Analysis and modeling of wind/diesel systems without storage" (1994). Doctoral Dissertations Available from Proquest. AAI9510487. http://scholarworks.umass.edu/dissertations/AAI9510487

[49] Elmitwally, A., and M. Rashed. "Flexible operation strategy for an isolated PV-diesel microgrid without energy storage." *IEEE Transactions on Energy Conversion* 26.1 (2011): 235-244.

[50] Ibrahim, H. et al. "No-storage wind-diesel system: Mechanical modeling based on power flow models." *IEEE 2011 Electrical Power and Energy Conference (EPEC 2011)*. IEEE, 2011.

[51] Uhlen, K., B. A. Foss, and O. B. Gjosaeter. "Robust control and analysis of a wind-diesel hybrid power plant." *IEEE Transactions on Energy Conversion* 9.4 (1994): 701-708.

[52] Chaiyatham, T., et al. "Design of optimal fuzzy logic-PID controller using bee colony optimization for frequency control in an isolated wind-diesel system." *IEEE 2009 Transmission & Distribution Conference & Exposition: Asia and Pacific*. IEEE, 2009.

[53] Torres, M., and L. A. C. Lopes. "Virtual synchronous generator control in autonomous wind-diesel power systems." *IEEE 2009 Electrical Power & Energy Conference (EPEC 2009)*. IEEE, 2009.

[54] Hasanien, H. M., S. M. Muyeen, and J. Tamura. "Frequency control of isolated network with wind and diesel generators by using fuzzy logic controller." *IEEE 2009 International Conference on Electrical Machines and Systems (ICEMS 2009)*. IEEE, 2009.

[55] Marzband, M. et al. "Frequency control of isolated wind and diesel hybrid MicroGrid power system by using fuzzy logic controllers and PID controllers." *IEEE 2011 International Conference on Electrical Power Quality and Utilisation (EPQU 2011)*. IEEE, 2011.

[56] Kassem, A. M., and A. M. Yousef. "Robust control of an isolated hybrid wind–diesel power system using Linear Quadratic Gaussian approach." *International Journal of Electrical Power & Energy Systems* 33.4 (2011): 1092-1100.

[57] Das, D. C., A. K. Roy, and N. Sinha. "GA based frequency controller for solar thermal–diesel–wind hybrid energy generation/energy storage system." *International Journal of Electrical Power & Energy Systems* 43.1 (2012): 262-279.

[58] Kassem, A. M. and A. M. Yousef. "Voltage and frequency control of an autonomous hybrid generation system based on linear model predictive control." *Sustainable Energy Technologies and Assessments* 4 (2013): 52-61.

[59] Wies, R. W., E. Chukkapalli, and M. Mueller-Stoffels. "Improved frequency regulation in mini-grids with high wind contribution using online genetic algorithm for PID tuning." *IEEE 2014 Power and Energy Society General Meeting (2014 PESGM)*. IEEE, 2014.

[60] Gampa, S. R., and D. Das. "Real power and frequency control of a small isolated power system." *International Journal of Electrical Power & Energy Systems* 64 (2015): 221-232.

[61] Kim, Y. S., E. S. Kim, and S. I. Moon. "Frequency and voltage control strategy of standalone microgrids with high penetration of intermittent renewable generation systems." *IEEE Transactions on Power Systems* 31.1 (2016): 718-728.

[62] Sebastian, R. et al. "Approaching hybrid wind-diesel systems and Controller Area Network." *IEEE 2002 Annual Conference of the Industrial Electronics Society (IECON 2002)* Volume 3. IEEE, 2002.

[63] Zoka, Y. et al. "An interaction problem of distributed generators installed in a MicroGrid." *IEEE 2004 International Conference on Electric Utility Deregulation, Restructuring and Power Technologies (DRPT 2004)* Volume 2. IEEE, 2004.

[64] Katiraei, F., and M. R. Iravani. "Power management strategies for a microgrid with multiple distributed generation units." *IEEE Transactions on Power Systems* 21.4 (2006): 1821-1831.

[65] Miao, Z., A. Domijan, and L. Fan. "Investigation of microgrids with both inverter interfaced and direct AC-connected distributed energy resources." *IEEE Transactions on Power Delivery* 26.3 (2011): 1634-1642.

[66] Soni, N., S. Doolla, and M. C. Chandorkar. "Improvement of transient response in microgrids using virtual inertia." *IEEE Transactions on Power Delivery* 28.3 (2013): 1830-1838.

[67] Bhatti, T. S., A. A. F. Al-Ademi, and N. K. Bansal. "Load frequency control of isolated wind diesel hybrid power systems." *Energy Conversion and Management* 38.9 (1997): 829-837.

[68] Nehrir, M. H., and B. J. LaMeres. "A multiple-block fuzzy logic-based electric water heater demand-side management strategy for leveling distribution feeder demand profile." *Electric Power Systems Research* 56.3 (2000): 225-230.

[69] Johnson, C. et al. "Design and modeling of dispatchable heat storage in wind/diesel systems." *Renewable Energy Research Laboratory, Dept. of Mechanical and Industrial Engineering, University of Massachusetts, Amherst, MA* 1003 (2002).

[70] Madureira, A., C. Moreira, and J. Peças Lopes. "Secondary load-frequency control for microgrids in islanded operation." *2005 International Conference on Renewable Energy Power Quality* (2005).

[71] Lu, N., and D. J. Hammerstrom. "Design considerations for frequency responsive grid friendly TM appliances." *IEEE 2005/2006 PES Transmission and Distribution Conference and Exhibition*. IEEE, 2006.

[72] Short, J. A., D. G. Infield, and L. L. Freris. "Stabilization of grid frequency through dynamic demand control." *IEEE Transactions on Power Systems* 22.3 (2007): 1284-1293.

[73] Callaway, D. S. "Tapping the energy storage potential in electric loads to deliver load following and regulation, with application to wind energy." *Energy Conversion and Management* 50.5 (2009): 1389-1400.

[74] Vandoorn, T. L. et al. "Active load control in islanded microgrids based on the grid voltage." *IEEE Transactions on Smart Grid* 2.1 (2011): 139-151.

[75] Molina-Garcia, A., F. Bouffard, and D. S. Kirschen. "Decentralized demand-side contribution to primary frequency control." *IEEE Transactions on Power Systems* 26.1 (2011): 411-419.

[76] Shafiee, Q., J. C. Vasquez, and J. M. Guerrero. "Distributed secondary control for islanded MicroGrids-A networked control systems approach." *IEEE 2012 Annual Conference of the Industrial Electronics Society (IECON 2012)*. IEEE, 2012.

[77] Zhao, C. et al. "Design and stability of load-side primary frequency control in power systems." *IEEE Transactions on Automatic Control* 59.5 (2014): 1177-1189.

[78] Shafiee, Q., J. M. Guerrero, and J. C. Vasquez. "Distributed secondary control for islanded microgrids—A novel approach." *IEEE Transactions on Power Electronics* 29.2 (2014): 1018-1031.

[79] Trudnowski, D., M. Donnelly, and E. Lightner. "Power-system frequency and stability control using decentralized intelligent loads." *IEEE 2005/2006 PES Transmission and Distribution Conference and Exhibition*. IEEE, 2006.

[80] Johnson, C., J. F. Manwell, J. G. Abdulwahid, and A. Rogers. "Design and modelling of Dispatchable Heat storage in Remote Wind-Diesel Systems." *Renewable Energy Research Laboratory, Dept. of Mechanical and Industrial Engineering, University of Massachusetts, Amherst, MA* 1003 (2002).

[81] Hughes, L. "Meeting residential space heating demand with wind-generated electricity." *Renewable Energy* 35.8 (2010): 1765-1772.

[82] Sateriale, M. E. "Modeling and analysis of masonry electro-thermal heating and storage for optimal integration with remote stand-alone wind-diesel systems." Master of Science Thesis, University of Alaska-Fairbanks, 2013.

[83] Coleman, W. R. and C. M. Grastataro. "American electric power system electric thermal storage program: an evaluation of performance within the home." *IEEE Transactions on Power Apparatus and Systems* 12 (1981): 4741-4749.

[84] Adams, M. D. "American-Electric Power System Electric Thermal Storage Program: An Evaluation of the Impact on the Generation System." *IEEE Transactions on Power Apparatus and Systems* 4 (1982): 886-894.

[85] Roberge, M. A., et al. "Model of room storage heater and system identification using neural networks." *2000 Proceedings of CLIMA*. 2000.

[86] Bedouani, B. Y., et al. "Central electric thermal storage (ETS) feasibility for residential applications: Part 1. Numerical and experimental study." *International Journal of Energy Research* 25.1 (2001): 53-72.

[87] Bedouani, Ben Youcef, et al. "Central electric thermal storage (ETS) feasibility for residential applications: Part 2. Techno-economic study." *International Journal of Energy Research* 25.1 (2001): 73-83.

[88] Molina, A. et al. "Electrical thermal storage modeling: a tool to evaluate new opportunities and bids for residential users in a deregulated market." *IEEE 2003 Power Tech Conference Proceedings* 4. IEEE, 2003.

[89] Gomez, E. "A physically based load model of residential electric thermal storage: Application to LM programs." *International Journal of Power and Energy Systems* 24.1 (2004).

[90] Zhang, K., B. Han, and X. Yu. "Electrically conductive carbon nanofiber/paraffin wax composites for electric thermal storage." *Energy Conversion and Management* 64 (2012): 62-67.

[91] McGowan, J. G., and J. F. Manwell. "Hybrid wind/PV/diesel system experiences." *Renewable Energy* 16.1 (1999): 928-933.

[92] Wies, R. W. et al. "Review and testing of Steffes electric thermal storage unit with grid-interactive frequency regulation." *Intelligent Energy Systems Llc, Anchorage, AK, Technical Report* (2013).

[93] Wies, R. W. et al. "Autonomous Distributed Secondary Loads for Sole Frequency Regulation in High Penetration Wind-Diesel Microgrids." *2017 IEEE PES General Meeting* (2017).

Chapter 2. Summary of Measurement and Modeling Methodologies

This chapter provides a brief overview of the strategies used to mathematically describe the model components and measurement techniques. Model developments specific to the thermal, mechanical, and electrical components are described in detail within the respective sections of this dissertation.

Chapter 3 is a heat transfer study, and thus, the modeling and measurement methodologies of this section are rather unique within the dissertation. They are described here in sections 2.1 and 2.2. Chapter 4 involves data collection, modeling, and validation of a full-scale hybrid wind-diesel test bed. Electromechanical dynamics measurement methods are discussed in 2.3. Chapters 5 and 6 reference the same model developed in Chapter 4, and therefore, share many of the same methods. Electromechanical dynamics modeling methods are discussed collectively in 2.4.

2.1 Numerical Heat Transfer - Measurement

A numerical finite difference heat transfer study is carried out in Chapter 3. The objective of the study is to determine the effects of air flow rate, material properties, and core geometry on the discharge behavior of the ETS core. The study is conducted using Comsol Multiphysics®.

Primarily, this heat transfer study is concerned with the transient discharge characteristics of the heater core. The embodied energy within the core is quantified with a "State of Charge" (SOC) calculation. This is measured by integration of temperature over the volume of the solid, multiplication by density and heat capacity of the material, and division by the energy content at a chosen "full charge". (See Chapter 3 for full details.)

When parameters are varied and simulation sweeps performed, the resulting discharge curves are linearized and regressed. The slopes of these regressions (with forced 0 intercepts)

provide an effective time constant for discharge. The time constants are summarized in the results section of Chapter 4 and can be used to predict the behavior of a wide range of ETS heater cores.

2.2 Numerical Heat Transfer - Physical Modeling

Comsol Multiphysics® is capable of finite element and finite difference modeling of several physical domains. For the present work, only the following physics were considered:

- Heat transfer in solids (conduction within the core masonry)
- Heat transfer in fluids (convection from the air in the channels to the masonry during discharge)

Radiative heat transfer from the ETS heating elements to the masonry (charging) was simplified as a uniform heat flux. Physics not considered in this study include:

- Fluid flow in the channel (No computational fluid dynamics are performed. Air velocity profile is assumed flat.)
- Negligible physics, such as stress/strain and thermal expansion
- Irrelevant physics, such as acoustics, electro-magnetism and chemical species transport

All simulations are time-dependent, transient (unsteady) scenarios during which heat flow patterns within the solid are modelled and observed.

2.3 Electromechanical Dynamics - Measurement

The foundation of Chapters 4-6 is a dynamic mathematical model of a full-scale hybrid wind-diesel test bed. Modeling techniques will be summarized in 2.4. However, field measurements were used to validate the model. Measurement methodologies for these field measurements are discussed in this section.

2.3.1 Field Measurements

To measure the dynamics of the test bed when subject to various perturbations in load and wind power, the system was given a set of step and ramp inputs while voltage and current measurements were made. Due to limitations in the hardware, only the following six channels were selected (see Figure 2.1).

- Phase A bus line-to-neutral voltage, V_{an} *(V)*
- Phase B bus line-to-neutral voltage, V_{bn} *(V)*
- Phase C bus line-to-neutral voltage, V_{cn} *(V)*
- Phase A bus current, $I_{a,bus}$ *(A)*
- Phase A diesel electric generator (DEG) current, $I_{a,DEG}$ *(A)*
- Phase A wind turbine generator (WTG) current, $I_{a,WTG}$ *(A)*

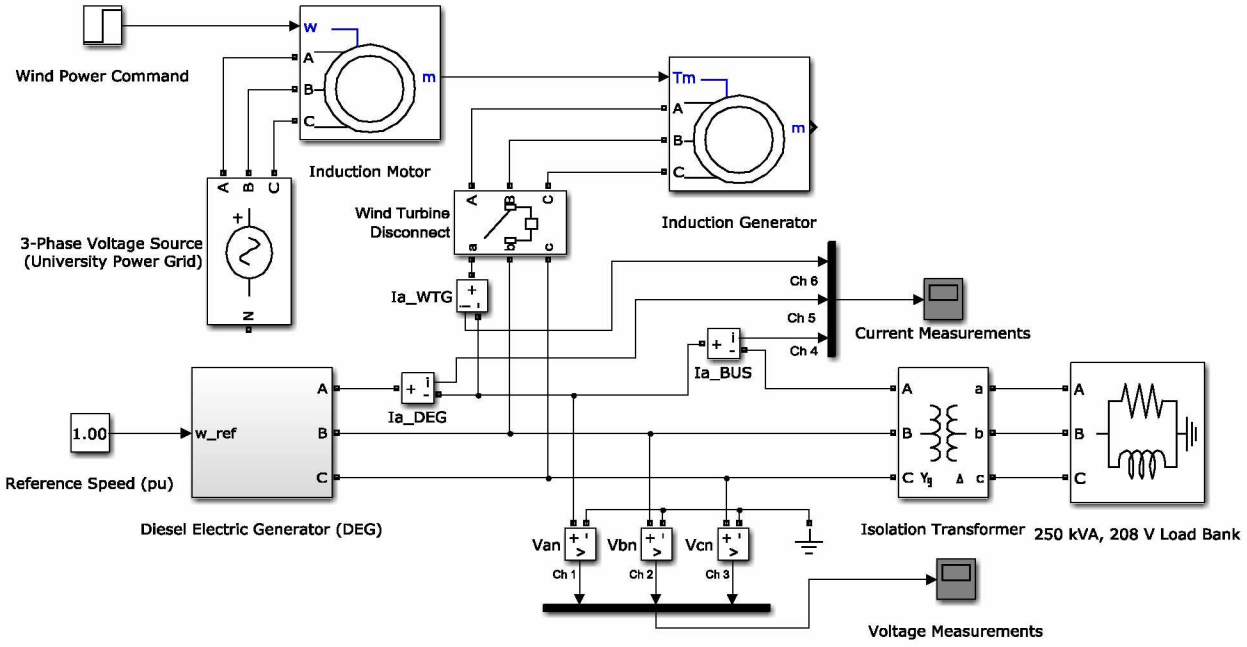

Figure 2.1. Hybrid wind-diesel test bed model block diagram with data collection configuration.

Three high-voltage differential probes with 500X attenuation were placed between each phase and the neutral point, all at the bus. Current probes used were Hall Effect Fluke i410 AC/DC current clamps with a 1 mV/A output. Automatic measurements of all six channels were performed by using a National Instruments™ PCI-6221 Data Acquisition System (DAQ) and breakout box with a LabVIEW interface. The outputs of the current and voltage probes were 256-bit 0-5 V signals, which were routed directly to the breakout box and sampled at 6000 Hz.

2.3.2 Raw Data

When the AC 60 Hz system is sampled at a rate of 6000 Hz, each cycle is represented by 100 data points per channel. Plotted raw data shows expected sinusoidal voltage and current waveforms at the anticipated magnitudes (see Figure 2.2).

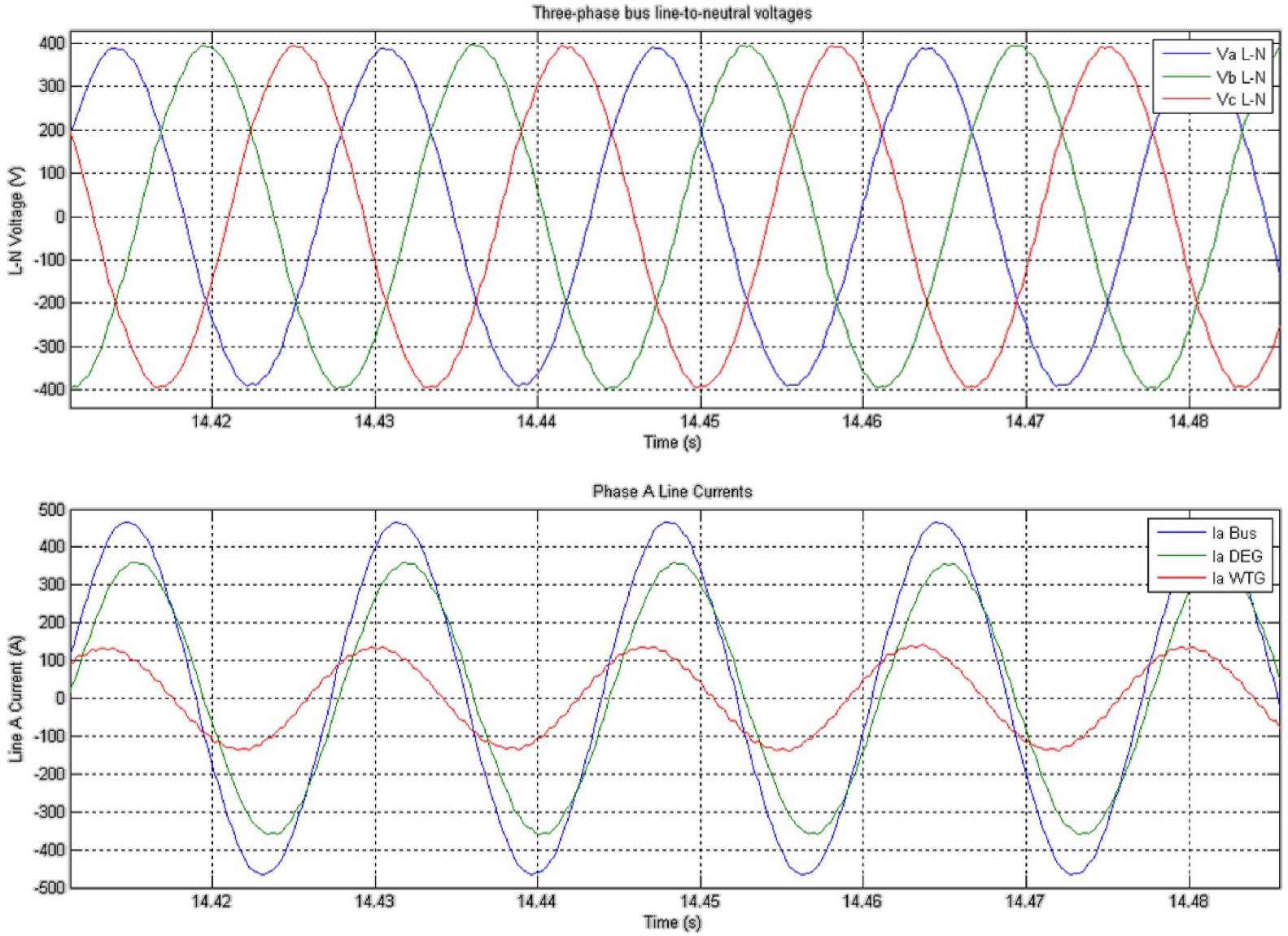

Figure 2.2. Three-phase line-to-neutral (L-N) voltages and phase A line currents for five complete cycles.

2.3.3 Post Processing: RMS Values

From the voltage and current measurements taken on the hybrid wind-diesel test bed, additional variables were calculated directly using MATLAB®. Of particular interest are the root mean square (RMS) values of voltage and current. These values more practically represent the signals over the time scale of interest (seconds and minutes, as opposed to sub-second). The following signals were derived from the measured channels of raw data.

- Phase A, B, and C RMS voltages [V] (Figure 2.3) - Calculated in a sliding window of 600 samples (6 cycles)
- Phase A RMS currents [A] for bus, DEG, and WTG (Figure 2.4) - Calculated in a sliding window of 600 samples (6 cycles)

Three-phase RMS line-to-neutral (L-N) voltages show a nominally balanced load with phase A carrying slightly less voltage than the other two. RMS magnitudes are at about 277 V L-N, as would be expected in a 480 V line-to-line (L-L) system. Perturbations in the load can be seen as voltage deviations from such nominal values in Figure 2.3.

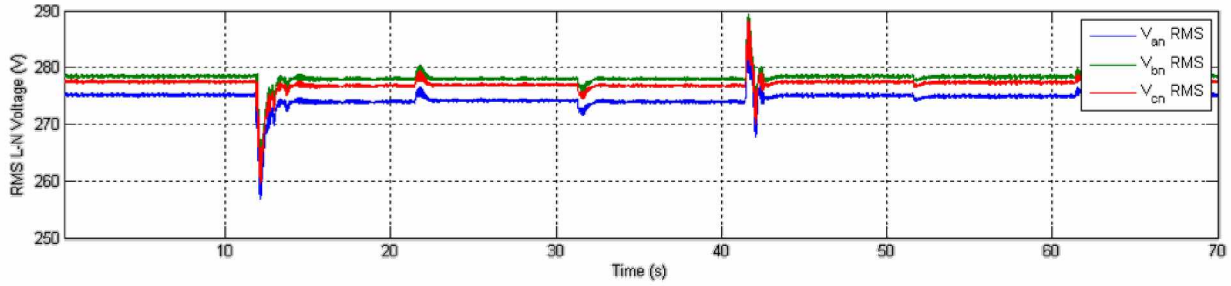

Figure 2.3. Sample of calculated RMS line-to-neutral voltages for all three phases.

RMS line currents (see Figure 2.4) show a series of steps, which are purposely introduced to determine the effect of load steps on machine dynamics. Bus and DEG currents are in near perfect alignment, as would be expected when no current is flowing out of the WTG. (Energy

balance would dictate that instantaneous generation match consumption.) Values shown range between 0 and 400 A, which almost cover the full measurement range of the current probes.

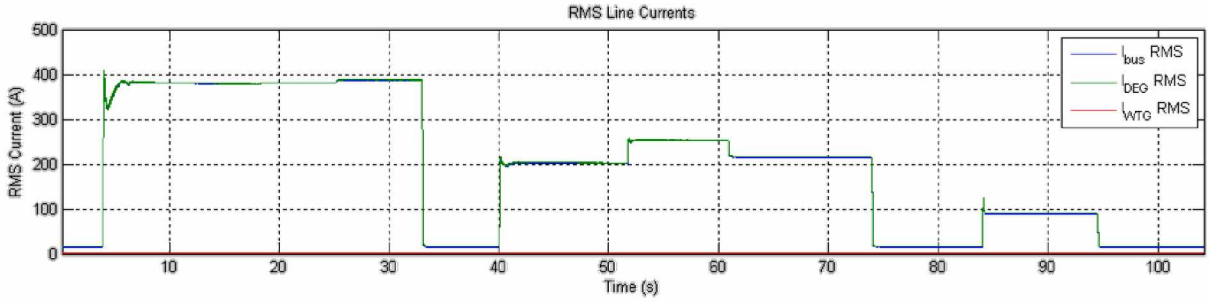

Figure 2.4. Sample of calculated RMS phase A line currents for all three components.

Other variables of interest, such as frequency and power factor, can be calculated directly from the raw data waveforms as well. These methods will be covered in the following section.

2.3.4 Post Processing: Frequency and Power Factor

Frequency and power factor are both calculated cycle-to-cycle. Here, frequency refers to the frequency of the voltage waveform, which can apply to any of the three phases. It can be shown, however, that frequencies are essentially the same between phases, as would be expected if the poles of the synchronous machine are fixed. A common method for calculating frequency is used here (see Figure 2.5), whereby zero-crossings of the voltage signal (on the rise) are interpolated. The inverse of their period (measured in units of time, seconds) indicate the frequency (in Hertz).

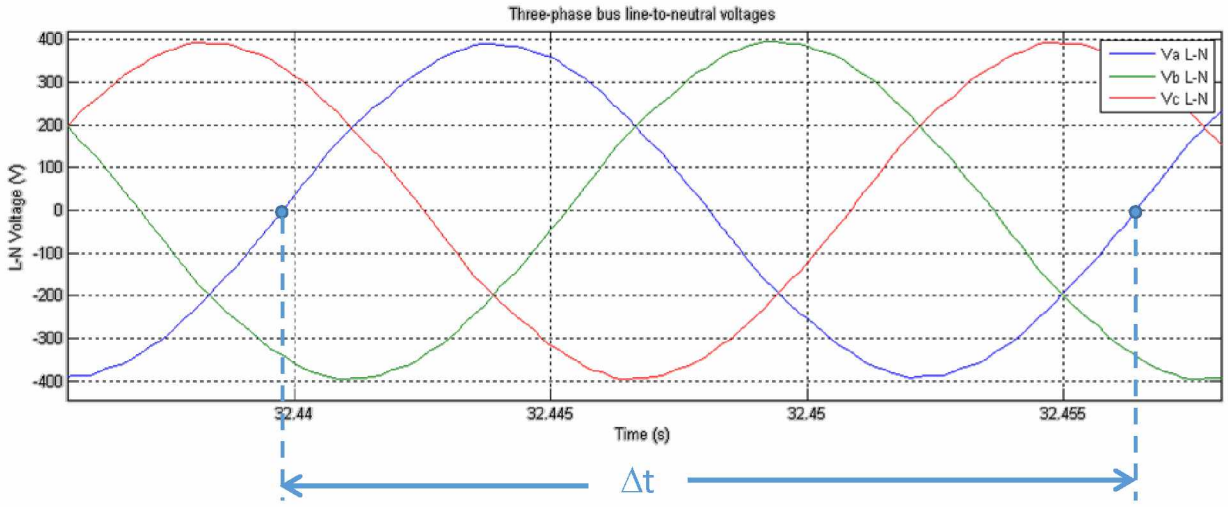

Figure 2.5. Frequency is calculated by interpolation of the voltage zero-crossings, on the rise.

Power factor refers to the cosine of the angle between the voltage and current waveform, which also may vary by phase. Since only phase A line currents were measured, power factor will be defined based on phase A voltage and phase A line currents. The power factor angle is calculated from the measured time difference Δt in Equation 2.1.

$$PF = \cos(\theta) = \cos\left(360\frac{\text{deg}}{cycle} \cdot 60\frac{cycles}{\text{sec}} \cdot \Delta t\right) \tag{2.1}$$

The example in Figure 2.6 shows a lagging power factor with a time difference of 0.0020 seconds. Per (2.1), the power factor for such a time difference would be cos (43.2°), or about 0.729 lagging.

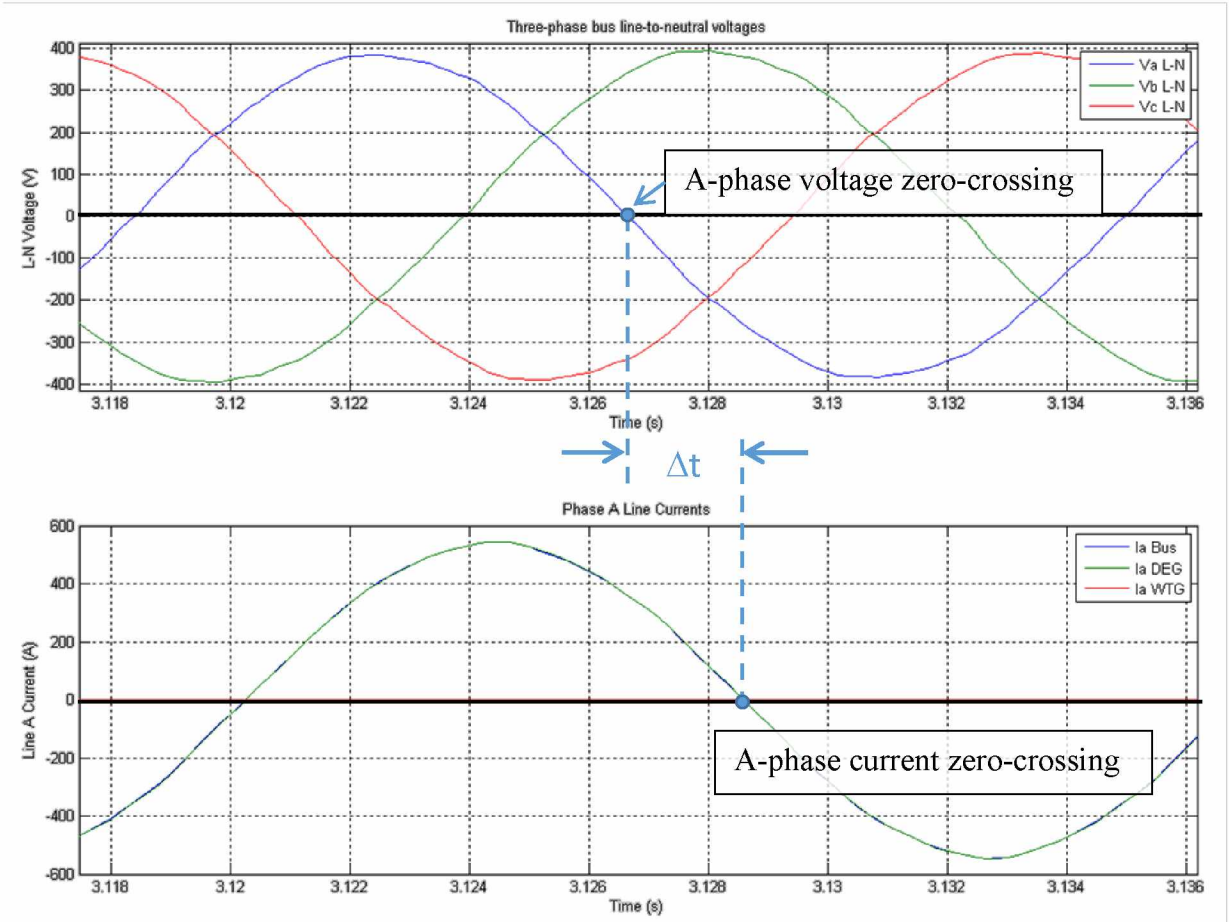

Figure 2.6. Power factor is calculated by the angle difference between the voltage and current zero-crossings.

2.3.5 Post-Processing: Impedance, Real Power, and Reactive Power

With three-phase RMS voltages, phase A RMS line currents, frequency, and power factors identified, the following variables could then be calculated using simple power relationships and a balanced load assumption (phase A as representative).

- Real power P for the main bus, DEG, and WTG (kW)
- Reactive power Q for the main bus, DEG, and WTG (kVAR)
- Impedance Z for the main bus, DEG, and WTG (Ω)

with the following equations for real power (2.2), reactive power (2.3), and impedance (2.4).

$$P = (V_{an} + V_{bn} + V_{cn}) \cdot I_a \cos(\theta) \tag{2.2}$$

$$Q = P \tan(\theta) \tag{2.3}$$

$$Z = (V_{an} + V_{bn} + V_{cn}) / 3I_a \tag{2.4}$$

The variables calculated in the previous sections are thus used to compare with and validate the response of the electromechanical dynamics model. Development of the model will be discussed in 2.4.

2.4 Electromechanical Dynamics - Modeling

As the intent of the dynamic modeling is to understand the electromechanical interactions of the system components, it is important to focus on the appropriate time scale. The electromechanical model developed in this dissertation focuses on the dynamic performance at a *millisecond* time scale. This is in contrast to the numerical heat transfer model of the ETS core, which is concerned with hour-to-hour and day-to-day performance. Conversely, it is also in contrast to the ultra-fast sub-cycle *microsecond* switching of DC power electronic components which are not used here.

2.4.1 Model Structure

The inputs of the model (see Figure 2.7) include variable wind speed and consumer demand profile. These linearly interpolated one-second signals perturb the model in such a way as to represent a realistic isolated wind-diesel power system environment and allow the responding control mechanisms to make continuous changes to the state of the machines. The primary outputs of the model include frequency and line-to-line voltages. Also calculated are line currents, real and reactive power flows, power factors, and component impedances. However, the primary

parameters of interest for this work are the frequency and voltage of the system, as these are the standard metrics by which system stability is evaluated.

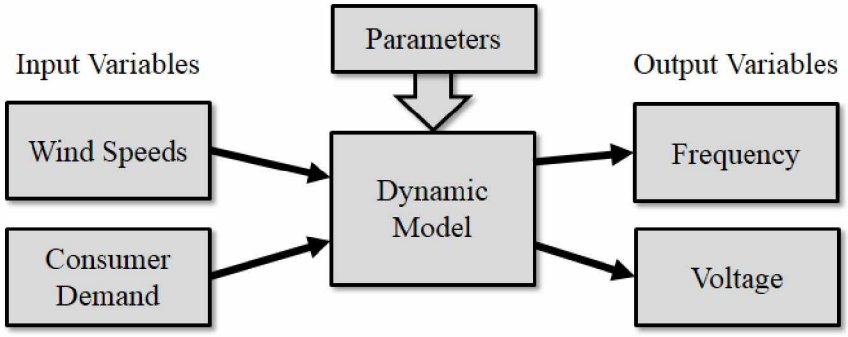

Figure 2.7. Flow chart of dynamic model showing the relevant inputs and outputs.

The components that form the dynamic model are discussed in further detail in Chapters 4-6. These include the diesel engine (which drives the synchronous generator), the wind turbine rotor (which drives the asynchronous/induction generator), the consumer bus, and the secondary load (ETS). Mathematical models for each generation component are appropriately applied, as illustrated in Figure 2.8. Each mechanical component (engine, turbine) converts a fuel (diesel, wind) to a mechanical torque, which is applied to the respective generator. The generator is where the mechanical and electrical interactions occur and, in both cases, is governed by the swing equation. This equation is essentially a force balance between the electrical torque (T_e) and mechanical torque (T_m) expressed as a time domain differential equation. The electrical torque is then determined by the equivalent circuit for the respective generator (Figures 2.9 and 2.10), which, in both cases, is expressed in the rotating (dq) reference frame. The rotating reference frame

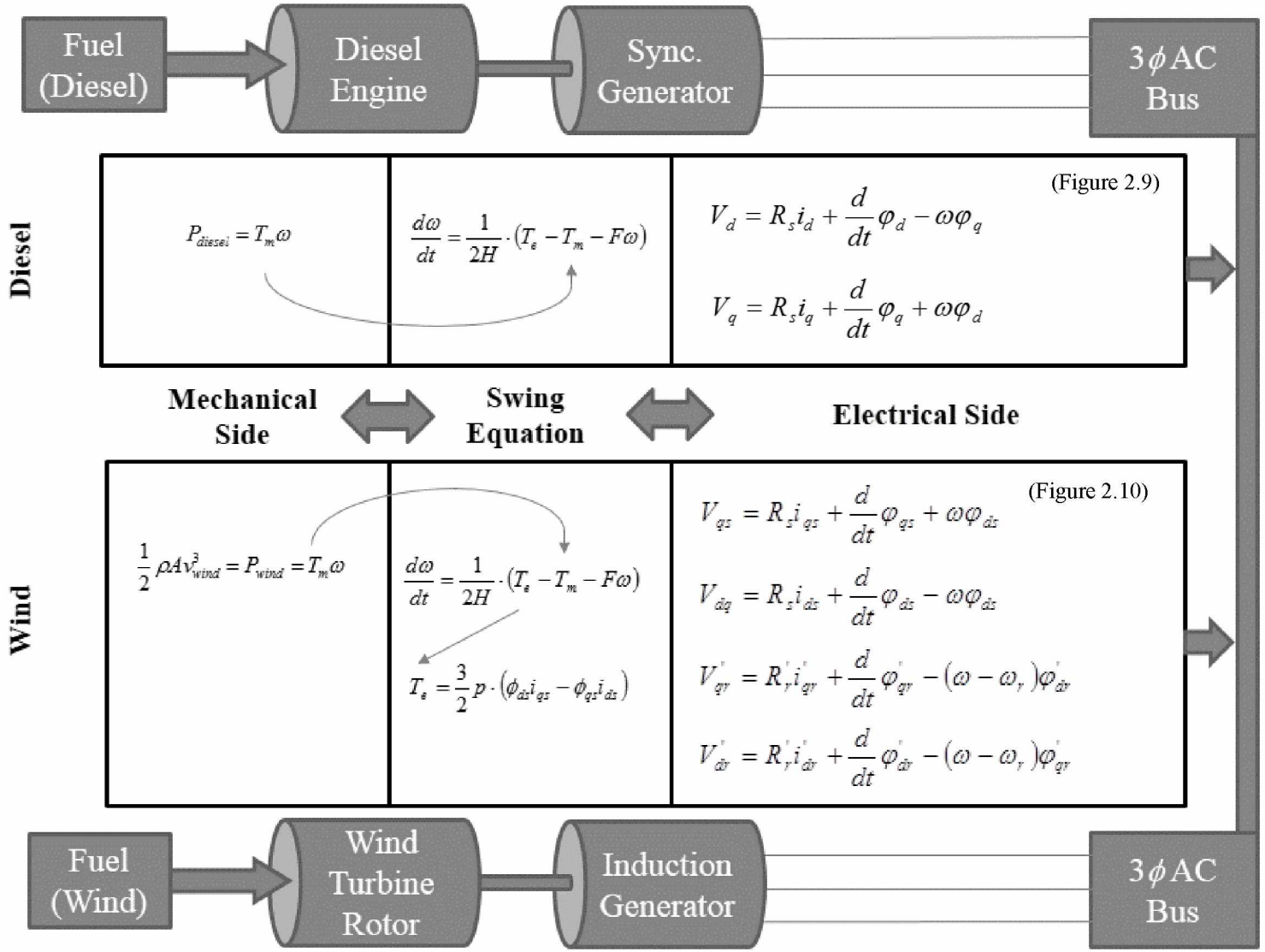

Figure 2.8. Structure of the electromechanical wind-diesel system model [1-3].

is commonly used to simplify the analysis of electrical machines by referring quantities to the rotor, thus eliminating the effect of time-varying inductances.

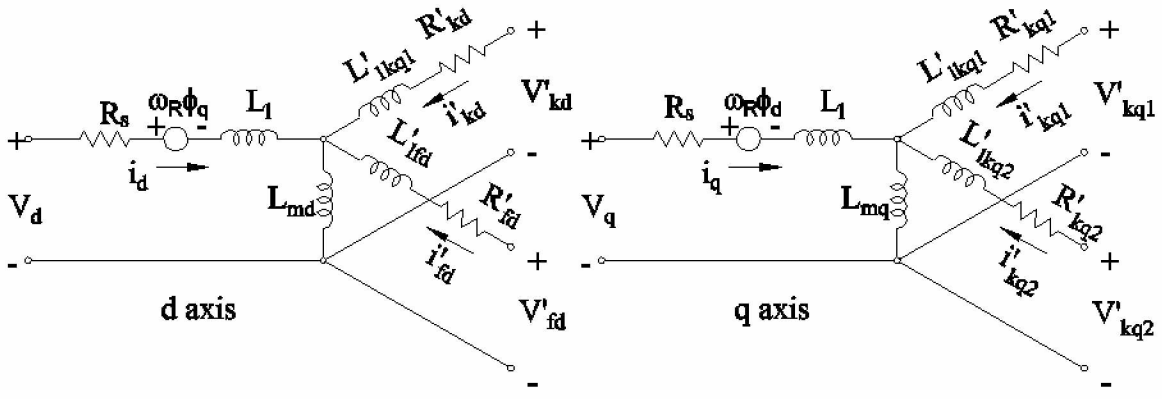

Figure 2.9. Circuit model for the synchronous machine [1-2].

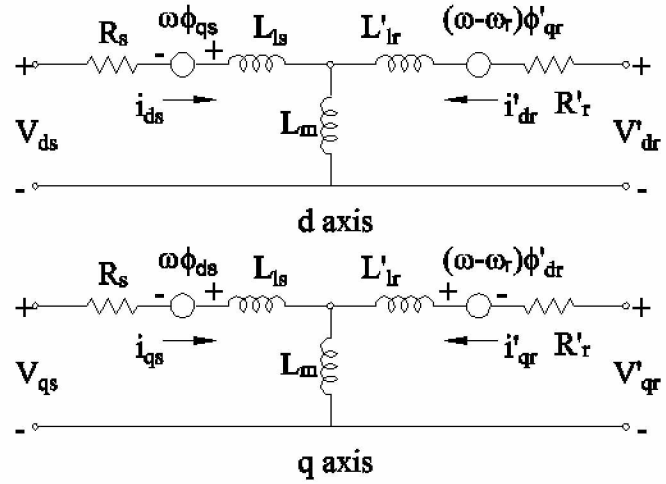

Figure 2.10. Circuit model for the asynchronous machine [3].

2.4.2 Equivalent Circuit Simulation Process

As stated earlier, the primary interest is in the electromechanical oscillations of the system. The equivalent circuits for both the synchronous and asynchronous (induction) generators can thus be solved using the *phasor* method in Simscape Power Systems™, as only the changes in

magnitude and phase of the voltages and currents are of interest—we do not need to solve all differential equations resulting from the interaction of R, L, and C circuit elements (i.e. the "state space" model). This simplification saves a significant amount of computational resources by solving a simpler set of algebraic equations.

Simscape Power Systems™ is an add-on to Simulink, which runs in the MATLAB® environment. The steps of the Simscape Power Systems™ *phasor* type simulation are illustrated in Figure 2.9 and discussed here in further detail. [4]

1. When a simulation is called, an initialization routine converts the Simscape Power Systems™ model into an equivalent system which can be solved by Simulink®. Each network node is given a node number.
2. The system blocks are then stored in the Simscape Power Systems™ 'Powergui' tool.
3. The blocks are separated into linear and nonlinear groups. For the electromechanical model developed in Chapter 4, the linear blocks include the diesel engine and governor, the wind turbine, the resistive and inductive loads, all measurement blocks, the synchronous machine exciter, and all controllers developed. Nonlinear blocks include the synchronous machine, the asynchronous machine, and all switches.
4. The state-space matrices (A, B, C, and D) of the linear part are formed. (See Equation 2.5)
5. The state-space model is immediately replaced with the complex transfer matrix $H(j\omega)$, which relates voltage and current phasors at the fundamental frequency (60 Hz).
6. The Simulink® "S-Function" block computes the linear portion of the system.
7. All nonlinear blocks are modeled as controlled current sources. Their inputs are the corresponding voltage outputs of the linear portion and their outputs are fed into the inputs

of the linear portion as the input sub matrix $\mathbf{u}_2$ (Figure 2.11). An additional sub matrix ($\mathbf{u}_1$) is made from the outputs of the independent voltage and current sources. Appropriate Simulink blocks are used for modeling the nonlinear blocks and the independent sources.

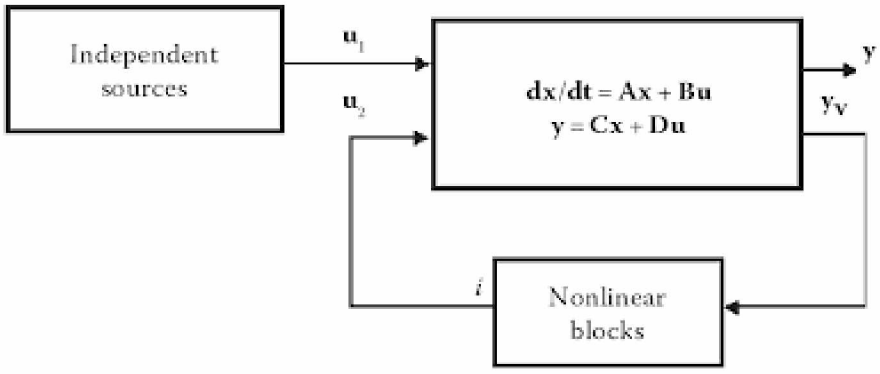

Figure 2.11. Simscape Power Systems™ simulation strategy block diagram [4].

As mentioned, the state-space representation of the first order linear differential electrical system is generated in step 5. The equations take the following form

$$\frac{dx}{dt} = Ax + Bu\,,\ \ y = Cx + Du \tag{2.5}$$

where x is a vector comprised of the capacitor voltages and the inductor currents, u is the system input vector, and y is the output vector. Matrices A, B, C, and D form the linear state-space model. However, if the phasor method is used, the faster modes are ignored by evaluating the system near the fundamental frequency and the state-space model can be replaced with the complex transfer matrix (H) defining the network algebraic equations.

2.4.3 Solution of Nonlinear Ordinary Differential Equations (ODEs)

Although the equivalent circuits can be reduced to a set of algebraic equations, the electromechanical interactions are still governed by the 2nd order nonlinear differential equation

known as the "swing equation" (see Equation 1.2). The swing equation harbors frequencies that span a range of several orders of magnitude and is numerically unstable with most solution methods. Thus, a continuous variable-step "stiff" solver must be applied.

MATLAB®'s stiff solvers include the following.

- ode15s, a general use variable-step, variable-order solver
- ode23s, an efficient single step solver
- ode23t, an implementation of the trapezoidal rule for only moderately stiff problems
- ode23tb, a highly efficient two-stage solver

Various solvers were tested with the electromechanical model, subject to a wide range of conditions and loads. Ode15s had problems at step changes in load impedance. Ode23s was effective, but computationally intensive. Ode23t and ode23tb both performed well under a wide range of conditions and were able to simulate at a rate of approximately 50% of real time—much faster than other solvers. Development of the electromechanical model called for the use of multiple solvers with various configuration parameters. Ultimately, ode23tb was selected based on its performance, flexibility, and recommendations from the literature [4].

Ode23tb uses an implicit Runge-Kutta algorithm with two distinct stages: 1) a trapezoidal rule step and 2) a second order backward differentiation formula. The solver is highly efficient, in part due to its application of the same iteration matrix in both steps [4]. Like all MATLAB® ode solvers, it is equally capable of solving the set of algebraic equations generated from the equivalent electrical circuits (see Figure 2.11).

These electrical, mechanical, and thermal modeling and measurement methodologies are thus applied in the following chapters of this thesis.

2.5 References

[1] Krause, P. C. *Analysis of Electric Machinery*. McGraw-Hill (1986) Section 12.5.

[2] Kundur, P. *Power System Stability and Control.* McGraw-Hill (1994).

[3] Krause, P. C., O. Wasynczuk, and S. D. Sudhoff. *Analysis of Electric Machinery*. IEEE Press (2002).

[4] Perelmuter, V. M. *Electrotechnical Systems: Simulation with Simulink® and Simscape Power Systems™*. CRC Press (2013).

Chapter 3. Generalized Heat Flow Model of a Forced Air Electric Thermal Storage Heater Core[1]

3.1 Abstract

Electric Thermal Storage (ETS) devices can be used for grid demand load-leveling and off-peak domestic space heating. A high-resolution 3D finite element model of a forced air ETS heater core is developed and employed to create a general charge/discharge model. The effects of thermal gradients, air flow characteristics, material properties, and core geometry are simulated. A simplified general stove discharge model with a single time constant is presented based on the results of the numerical simulations. This simplified model may be used to stimulate economic/performance case studies for cold climate communities interested in distributed thermal energy storage.

3.2 Introduction

Electric heat from resistive "baseboard" heaters is a common form of Domestic Space Heat (DSH) in cold climates. These systems are relatively inexpensive to purchase, easy to install, simple to control, and clean (from the end-user's standpoint). However, they require an instantaneous supply of electricity from the grid. When a large number of units are installed, the aggregate has the effect of potentially creating large peaks in grid demand during cold spells and the utility may struggle to avoid a capacity deficit.

---

[1] Janssen, N.T., R.A. Peterson, and R.W. Wies. "Generalized Heat Flow Model of a Forced Air Electric Thermal Storage Heater Core." *Journal of Thermal Science and Engineering Applications* 9.4 (2017): 041008. Funding provided by the U.S. Department of Energy, Office of Science, Basic Energy Sciences, under Award # DE-SC0004903

A previous modeling effort [1] investigated controlling the temperature set points of electric heaters without storage to reduce the peak behavior of thermostatic loads using programmable communicating thermostats. This method is less effective for smaller thermal masses and requires additional installed communication infrastructure.

Perhaps the most widely accepted solution to electric heat demand load levelling is the use of Electric Thermal Storage (ETS) heaters (See Figure 3.1). ETS heaters allow the consumer to decouple their residence's heat demand from the availability of electrical capacity on the grid by storing heat in a dense core of ceramic storage media. Heat can be released thermostatically by forcing air (or a liquid heat transfer fluid) through the core and into the residence as needed. Charging may occur during off-peak hours, or in accordance with excess power availability. On small, wind-powered microgrids, charging will primarily occur during periods of high wind availability.

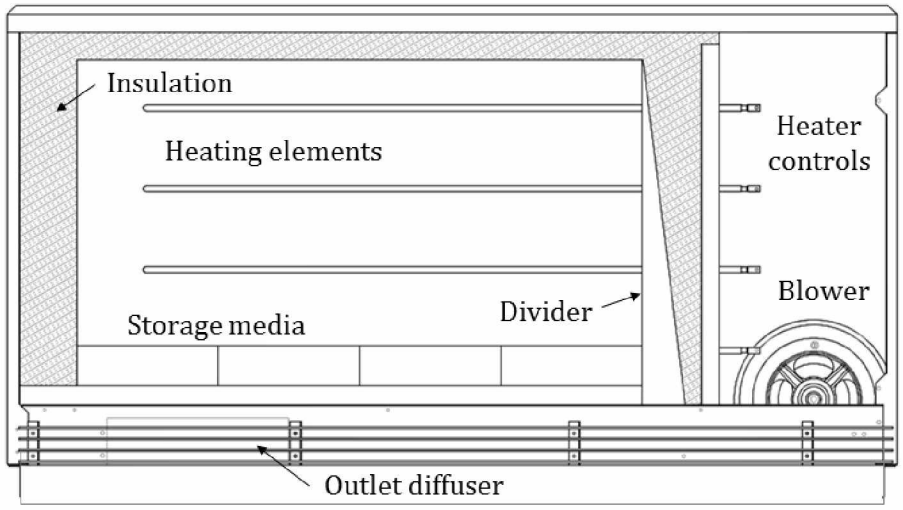

Figure 3.1. Primary components of a Steffes 2105 electric thermal stove [2].

Typical ETS units will maintain a target state of charge (SOC), which can be manually or automatically set. In general, the SOC should be higher when more heat demand is anticipated

(e.g. periods of colder weather). As the core's SOC drops with the average stove temperature, the ability for the ETS unit to provide heat at full output is diminished. Hence, a key design consideration is the discharge behavior of the stove as it cycles from a full SOC to a dead, empty state.

An important design consideration for islanded wind-powered microgrids is total ETS fleet size. Case studies can be found in the literature [3-5] which are conducted in order to adequately size a fleet of ETS units for a particular grid. A surplus of ETS units generally means a smaller fraction of off-peak power, or wind energy, per consumer. A deficit of ETS units reduces the aggregate storage capacity of the fleet. Though there are various methods for optimization, a good understanding of the transient behavior of the particular ETS device is an advantage in these analyses.

One particular study [6] integrates a 1D finite difference core model into the performance analysis, avoiding additional details in exchange for computational efficiency. For an even simpler analysis, Sateriale [7] makes the assumption that the stove outlet power is constant and independent of the SOC. Some effort has been made in the literature outlining approaches to developing ETS discharge models [8], though they leave it to the designer to follow such methods. Clearly, a simple yet accurate charge/discharge model of a typical room ETS unit is needed to further research and implementation in this area.

This study develops a generalized lumped thermal model for a typical forced air room ETS core. Factors such as core geometry, material, and air flow characteristics are studied using a numerical finite element model. The results are summarized and outline the transient behavior of a general ETS core, given any combination of these factors. Potential additional variables such as stove thermal insulation and air chamber mixing are omitted for reasons of generalization.

3.3 Model

The primary objective of the present work is to develop a generalized performance model of a typical forced air room ETS heater core. With decoupled charge and discharge commands, there are an infinite number of potential input patterns. These patterns could result in numerous time-temperature histories within the storage media. The first and primary step of the analysis is to determine the degree to which certain factors affect the charge and discharge behavior of the core.

The charging behavior alone is not given extensive attention in this study, and the heat addition is modeled as a constant heat flux into an insulated simulation region. This is an accurate description as long as the voltage is supplied consistently and the impedance of the heating elements does not change with temperature. (Some slight increase in impedance will occur as the core temperature rises.) A linear accumulation of sensible thermal energy is the result. However, the discharge characteristics of the core are apt to be a function of the core material properties, the air flow characteristics, and the distribution of thermal energy within it.

3.3.1 Definitions

Two important unitless quantities can be defined for use in the analysis: State of Charge (SOC) and Storage Disparity (SD). In the case of sensible thermal energy, the SOC is defined as

$$SOC = \frac{\int (T - T_0) \cdot dV}{(T_h - T_0) \cdot V} \tag{3.1}$$

where T is the temperature at any point in the storage volume, V. T_0 and T_h represent the low and high limits (respectively) on the possible range of temperatures within the core. The density and

specific heat of the solid are assumed not to be functions of temperature and therefore cancel in the ratio. The state of charge is thus a non-dimensional quantity.

The storage disparity represents the level to which thermal gradients in the core exist. It is a function of the maximum and minimum temperatures within the solid as well as the lowest possible core temperature, T_{∞}.

$$SD = \frac{T_{\max} - T_{\min}}{T_{\max} - T_{\infty}} \tag{3.2}$$

When the temperature at every point in the core is the same (perfect thermal equilibration), *SD=0*. If the minimum temperature approaches T_{∞}, *SD* approaches unity. This metric can be used as a means of quantifying the degree of thermal equilibrium as *SD* varies between 0 and 1.

3.3.2 Structure

A time-variant (transient) COMSOL© Multiphysics® model was developed based on the general layout and brick geometry of the Steffes 2102 room unit. Figure 3.2 shows a cross-section of the 2102 with a box encircling the simulation region. The core consists of eight layers of ceramic storage media with paired air channels between each layer. Four sets of resistive electric heating elements reside in alternate air channels, providing heat flux to the core. A baffle divides the inlet side from the outlet, forcing inlet air through the depth of the core, around a 180° turn, and out through the opposite side.

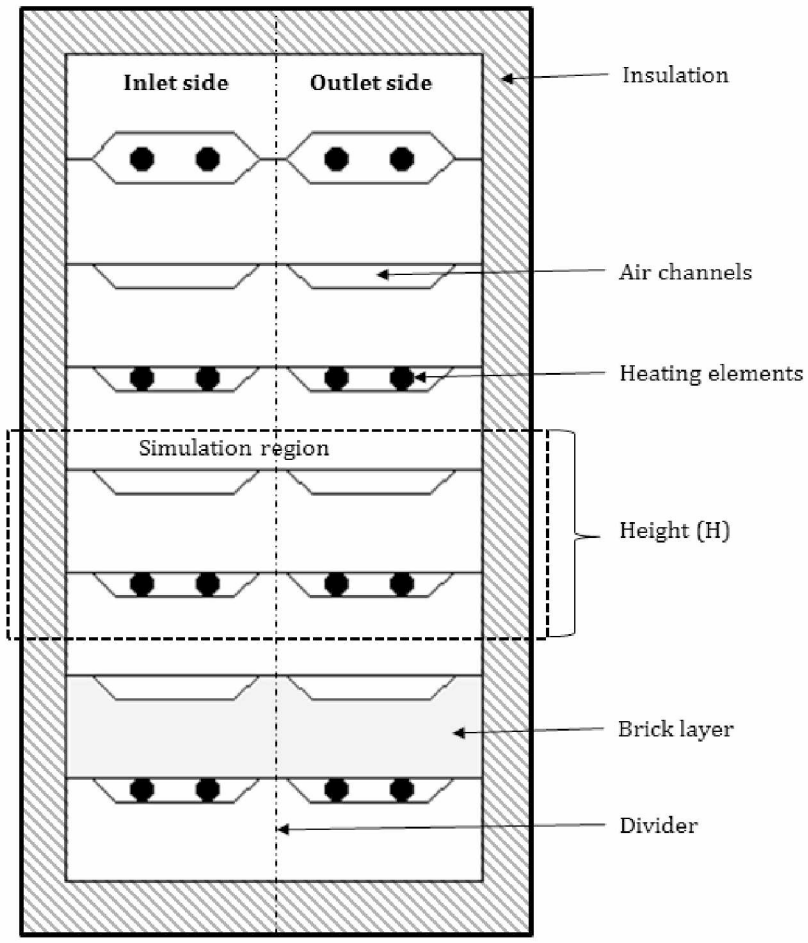

Figure 3.2. Cross-section of Steffes 2102 core.

A representative simulation region was chosen in order to reduce the size of the numerical model (Figure 3.3). The region encompasses two insulated brick layers and two air channels (one with heating elements, one without). A periodic boundary condition was applied to the upper and lower surfaces of the region to represent a repeating stack of regions. The front, back, and side surfaces are insulated ($\dot{Q}$ =0) and heat is generated on the charging surfaces at a constant heat flux. Conduction in the ceramic media and convection in the air flow channels are the operative modes of heat transfer throughout the simulation region. Fluid velocity profiles inside the channel are specified.

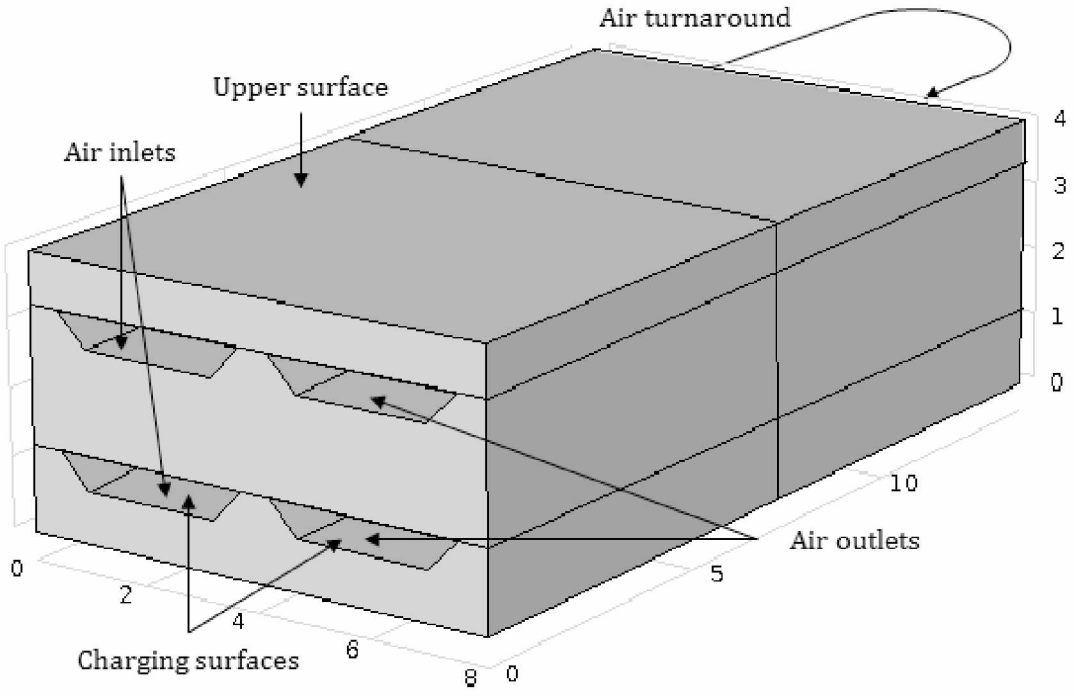

Figure 3.3. Simulation region anatomy (length units in inches).

3.3.3 Governing Equations

Transient heat conduction in the ceramic core (subscript "c") is governed by Fourier's law, expressed here in terms of the ceramic material properties (density [ρ], specific heat [C_p], thermal conductivity [k]), heat flux ($\dot{Q}$), temperature (T) and time (t).

$$\rho_c C_{p,c} \frac{\partial T}{\partial t} = \nabla \cdot (k_c \nabla T_c) + \dot{Q} \tag{3.3}$$

Similarly, heat transfer in the air flow channels (subscript "a") is described with an additional convective term

$$\rho_a C_{p,a} \frac{\partial T}{\partial t} + \rho_a C_{p,a} \vec{u} \cdot \nabla T = \nabla \cdot (k_a \nabla T_a) + \dot{Q} \tag{3.4}$$

where $\vec{u}$ is the fluid velocity vector. The fluid velocity field is specified, and various profiles are considered.

3.3.4 Boundary Conditions

Apart from the insulated ($\dot{Q}=0$) and periodic boundaries, the inlet, outlet, and charging surface boundary conditions are defined as follows

$$\dot{Q} = h \cdot \left(T_{\infty} - T_{a}\right) \tag{3.5}$$

where T_{∞} is the room air temperature and h is the convective heat transfer coefficient. If the thermostatically-controlled blower is off, $h=0$ at the inlet and the boundary is insulated. When the blower activates, drawing air into the channels, h is set to infinity in order to represent an isothermal boundary at $T_{a} = T_{\infty}$. Both channel outlet boundary conditions are advective outflow, which can also be modeled using $h=0$ combined with a finite value of $\vec{u}$.

At the charging surfaces, the heat flux is given as

$$\dot{Q} = \dot{Q}_{chrg} \tag{3.6}$$

In this study, the specific heat flux is 2660 W/m^2, which is the rated power of the Steffes 2102.

3.3.5 Material Properties

Typical parameters for the materials in an actual Steffes 2102 were used for the initial simulation and are specified in Table 3.1. These values are varied between realistic low and high limits in the parameter sweeps of section 3.4 and offer a representative starting point for analysis of the transient core SOC. Air properties including thermal conductivity, density, and specific heat are analytic functions of temperature provided within the software.

Table 3.1. Nominal parameters.

Property	Var.	Unit	Value
Ceramic Media			
Thermal Conductivity	k_c	W/mK	1.00
Density	ρ_c	kg/m^3	3145
Specific Heat	$c_{p,c}$	J/kgK	1050
Sim. Region Height	H	in	4
Air			
Ratio of Spec. Heats	γ	-	1.4
Thermal Conductivity	k_a	W/mK	Analytic
Density	ρ_a	kg/m^3	Analytic
Specific Heat	$c_{p,a}$	J/kgK	Analytic
Bulk Velocity	u	m/s	4.0

3.4 Analysis

The initial part of the analysis used the baseline numerical model with the typical material properties from Table 3.1 in order to gain insight into the stove's general discharge behavior as a function of time.

3.4.1 Solution Linearization and Air Velocity Profile

Given the nominal material parameters (Table 3.1), the output of the stove core can be modeled for varying degrees of bulk air flow, which will directly affect the discharge rate of the core. A range of 2-8 m/s was investigated based on laboratory measurements of the Steffes 2102. The initial temperatures are specified at every point in the storage material to the maximum allowable temperature in the core (900K) for an initial SOC of 100%. Initially a flat velocity profile

is specified in the air channel.

The resulting surface temperature of the simulation region is shown in Figure 3.4 (for $u=8$ *m/s*) several minutes after the initiation of a discharge. Cold room air enters the left side, and leaves on the right after doubling back in the rear of the stove. The coldest region is, expectedly, the area around the inlet channels. A localized hot spot can be seen in the corner opposite the inlet side. A strong gradient is visible between the inlet and outlet channels of the brick. The effects of charging-induced gradients are not visible in the bottom channels versus the top, as they quickly disappear after the initiation of a discharge.

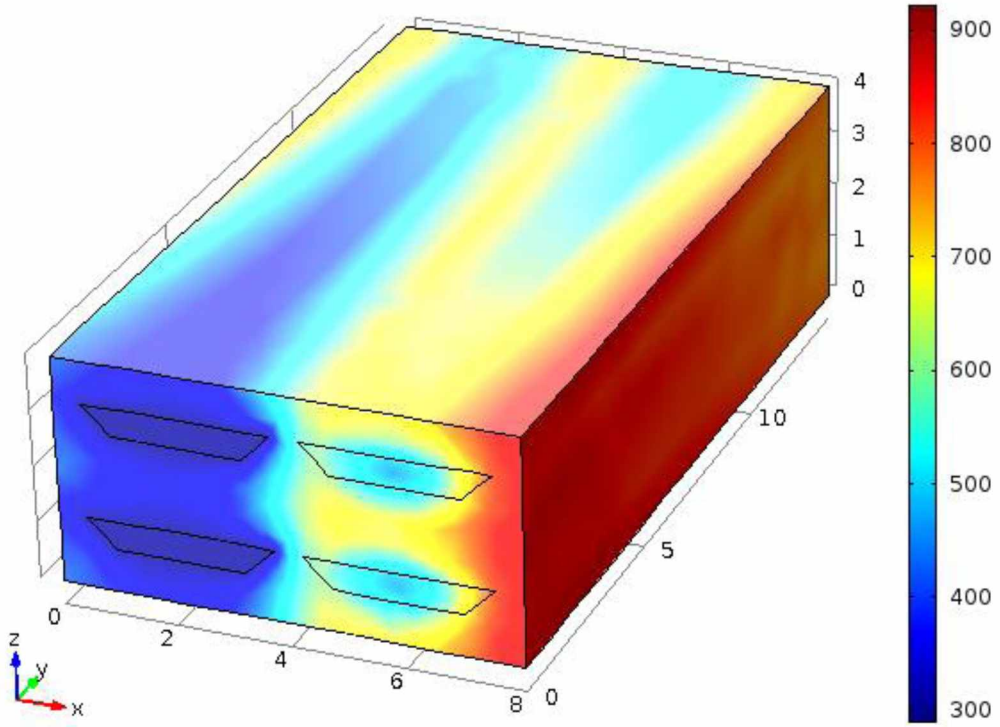

Figure 3.4. Surface temperature solution for nominal parameter case.

Given the numerical temperature solution at each tested air velocity, Equation 1 can then be used to calculate SOC as a function of time. The resulting stove discharge curves follow an approximate exponential decay pattern (Figure 3.5) with a single time constant. The general state

of charge can then be modeled as a function of time as

$$SOC = SOC_0 e^{\frac{-t}{\tau}} \tag{3.7}$$

where SOC_0 is the initial state of charge (when the discharge command is given) and τ is the time constant. The time constant is determined using a linear regression of ln (SOC) versus t. The time constant (τ) is therefore the negative inverse of the slope of the linearized discharge curve.

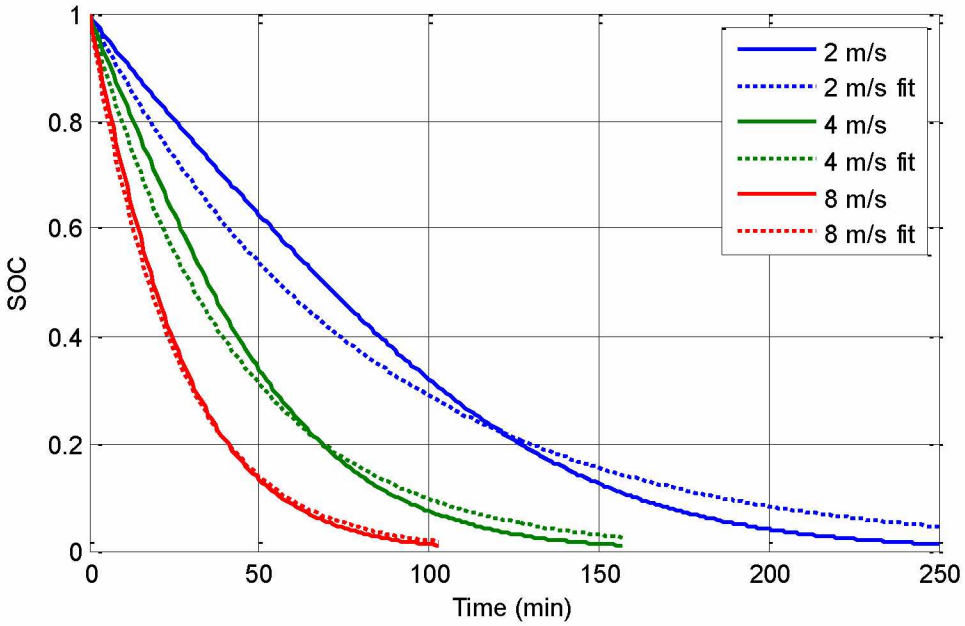

Figure 3.5. Discharge curves for flat velocity profile with fits shown.

The results of three simulations in the typical velocity range are shown along with their respective least-squares fit in Figure 3.5. Two things are readily apparent: 1) higher velocities increase the discharge rate of the core, and 2) the 1-parameter curve fit is less accurate at lower velocities.

To quantify error between two discharge curves, the mean square error (mse) is defined as

$$mse = \frac{1}{t_f - t_0} \int_{t_0}^{t_f} \sqrt{(SOC_a - SOC_b)^2}\, dt \tag{3.8}$$

where (t_0, t_f) is the interval of time under consideration and the subscripts a and b denote the two curves being compared. The typical interval used in this study will be from t_0=0 to the time at which the stove has reached SOC=0.01.

The mse of the three velocities modeled in Figure 3.5 are shown in Table 3.2, in addition to an identical simulation except using a parabolic velocity profile in the air channel. The time constants are equal to within 0.1%, indicating the shape of the air channel velocity profile has negligible effect on the discharge behavior of the stove. The mse data also show that the flat and parabolic velocity curves at each flow rate are nearly identical to each other. Therefore, a flat velocity profile is used for the remainder of the study.

Table 3.2. Mean squared error of various velocities.

Bulk Velocity (m/s)	Flat Vel. Profile		Parabolic Vel. Profile		*mse* between
	τ (min)	mse_{fit}	τ (min)	mse_{fit}	
2	80.37	7.22E-05	80.47	7.15E-05	4.80E-07
4	42.74	7.24E-05	42.90	7.13E-05	9.87E-07
8	25.28	4.16E-05	25.41	3.81E-05	2.43E-06

3.4.2 Thermal Gradients

As the ETS core charges when excess electric power is available (e.g. high wind event), and discharges due to thermostatic demand, thermal gradients can build up within the storage media over time. The extent to which these gradients affect the subsequent discharge behavior of the stove can be quantified. This relationship will depend on the core material, geometry, air flow rate, and charge-discharge history.

Here, the typical parameter values from Table 1 are used for comparison between two cases at various states of charge: *immediate* and *equilibrated* discharge. In the case of immediate

discharge, a strong thermal gradient is induced by allowing the core to charge from 0 to SOC_0 at the full electric charge rate, followed immediately by discharging until SOC = 0 (Figure 3.6). The equilibrated case allows for a short period of time after charging to remove thermal gradients before subsequent discharge. The resulting time constants and mse values for these two different simulations are shown in Table 3.3. The air velocity was 4 m/s in both simulations.

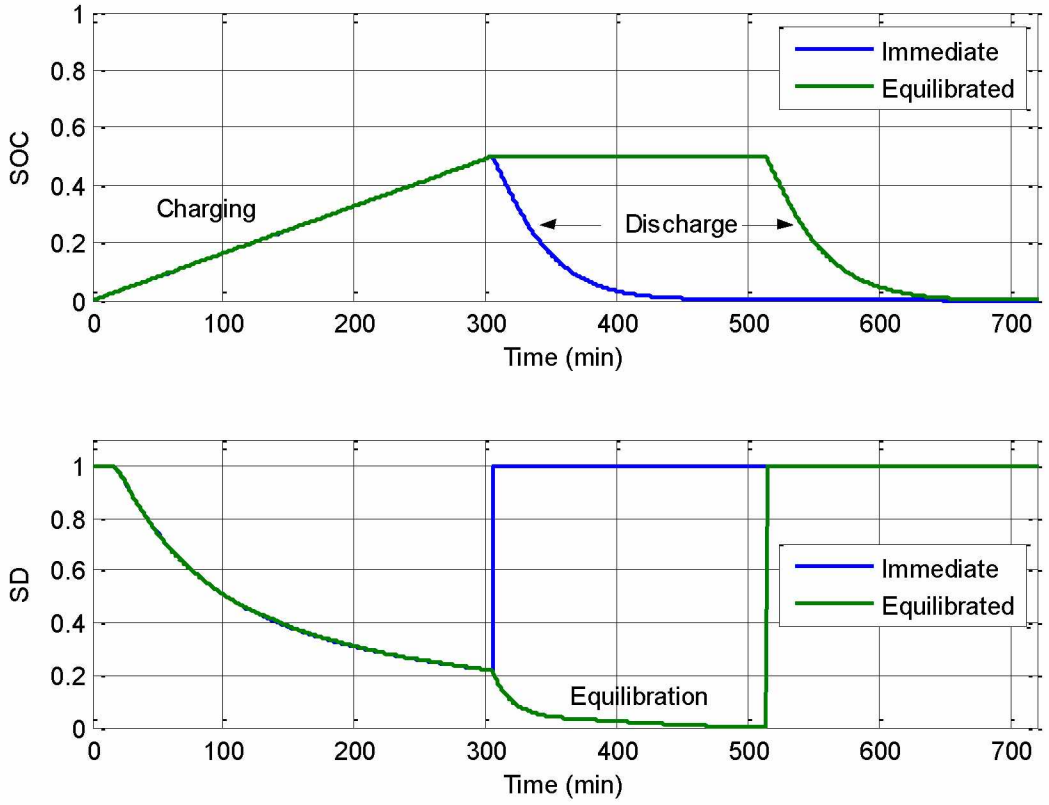

Figure 3.6. SOC and *SD* curves for $SOC_0 = 0.5$ and $u = 4$ m/s.

Table 3.3. Mean squared error by discharge and SOC_0.

	Immediate Discharge		Equilibrated Discharge		
SOC_0	τ (min)	mse_{fit}	τ (min)	mse_{fit}	mse between
0.25	34.87	4.53E-05	34.20	3.86E-05	1.88E-06
0.50	37.45	1.10E-04	38.33	1.01E-04	5.83E-06
0.75	39.24	2.14E-04	39.40	2.06E-04	7.60E-06
1.00	41.40	3.69E-04	41.74	3.81E-04	1.38E-06

The mse between immediate and equilibrated discharges for each SOC_0 tested are very small, on the order of 10^{-6}, indicating minimal correlation between the presence of a thermal gradient and the ETS discharge behavior. However, there is some small variability (<2%) in the value of the time constant for discharge. These results are valid for charge rates at or below 2660 W/m^2.

3.4.3 Parameter Sweep

Thus far it is has been shown that the air velocity profile in the core channels, and the thermal gradients within the media do not significantly affect the discharge behavior of the core. The next analysis will show that the core material properties and core geometry have a much more substantial effect on SOC*(t)*. Furthermore, the bulk air flow velocity (u) will also be shown to have a significant effect as well. A range of the three fundamental parameter values are tested in a sweep study.

3.4.3.1 Material Properties

A close look at the governing equation (3.3) confirms the three core material properties are density (ρ), specific heat (C_p) and thermal conductivity (k). However, the ability for heat to diffuse through the core over time is best described by the thermal diffusivity (α) which is a function of

these three properties.

$$\alpha = \frac{k}{\rho \cdot C_p} \tag{3.9}$$

When these individual properties are varied over the range in Table 3.4, the thermal diffusivity will span a range between 1/8 and 6 times its nominal value.

Table 3.4. Fundamental parameter space.

	k [W/mK]	*ρ* [kg/m^3]	*Cp* [J/kgK]	*α* [m^2/s]	*H* [in]	*u* [m/s]
Low	0.5	6290	2100	3.79E-08	3.0	2.0
Nominal	1.0	3145	1050	3.03E-07	4.0	4.0
High	1.5	1573	525	1.82E-06	5.0	8.0

3.4.3.2 Core Geometry

The nominal four-inch (10.2 cm) height of the simulation region H (Figure 3.2) is varied within a range of three to five inches (7.6 – 12.7 cm) to simulate the effect of varying core geometry (Table 3.4).

3.4.3.3 Bulk Air Velocity

The same range of velocities shown to affect the stove discharge curve (section 3.3.2) will be analyzed here, in combination with the other fundamental variables (Table 3.4).

A complete permutation of these three fundamental parameters results in a 3^3 study (27 simulation points). The results are presented and discussed in section 3.5.

3.5 Results and Discussion

As shown in section 3.4, three fundamental parameters drive the behavior of the stove core's time-dependent output, which can be modeled as an exponential discharge (3.7). The

material properties, core geometry, and air flow rate can be combined into a single independent parameter and generally used to describe the output of a range of core designs and operating scenarios. This section explores the shape and accuracy of a generalized one-parameter time constant model and an alternative two-parameter (quadratic) exponential model.

3.5.1 One-Parameter Model

The three fundamental parameters driving the discharge behavior of the core can be represented in a single independent dimensionless quantity of a modified Graetz number similar to that introduced in [9]. This modified Graetz number (Gz*) is the product of the Reynolds number (Re), the Prandtl number (Pr) and the dimensionless quantity L/D_H.

$$Gz^* = \mathrm{Re}\,\mathrm{Pr}\frac{L}{D_H} = \left(\frac{uD_H}{\nu}\right)\left(\frac{\nu}{\alpha}\right)\left(\frac{L}{D_H}\right) = \left(\frac{uL}{\alpha}\right) \tag{3.10}$$

In (10), u is the bulk fluid velocity. The fluid dynamic viscosity, ν cancels and does not appear in Gz*. In the case of channel flow, the hydraulic diameter, D_H would be four times the ratio of channel cross sectional area over perimeter ($4A/P$). However here, D_H cancels and leaves L in Gz*, where L is the length parallel to the flow direction. In order to retain the effect of the finite thickness of the storage medium, a characteristic length L is defined as the ratio of storage medium volume over the heat transfer area inside the channel (effectively the channel length, and reducing to that exactly for small storage medium volumes, analogous to a thin-walled pipe). The thermal diffusivity, α (9), contains the material properties relevant to heat transport.

This modified Graetz number is the independent variable of the parameter sweep. The study dependent variable describes the output of the stove core. In (7), the single parameter that describes this output is the time constant, τ.

The time constants derived from the least squares fit (section 3.1) can be calculated for each simulation in the parameter sweep (section 3.3). τ is a function of the convective heat transfer coefficient, h, and the mass (m), specific heat (c_p) and heat transfer surface area (A) of the simulation region (11).

$$\tau = \frac{mc_p}{hA} \tag{3.11}$$

The heat transfer coefficient, h, is present (along with other known simulation parameters) in the Biot number

$$Bi = \frac{hV_{body}}{kA} \tag{3.12}$$

In addition to h, Bi is also a function of the volume of the ceramic within the simulation region (V), the thermal conductivity of the heat transfer media (k) and the total heat transfer surface area (A). The Biot number represents the ratio of heat transfer at the outside of a body to the heat transfer within it. In this study, the Biot number is the dependent variable plotted against the independent variable, Gz*. The results of the parameter sweep are shown in Figure 3.7 spanning several powers of ten.

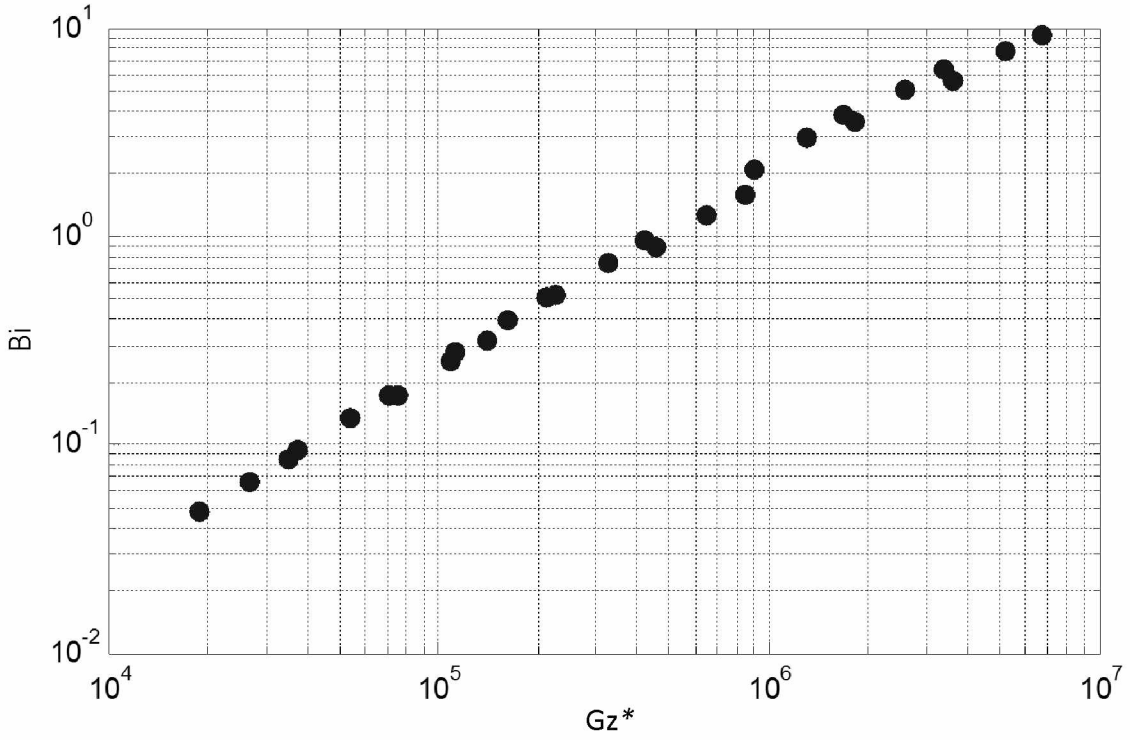

Figure 3.7. Results of the parameter sweep.

The direct and nearly linear relationship between Bi and Gz* could be expected as the mode of heat transfer at the surface of the channel is entirely advective. Similarly, for low values of Gz* (convective driven heat transport), heat transfer within the body (low values of Bi) overtakes heat transfer on the outside. A linear fit can be applied to Figure 3.7, relating Bi to Gz* as

$$\log_{10}(Bi) = 0.9218 \cdot \log_{10}(Gz^*) - 5.225 \tag{3.13}$$

Note that it is common for a lumped parameter model to be restricted to Biot numbers no greater than 10^{-1}. This accounts for only 10% of the data in Figure 3.7. To resolve the error associated with heat gradients within the core, a second parameter can be used.

3.5.2 Two-parameter Model

The single parameter model presented in 3.5.1 covers a wide range of foreseeable material properties, core geometries and air flow rates. However, error is introduced at high Biot numbers. This error can be removed with an added quadratic term in the exponential model. The discharge curve is then

$$SOC = SOC_0 e^{at^2+bt} \tag{3.14}$$

where a and b are the two parameters that describe the fit.

One such improvement is shown in Figure 3.8. The one-parameter general fit is a plot of equation (3.7) using a time constant calculated from equations (3.10 - 3.13). The two-parameter regressive fit uses a least squares method to find the coefficients of equation (3.14). An 84% improvement in the mse is achieved with the additional parameter.

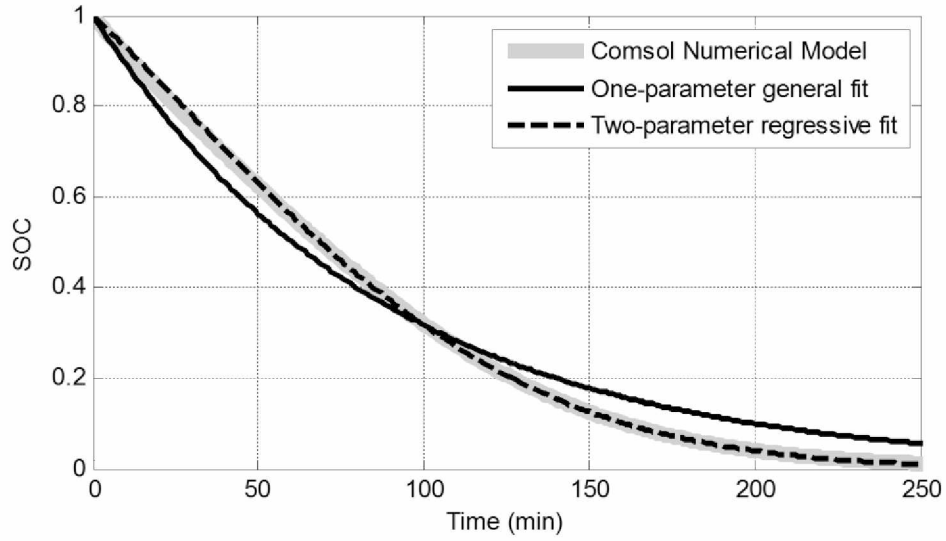

Figure 3.8. Improvement in fit using two-parameter regression (u = 2 m/s).

Analysis of the two-parameter model for all simulations indicates that the b parameter is a strong function of u/H. However, a may range from -10^{-8} to $+5\text{x}10^{-8}$ with little correlation to u, H,

or α. It is therefore recommended that the single time constant model be used for economic feasibility studies and general system performance analyses when high precision accuracy is not necessary to capture the desired behavior characteristics.

3.5.3 Core Energy Balance

A comprehensive core energy balance (in rate form) can now be stated. The sensible energy (E) within the core is

$$E = \rho_c c_{p,c} \int (T_c - T_0) \cdot dV \tag{3.15}$$

where E has unis of energy (Joules) and depends on the density, specific heat, and temperature within the core volume.

Consider such an ETS core subject to two digital signals: the charge command (*cc*) and discharge command (*dc*). When one of these values is zero, no energy transfer occurs in its respective mode. For example, if *dc=0*, the core is not discharging because the thermostat does not demand heat. A generalized energy balance of the ETS core presented herein can then be expressed as

$$\dot{E} = (\dot{Q}_{chrg}) \cdot cc(t) - (\dot{Q}_{dischrg}) \cdot dc(t) - \dot{Q}_{loss} \tag{3.16}$$

In rate form, the storage term ($\dot{E}$) is the sum of the charge (positive), discharge (negative), and loss terms. The charge rate (first term) is a function of only the charge command (*cc*) and the charge power ($\dot{Q}_{chrg}$). The charging heat flux should be within or around the 2660 W/m^2 used in this study in order to observe the lumped capacitance assumption.

The controlled discharge rate (middle term) is the product of the discharge command (*dc*) and the forced discharge rate (time derivative of equation 3.7), expressed in *W*.

$$-\dot{Q}_{dischrg} = \frac{d}{dt}\left(E_0 e^{\frac{-(t-t_0)}{\tau}} \right) = \frac{-E_0}{\tau} e^{\frac{-(t-t_0)}{\tau}} \tag{3.17}$$

The time constant (τ) can be obtained from equations (3.10-13). The value of E_0 becomes the current sensible energy of the core whenever a discharge event initiates (at t_0).

The uncontrolled discharge (loss) term in equation (3.16) is a function of the insulation and stove body around the core,

$$\dot{Q}_{loss} = h_{stove} A \left(T_w - T_\infty \right) \tag{3.18}$$

where A is the heat transfer surface area, T_w is the wall temperature of the core, and h_{stove} is a heat transfer coefficient for the entire stove, determined empirically.

3.5.4 Stove Modeling

Equation (3.16) can be used to model the charge and discharge cycles of an ETS core given the digital input signals and time constant. Mass and volume calculations can be made using either a representative stove simulation region (as in this paper) or using the entire core, as long as consistency is maintained. The model is compatible with changing room air temperatures, within reasonable proximity to 20°C, as would be seen with set-back thermostats. Colder room temperatures would tend to cause higher air mass flow rates in the channels and consequently increase the discharge rate.

Some ETS devices may use a variable speed forced air blower for air circulation throughout the core. This changes the bulk air velocity in the channels and alters the time constant. Such an effect would not change the values of *dc* and *cc*, which remain binary.

A final consideration in modeling an entire electric thermal stove is air mixing in the outlet manifold. With some designs, such as the Steffes 2102, a small fraction of the forced air is directed

through the core, with the majority being used to moderate the outlet temperature. (It is unsafe to allow 900K air to be released directly into a residence.) As such, the actual air flow rate *through the core* must be used in the calculation of the core's time constant.

3.6 Conclusions

A numerical model of a typical room size ETS heater core was developed and used to study the effects of material, core geometry, air flow rate (and velocity profile), and thermal gradients on discharge rate. Bulk air velocity, core dimensions, and material properties were shown to have the strongest effect on the discharge curve, which can be approximated by a simple exponential time constant and improved with a second parameter fit. Time constants were calculated for a wide range of parameters and summarized against a single non-dimensional modified Graetz number. It was shown that the SOC of a typical ETS heater core is only a function of its initial SOC (SOC_0) and the core time constant (τ). Heat gradients and air velocity profiles were shown to have a negligible impact. An energy balance equation was given in terms of the findings within the present study.

The information within this study can be put to practical use in the development of economic case studies for ETS applications in cold climates.

3.7 Acknowledgement

The authors would like to thank Dylan Cutler at the National Renewable Energy Laboratory for his thorough review of and helpful feedback on this manuscript. An additional thanks to Dennis Meiners at Intelligent Energy Systems for his support of our ETS research.

3.8 Funding

This work is supported by the U.S. Department of Energy (DOE), Office of Science, Basic Energy Sciences, under Award # DE-SC0004903.

3.9 Nomenclature

A	Heat transfer surface area
a	First coefficient for two-parameter fit
b	Second coefficient for two-parameter fit
Bi	Biot number
c_p	Specific heat
cc	Charge command (digital)
D_H	Hydraulic diameter
dc	Discharge command (digital)
E	Energy content of core
Gz*	Modified Graetz number
H	Height of simulation region
h	Convective heat transfer coefficient
k	Thermal conductivity
L	Characteristic length
m	Mass of simulation region
Pr	Prandtl number
$\dot{Q}$	Heat flux

Re	Reynolds number
SD	Storage Disparity
SOC	State of Charge
T	Temperature
T_0	Lowest potential core temperature
T_∞	Room air temperature
T_h	High temperature limit of core
T_{max}	Highest temperature in the core
T_{min}	Lowest temperature in the core
T_w	Wall temperature of core
t	Time
u	Bulk air velocity in channel
V	Volume
γ	Ratio of specific heats
ν	Fluid dynamic viscosity
ρ	Density
τ	Time constant

3.10 References

[1] Callaway, D. S. "Tapping the energy storage potential in electric loads to deliver load following and regulation, with application to wind energy." *Energy Conversion and Management* 50.5 (2009): 1389-1400.

[2] Steffes Corporation. (2015). *Owner's and Installer's Manual for Room Heating Units*. Retrieved from http://www.steffes.com/LiteratureRetrieve.aspx?ID=28566

[3] Hughes, L. "Meeting residential space heating demand with wind-generated electricity." *Renewable Energy* 35.8 (2010): 1765-1772.

[4] Johnson, C., J. Manwell, U. Abdulwahid, and A. Rogers. "Design and modelling of Dispatchable Heat storage in Remote Wind-Diesel Systems." *Renewable Energy Research Laboratory, Dept. of Mechanical and Industrial Engineering, University of Massachusetts, Amherst, MA* 1003 (2002).

[5] Hughes, L. "The technical potential for off-peak electricity to serve as backup in wind-electric thermal storage systems." *International Journal of Green Energy* 7.2 (2010): 181-193.

[6] Bedouani, B. Y. et al. "Central electric thermal storage (ETS) feasibility for residential applications: Part 1. Numerical and experimental study." *International Journal of Energy Research* 25.1 (2001): 53-72.

[7] Sateriale, M. E. "Modeling and analysis of masonry electro-thermal heating and storage for optimal integration with remote stand-alone wind-diesel systems." Master of Science Thesis, University of Alaska-Fairbanks, 2013.

[8] Roberge, M. A. et al. "Model of room storage heater and system identification using neural networks." *Proceedings of CLIMA Conference* Volume 265 (1997).

[9] Nellis, G. and S. Klein. *Heat Transfer*. Cambridge University Press. (2009): 663.

Chapter 4. Development of a Full-Scale-Lab-Validated Dynamic Simulink® Model for a Stand-Alone Wind-Powered Microgrid[2]

4.1 Abstract

Isolated hybrid wind microgrids operate within three distinct modes, depending on the wind resources and the consumer grid demand: diesel-only (DO), wind-diesel (WD) and wind-only (WO). Few successful systems have been shown to consistently and smoothly transition between wind-diesel and wind-only modes. The University of Alaska – Fairbanks Alaska Center for Energy and Power (ACEP) has constructed a full scale test bed of such a system in order to evaluate technologies that facilitate this transition. The test bed is similar in design to the NREL Power Systems Integration Laboratory (PSIL) and sized to represent a typical off-grid community. The objective of the present work is to model the ACEP test bed in DO and WD modes using MATLAB® SIMULINK® and then validate the model with actual full-scale laboratory measurements. As will be shown, the frequency responses are grouped into three classifications based on their behavior. The model is shown to be successful in describing the frequency response of relatively small (0.15 per unit) steps in load. Modifications to the excitation system model are discussed which could improve the accuracy for larger steps in load. The ACEP test bed and associated SIMULINK® model are to be used in future work to support investigating WO operation.

---

[2] Janssen, N.T., R.A. Peterson, and R.W. Wies. "Development of a Full-Scale-Lab-Validated Dynamic Simulink® Model for a Stand-Alone Wind-Powered Microgrid." *ASME 2014 Power Conference*. American Society of Mechanical Engineers, 2014. Funding provided by the U.S. Department of Energy, Office of Science, Basic Energy Sciences, under Award # DE-SC0004903.

4.2 Introduction

Many remote communities in the world generate electricity from a central plant powered by diesel electric generators (DEGs). These communities rely on expensive diesel fuel to power their grid. Rising fuel costs are rendering this approach financially unsustainable for many of these communities, which are now looking to use renewable resources, such as wind, to offset these costs. [1]

An islanded microgrid that uses a combination of diesel-electric generation and wind power in order to meet the electrical demand of the consumer is considered a Hybrid Wind Diesel (HWD) system [2]. A HWD system consists of at least one DEG, one or more Wind Turbine Generators (WTGs), and a dynamic consumer load. The system may also make use of an energy storage device (such as a lead-acid battery) and/or dump load. As the ratio of grid demand to wind power approaches unity, the need to dump excess energy to a secondary load becomes necessary

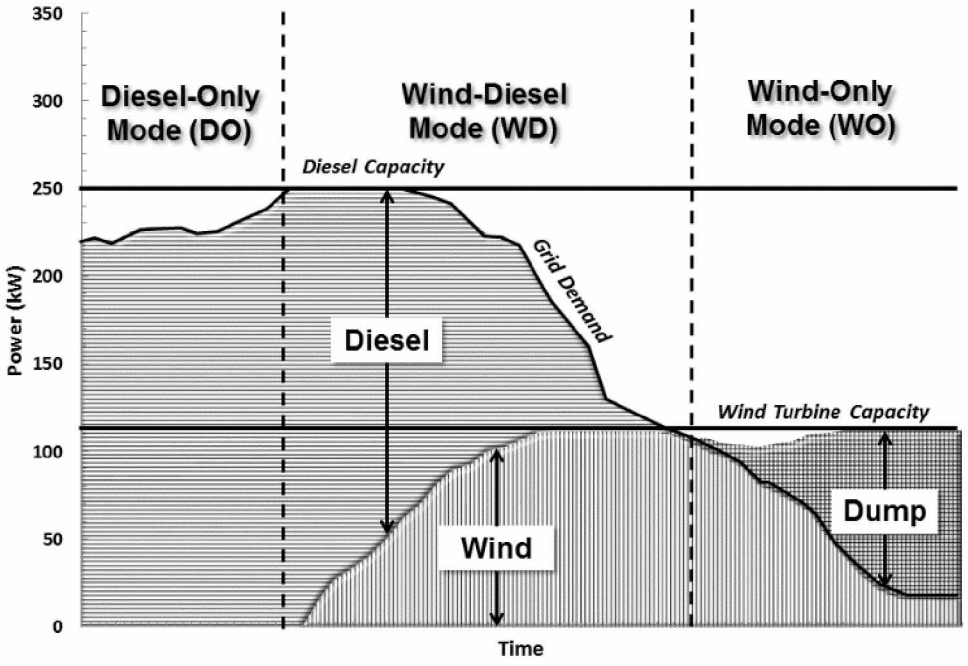

Figure 4.1. Energy balance of ACEP Hybrid Technologies Test Lab.

in order to avoid motoring the diesel engine. If the DEG can be successfully decoupled from the grid (mechanically or electrically) the system is classified as "high penetration" (or more recently "high contribution").

High contribution hybrid wind diesel systems (HCHWD) present many control challenges not encountered in larger, more stable electric grids [3]. With no source of base load generation or spinning reserve, the only way to achieve an instantaneous balance of real power generation and consumption with a varying source of wind power is for a secondary load controller to divert energy to a sink. The sink may either be a storage device or a dump load. Furthermore, when the DEG is decoupled from the system, a source of reactive power must be present to excite the WTG(s) and any reactive component of the consumer load.

Existing scientific literature has made some good effort in modeling the dynamics of a HWD system [4-7]. Neither lab nor field validation measurements were presented in [4] nor [5]. Tomilson et al [6] achieved a reasonable frequency response match with their test bed in DO mode, with no WD results presented. Jeffries [7] developed and validated a non-dimensional model with excellent agreement in both WD and DO modes (1994). However, DEG technology has changed much since the publication of both of these studies.

Furthermore, many publications have since been made that utilize some form of these typical SIMULINK® models [8-13] as a basis for their analysis. These models remain un-validated against the dynamics of full-scale modern hybrid systems, such as ACEP's PSIL.

ACEP has a full-scale hybrid wind diesel test bed (see Figure 4.2) that consists of a 320 kVA diesel electric generator (DEG), an 8-bit 250 kW resistive/inductive load bank, and a 150 HP induction machine driven by a motor/VFD, which represents a WTG. (The test bed also has a 1000

amp-hour lead-acid battery bank and inverter. However, these components were not used in the scope of the present research.)

Figure 4.2. ACEP's Power Systems Integration Lab (Photo Todd Paris).

The goal of the present work is to model the transient response of the ACEP HWD test bed in wind-diesel (WD) and diesel-only (DO) modes and compare the results with laboratory measurements. Future plans include the integration of storage technologies with the intent of exploring wind-only (WO) mode.

4.3 Mathematical Model

The key components of the ACEP test bed can be seen in the MATLAB® SIMULINK® block diagram shown in Figure 4.3. They are connected via a common 480V AC bus with voltage, current, real power, and reactive power measurement blocks. For simulations, the load bank model is replaced with a switchable load and breaker so as to introduce step load disturbances to the

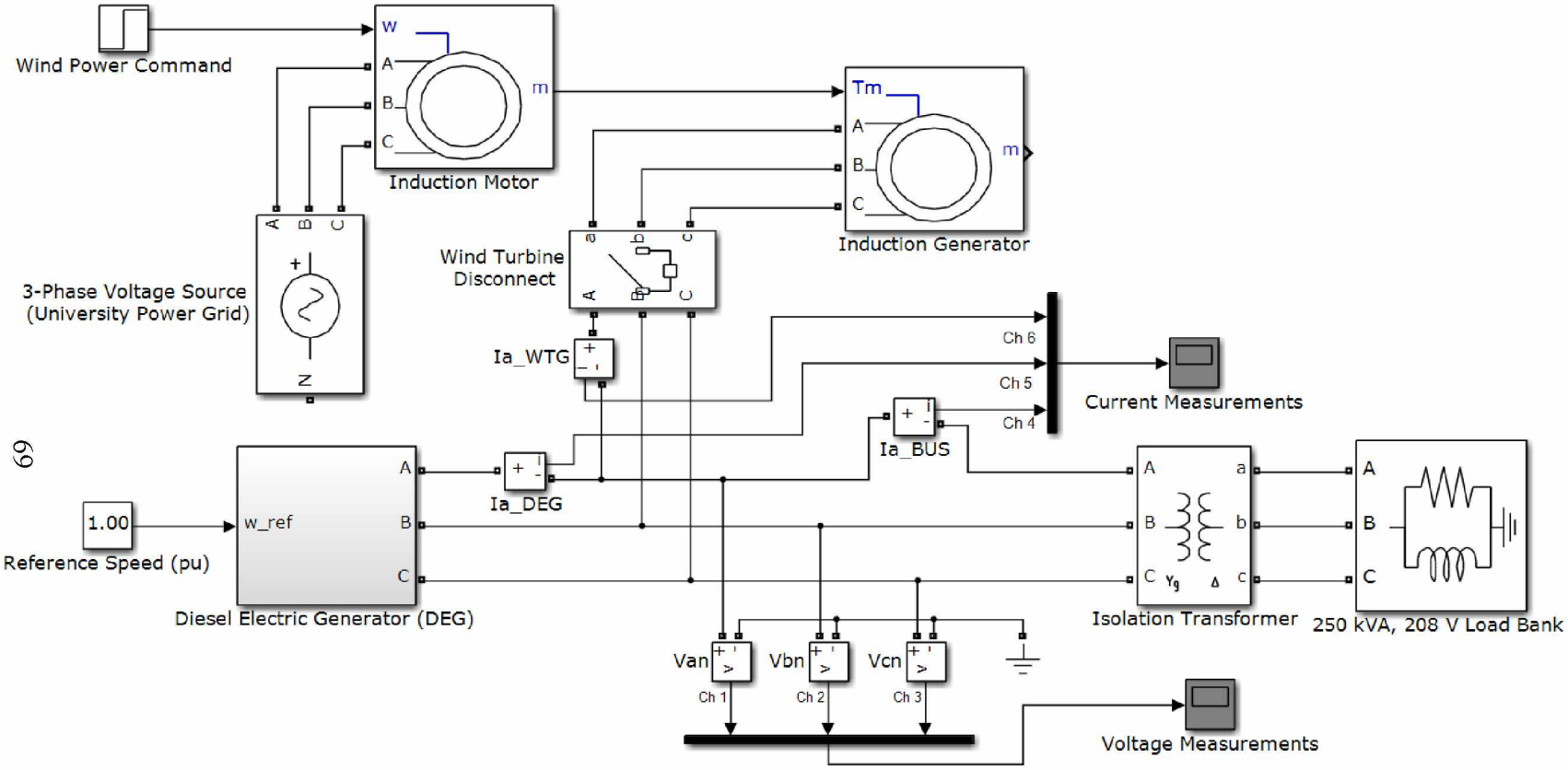

Figure 4.3. Laboratory test setup.

system. Simulating DO and WD modes requires a mathematical model be defined for four major system components: the diesel engine (DE) and speed governor, the synchronous generator (SG), the SG excitation system, and the induction generator (IG). The load is modeled as a constant-impedance with an ideal three-phase switch for load changes.

4.3.1 Diesel Engine/Governor Model

The DE and electronic speed governor block diagrams are typical of those found in the literature (see Figure 4.4) [4-15]. The PID type speed controller integrates the error in shaft angular velocity and forwards the resulting signal to the second-order actuator model introduced by Yeager et al [15]. The engine model is a simple first order transport delay, which represents the mean time for all cylinders to fire and for the resulting torque to develop. Time constants and gains were selected based on the consensus in literature with alterations made after lab measurement validation.

The speed governor on the diesel (electrically-driven, electrically-actuated) has the function of keeping the synchronous machine rotating at a constant angular velocity. The speed of the drive shaft is directly proportional to the frequency of the generator and grid.

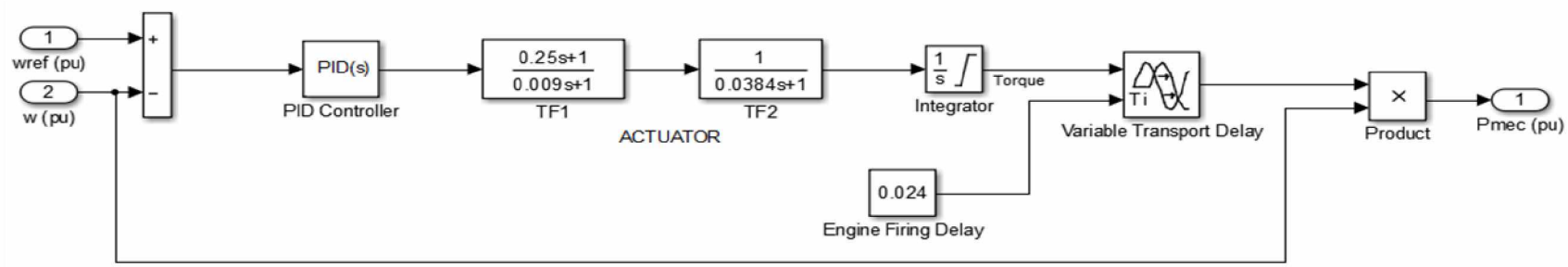

Figure 4.4. Block diagram of diesel engine and governor model.

4.3.2 Synchronous Generator Model

The synchronous generator model is available in the MATLAB® SIMULINK® SimPowerSystems™ toolbox and can be broken into two components: mechanical and electrical.

The mechanical portion of the synchronous generator model relates rotor speed (ω) to the inertial constant (H), mechanical torque (T_m), electrical torque (T_e), and damping/windage losses (F). This is an expression of the commonly used "swing equation".

$$\frac{d\omega}{dt} = \frac{1}{2H} \cdot (T_e - T_m - F\omega) \tag{4.1}$$

The electrical model of the wye-connected salient-pole synchronous machine is given in the two-axis 'dq' reference frame. Stator, rotor, and damper winding dynamics are represented (see Figure 4.5) in the equivalent circuit.

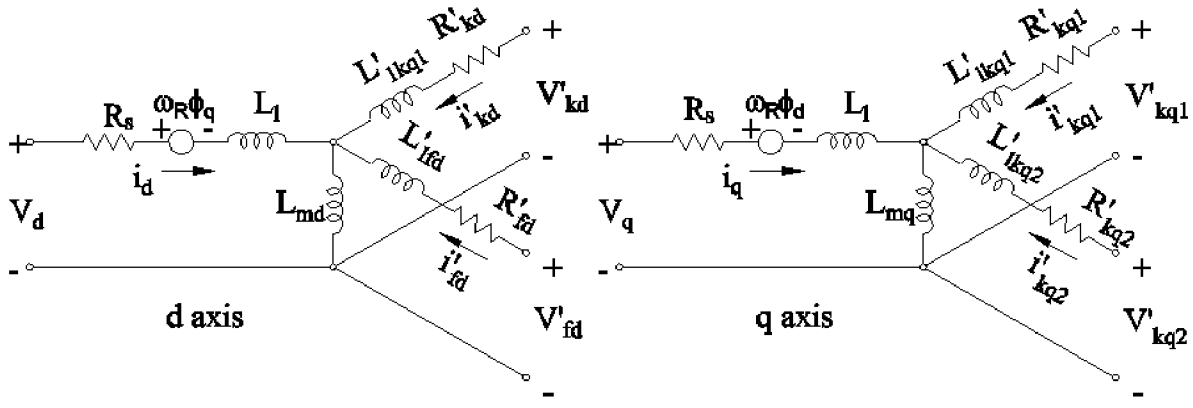

Figure 4.5. Synchronous machine equivalent circuit diagram [10].

4.3.3 Excitation System Model

The exciter (or "Automatic Voltage Regulator (AVR)") is responsible for controlling current to the rotor field windings, which directly affects the terminal voltage of the generator. The exciter on the ACEP test bed is of the AC brushless type.

The MATLAB® SIMULINK® exciter block models a DC type exciter, as described in [17] (see Figure 4.6). The terminal voltage error is fed through a main regulator with a proportional gain and time constant. A small amount of damping is fed back into the primary summing junction. The resulting DC field voltage sets up an opposing magnetic field between the rotor and stator. Limits are often imposed on the level of excitation in order to protect the machine's armature windings from overheating.

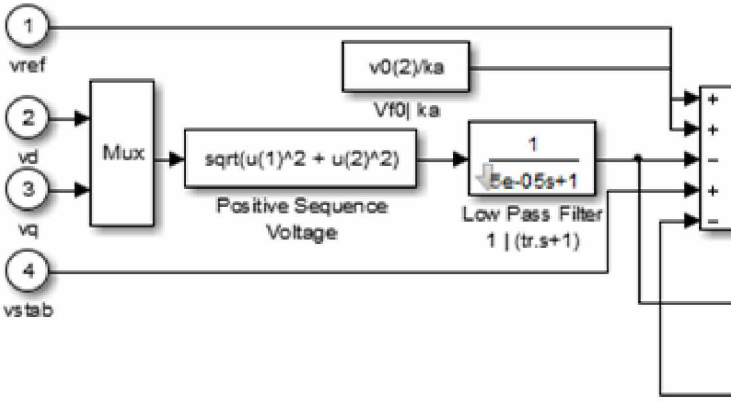

Figure 4.6. Block diagram of excitation system model.

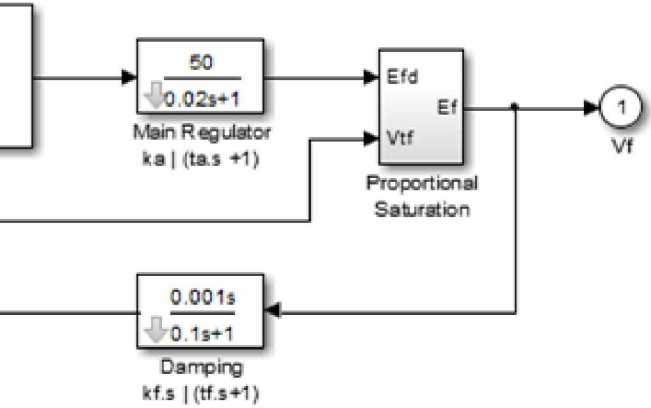
50
0.02s+1
Main Regulator
ka | (ta.s +1)
Efd
Ef
Vtf
Proportional
Saturation
1
Vf
0.001s
0.1s+1
Damping
kf.s | (tf.s+1)

4.3.4 Induction Generator Model

The induction generator, which represents the WTG, is a three-phase AC squirrel-cage machine and is modelled in MATLAB® SIMULINK® SimPowerSystems™ as follows.

The mechanical model of the squirrel cage IG is exactly the same as that of the SG (see Eq. 4.1). (It should be noted that the ACEP test bed does not have a wind turbine on the rotor of the IG. The total inertia under consideration in the mechanical model is therefore limited to the sum of the IG and drive motor rotor inertias.)

The electrical model of the three-phase, 60 Hz, wye-connected, squirrel cage IG varies from that of the SG previously presented (see Figure 4.7). The two-axis 'dq' reference frame is used; however, the field windings are excited internally by slip between the rotating magnetic field and the rotor angular velocities [16]. The following equation relates magnetic flux ϕ, stator current i, and number of pole pairs p, to electrical torque T_e.

$$T_e = \frac{3}{2} p \cdot \left(\phi_{ds} i_{qs} - \phi_{qs} i_{ds} \right) \tag{4.2}$$

The dq axis fluxes and induced stator currents are calculated by solution of the equivalent circuit (Figure 4.7). These equations are presented in further detail by Krause [16].

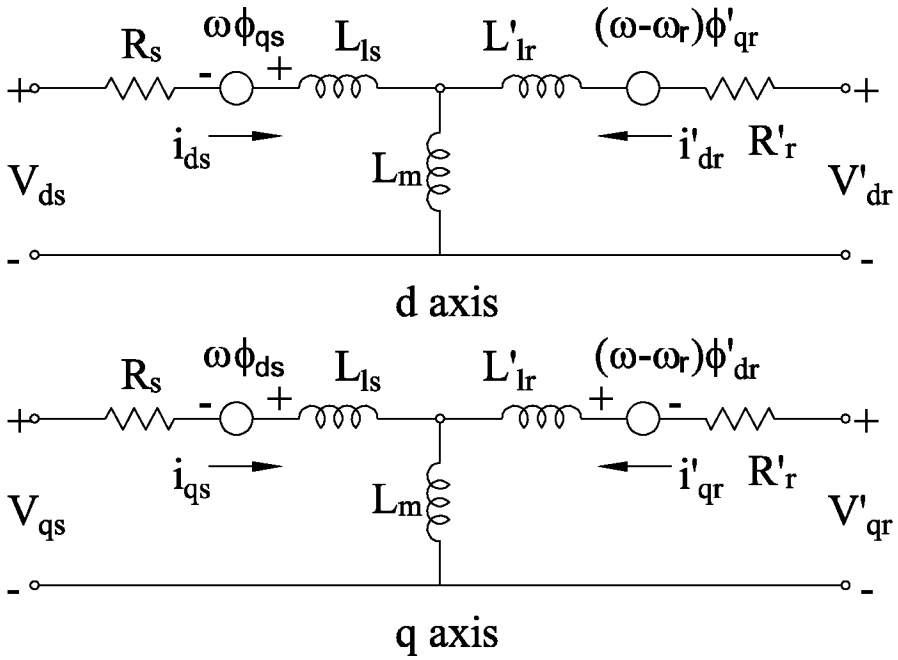

Figure 4.7. Induction generator equivalent circuit diagram [10].

4.4 Data Collection

All three phases of instantaneous bus voltage (V_{an}, V_{bn}, and V_{cn}) were measured as well as the phase 'a' line currents of the DEG, the WTG, and the load (see Figure 4.3). Lab measurements were performed on the ACEP HWD test bed in order to verify the mathematical model developed herein. The brief 3-4 second transient periods following various system disturbances were recorded and compared to model predictions. Of primary interest were frequency and voltage, though current probes were used in conjunction with high voltage differential probes in order to measure real power (P) and reactive power (Q). Signals were routed to a National Instruments (NI) PCI-6221 DAQ card and LabView data collection interface fixed to record at 6000 samples per second.

4.5 Results

4.5.1 Data Processing

Measured instantaneous voltages and currents were used to calculate RMS voltages, RMS line currents, frequency (f), power factor (PF), real power (P), reactive power (Q), and impedance (Z). Frequency and power factor calculations were made by interpolating zero-crossings of the phase voltage and line current waveforms. This allowed the mechanical response of the machine's angular velocity (ω) to be presented on a time scale, throughout the duration of the transient. RMS values were calculated with a sliding window of 600 data points (0.10 sec, or about 6 cycles).

4.5.2 Diesel Only (DO) Mode – Laboratory Results

In DO mode, the WTG is electrically isolated from the system and the DEG takes 100% of the dynamic consumer load. Load steps of various magnitudes were performed at multiple power factors (PF) as well as at various DEG loading levels.

Initial observations show three distinct responses whose shapes depend primarily on the size of the load step (see Figure 4.8). Large steps (0.80 per unit) up or down (Figures 4.8a and 4.8d) in load and medium steps (0.40 per unit) down (Figure 4.8e) in load result in "type 1" responses, which exhibit a linear recovery region before settling out to steady state. Medium steps (about 0.40 per unit) up in load (Figure 4.8b) result in a distinct shape that oscillates essentially undamped at a frequency of about 2.3 Hz for no more than 3 seconds before sharply attenuating (type 2). Smaller steps (0.15 per unit) result in small, single oscillations, termed here as "type 3" responses (Figures 4.8c and 4.8f). Good repeatability was observed in replicated experiments.

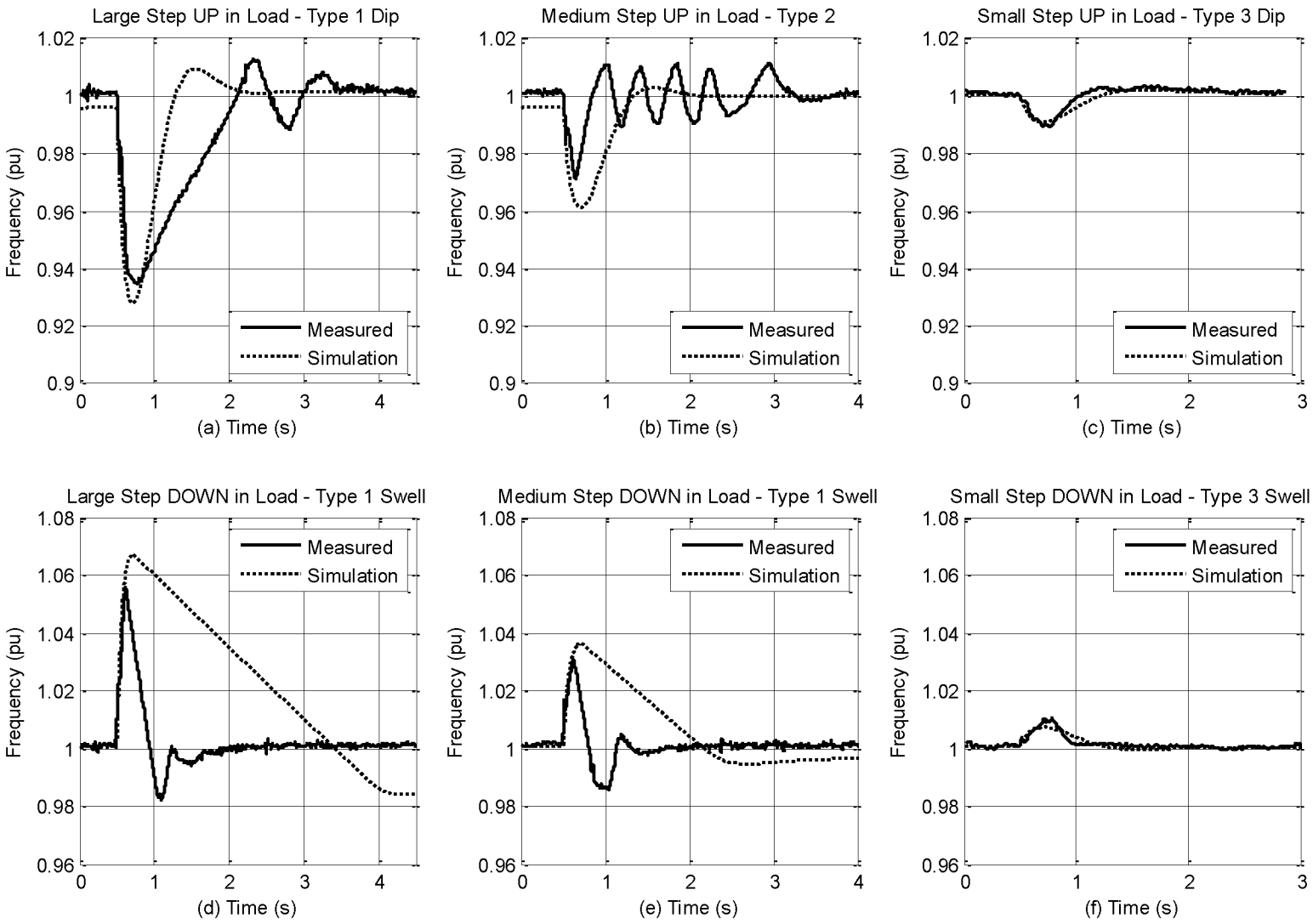

Figure 4.8. DO mode laboratory and simulation response characteristics.

4.5.3 Diesel Only (DO) Mode – Simulation Results

Model parameters were chosen to provide the best results over the range of inputs tested without significant deviation from nominal values. The results of the computer simulation are shown concurrently with their respective measured data from the laboratory experiment (Figures 4.8-13).

The simulation results of type 1 and 2 perturbations differ in shape significantly from those measured on the test bed. However, the magnitudes of the frequency excursions in the simulation are in error by no more than 1.1%. The model also significantly overestimates the settling time for medium to large steps down in load. Small (type 3) steps appear to be well predicted by the model.

Figures 4.9 and 4.10 show a collection of type 3 responses (steps of about 0.15 per unit) of the system in diesel-only mode. Good agreement with measured results is seen under moderate to heavy load across a range of power factors. Frequency deviations under low load are over-predicted by the model, but have the same general shape.

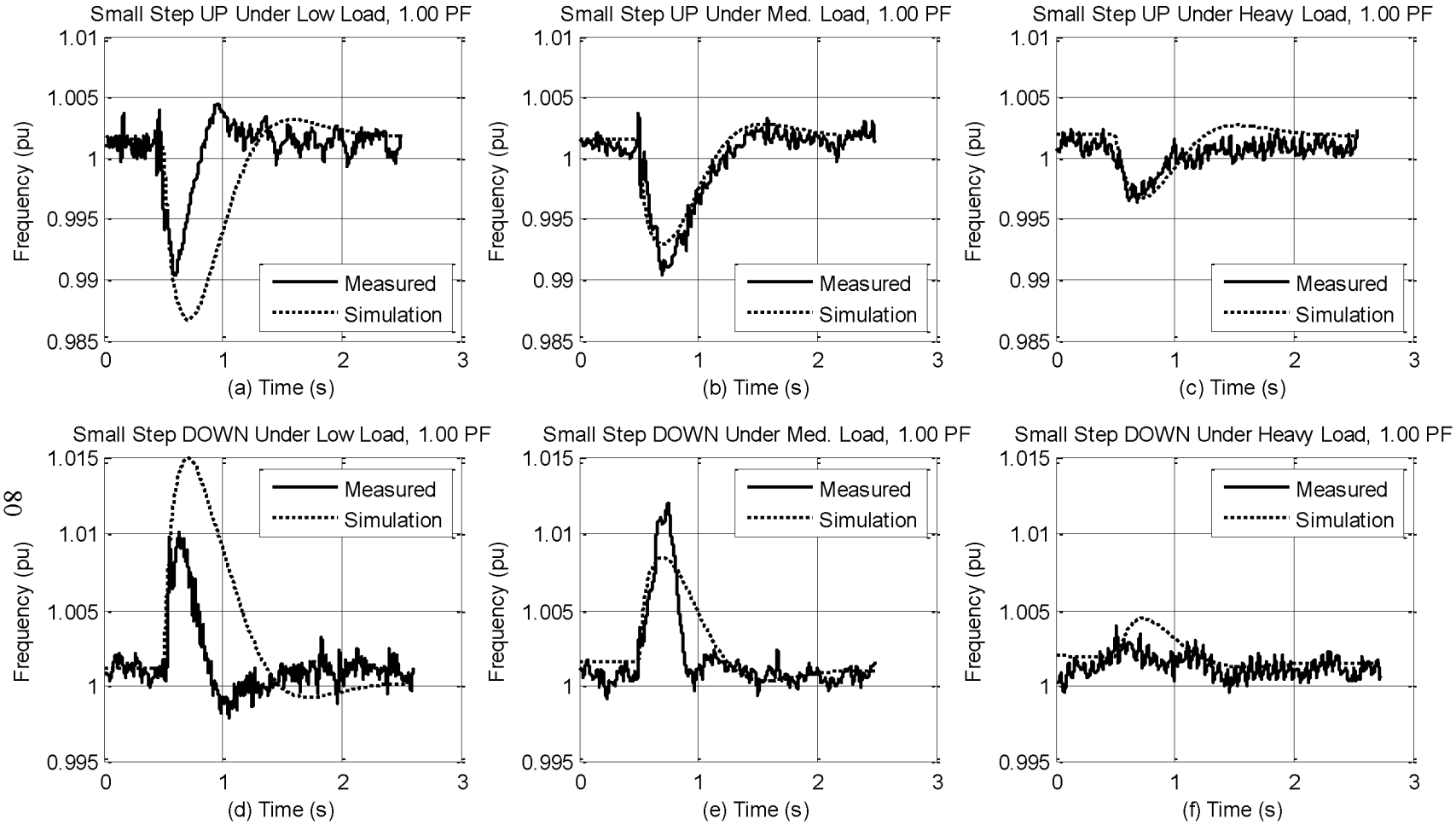

Figure 4.9. DO mode laboratory and simulation response characteristics, unity power factor.

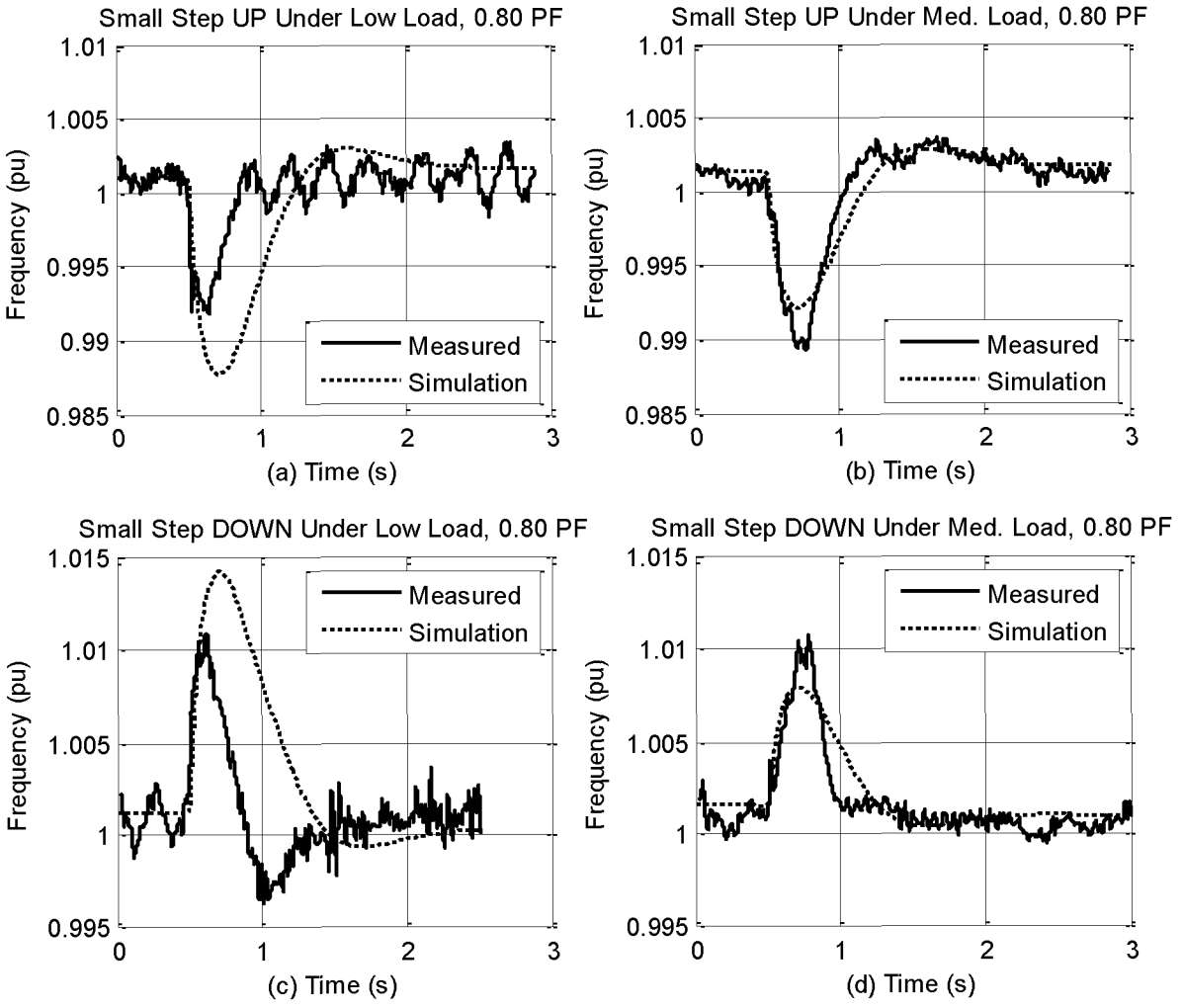

Figure 4.10. DO mode laboratory and simulation response characteristics, 0.80 lagging power factor. (Heavy load not tested.)

4.5.4 Wind-Diesel (WD) Mode

In WD mode, the IG is brought up to synchronous speed and electrically connected to the bus. The first set of design points were taken with the IG connected but under no drive motor torque (see Figure 4.11) in order to simulate light wind. Then, with the IG connected and under torque from the drive motor, two cases were considered: steps in load under constant wind power (Figure 4.12) and steps in wind power under constant load (Figure 4.13). General observations of model accuracy indicate good results at higher levels of DEG loading and with smaller perturbations.

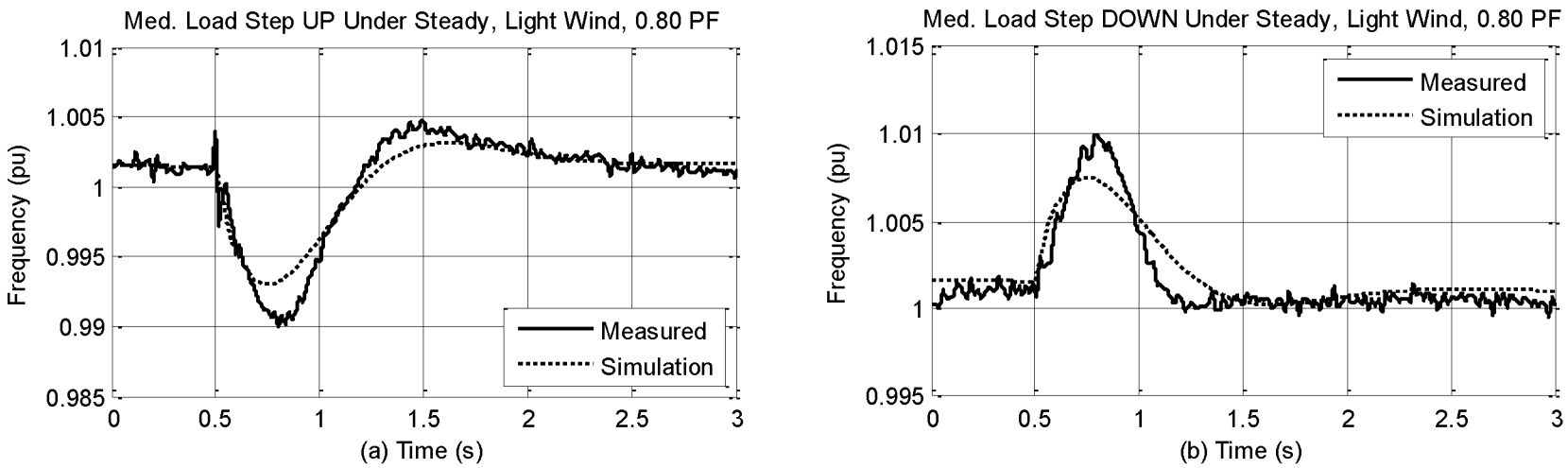

Figure 4.11. WD mode laboratory and simulation results. IM connected, but under no drive torque.

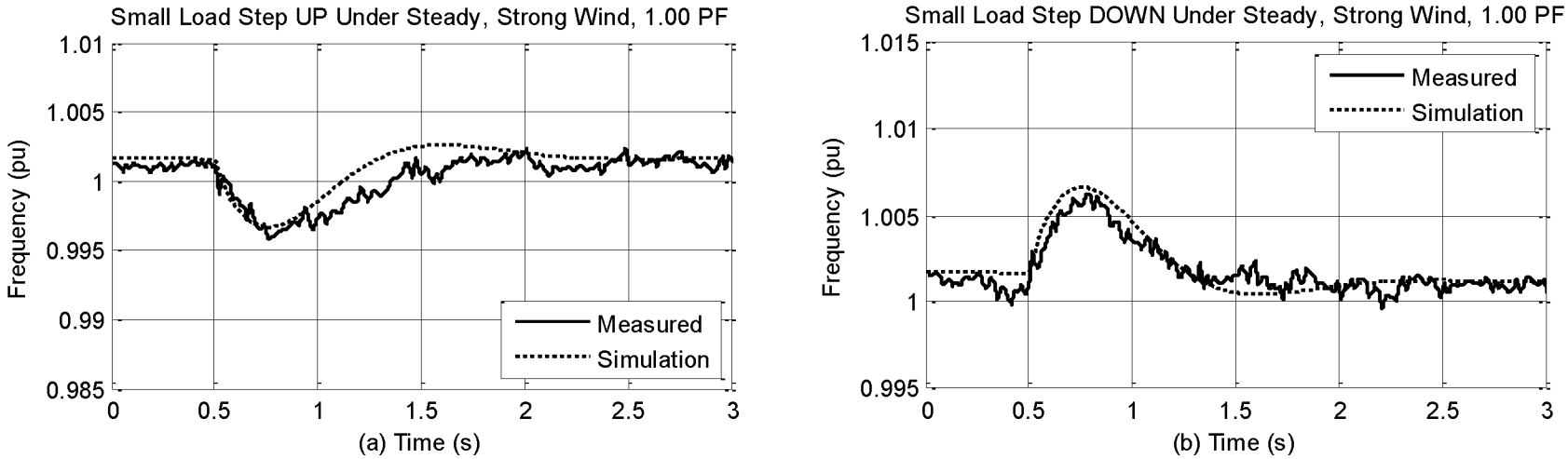

Figure 4.12. WD mode laboratory and simulation results. IM connected steady drive torque (strong wind).

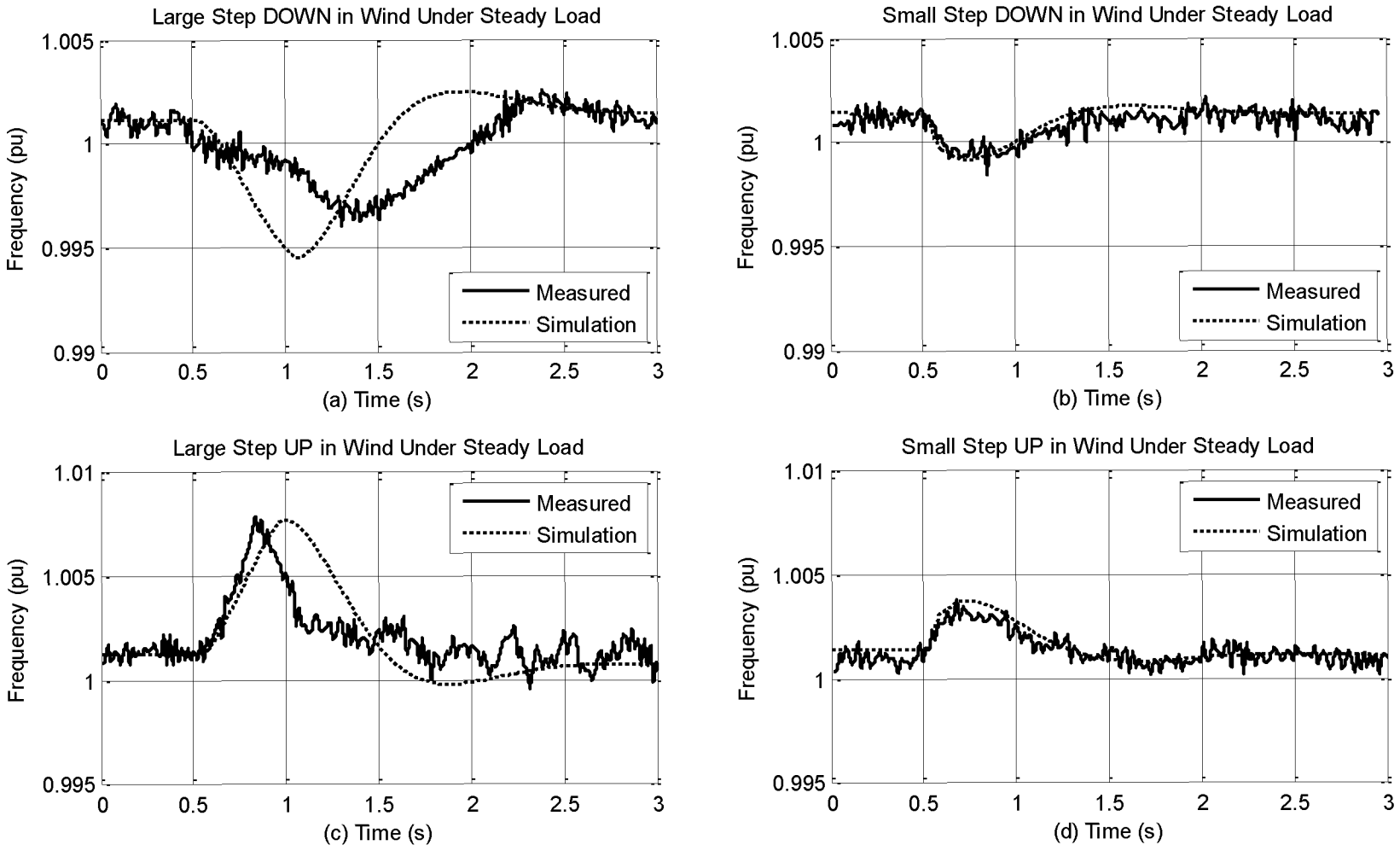

Figure 4.13. WD mode laboratory and simulation results. Steady 0.80 PF lagging load, steps in wind power.

4.6 Conclusions

Mathematical models of the major components of a HCHWD system were developed and compared with full-scale laboratory measurements in DO and WD modes. Three distinct frequency response shapes were observed based on the magnitude and direction of the disturbance in consumer load. The mathematical model gives good results at moderate to high levels of DEG loading and relatively small disturbances.

The results presented herein represent the best arrangement of the numerous machine parameters needed to fully define the model. It is clear that significant improvements need to be made to the structure of the model in some places, depending on its intended end-use.

1. The DEG speed controller may use adaptive tuning in order to set the P, I, and D gains on-the-fly.
2. The model of the AVR presented here is highly simplified.

Implementation of a "discontinuous" type exciter as described in [17] may improve the accuracy of the model. This type of AVR deliberately boosts the level of excitation current immediately following a system fault. This has the effect of increasing terminal voltage and air gap power, which assist in deceleration of the unit. However, it is beyond the scope of this research to reverse engineer the specific DEG controller and AVR design used by the equipment in the test laboratory.

4.7 Future work

In order to develop a reliable means of transitioning into WO mode, additional technologies will need to be investigated. ACEP is currently in the process of procuring a power electronic rectifier/inverter capable of fulfilling the role of frequency and voltage regulator in WO mode.

Integration of this inverter into the ACEP HWD test bed is planned for 2014. Further advancement of the model presented herein may be of value to this initiative, but would require knowledge of the proprietary software within the DEG's digital AVR.

4.8 Acknowledgements

This work is supported by the U.S. Department of Energy, Office of Science, Basic Energy Sciences, under Award # DE-SC0004903.

The authors would like to thank the following individuals for the integral part they played in collection of data and interaction with the ACEP HWD test bed.

Marc Mueller-Stoffels, PhD
Research Assistant Professor
Power Systems Integration Program Director
Alaska Center for Energy and Power
Institute of Northern Engineering
University of Alaska Fairbanks

David Light
Research Engineer
Alaska Center for Energy and Power
Institute of Northern Engineering
University of Alaska Fairbanks

4.9 References

[1] Isherwood, W. et al. "Remote power systems with advanced storage technologies for Alaskan villages." *Energy* 25.10 (2000): 1005-1020.

[2] Vandoorn, T. L., B. Renders, L. Degroote, B. Meersman, and L. Vandevelde. "Active Load Control in Islanded Microgrids Based on the Grid Voltage." *IEEE Transactions on Smart Grid* 2.1 (2011).

[3] Hunter, R. and G. Elliot. *Wind-Diesel Systems – A Guide to the Technology and Its Implementation.* Cambridge University Press, Cambridge (UK) (1994).

[4] Stavrakakis, G. S. and G. N. Kariniotakis. "A General Simulation Algorithm for the Accurate Assessment of Isolated Diesel-Wind Turbines Systems Interaction." *IEEE Transactions on Energy Conversion* 10.3 (1995): 577-583.

[5] Sebastián, R. "Smooth transition from wind only to wind diesel mode in an autonomous wind diesel system with a battery-based energy storage system." *Renewable Energy* 33.3 (2008): 454-466.

[6] Tomilson, A., J. Quaicoe, R. Gosine, M. Hinchey, and N. Bose. "Modelling an Autonomous Wind-Diesel System Using Simulink. " *IEEE 1997 Canadian Conference on Engineering Innovation*. Voyage of Discovery 1 (1997): 35-38.

[7] Jeffries, W. Q. "Analysis and modeling of wind/diesel systems without storage" (1994). Doctoral Dissertations Available from Proquest. AAI9510487. http://scholarworks.umass.edu/dissertations/AAI9510487

[8] Ibrahim, H., J. Lefebvre, J. F Methot, and J. S. Deschenes. "No-storage wind-diesel system: Mechanical modeling based on power flow models." *IEEE 2011 Electrical Power and Energy Conference (EPEC 2011)*. IEEE, 2011.

[9] Sedaghat, B., A. Jalilvand, and R. Noroozian. "Design of a multilevel control strategy for integration of stand-alone wind/diesel system." *International Journal of Electrical Power & Energy Systems* 35.1 (2012): 123-137.

[10] Rezkallah, M., Chandra, A., and Singh, B., "Three-leg four-wire voltage source inverters for hybrid standalone system feeding unbalanced load." *2013 IEEE Annual Conference of the Industrial Electronics Society (IECON 2013)*. IEEE, 2013.

[11] Sebastian, R., R. Pena-Alzola, and J. Quesada. "Peak shaving simulation in a wind diesel power system with battery energy storage." *2013 IEEE Annual Conference of the Industrial Electronics Society (IECON 2013)*. IEEE, 2013.

[12] Kassem, A. M., A. M. Yousef. "Voltage and frequency control of an autonomous hybrid generation system based on linear model predictive control." *Sustainable Energy Technologies and Assessments* 4 (2013): 52-61.

[13] Wies, R. W., E. Chukkapalli, and M. Mueller-Stoffels. "Improved Frequency Regulation in Mini-Grids with High Wind Contribution using Online Genetic

Algorithm for PID Tuning." *2014 IEEE Power and Energy Society General Meeting (IEEE PES 2014)*. IEEE, 2014.

[14] Luo, L., L. Gao, H. Fu. "The Control and Modeling of Diesel Generator Set in Electric Propulsion Ship." *International Journal of Information Technology and Computer Science (IJITCS)* 3.2 (2011): 31-37.

[15] Yeager, K. E and J. R. Willis. "Modeling of Emergency Diesel Generator in an 800 MW Nuclear Power Plant." *IEEE Transactions on Energy Conversion* 8.3 (1993).

[16] Krause, P. C., O. Wasynczuk, and S. D. Sudhoff. *Analysis of Electric Machinery and Drive Systems*. IEEE Press (2003): 109-190.

[17] "Recommended Practice for Excitation System Models for Power System Stability Studies." IEEE Standard 421.5 (1992).

Chapter 5. Frequency Regulation by Distributed Secondary Loads on Islanded Wind-Powered Microgrids[3]

5.1 Abstract

Frequency regulation is critical to the successful operation of remote wind-diesel electrical grids. When the grid is in 'wind-diesel' mode, frequency regulation is (classically) the sole duty of the diesel electric generator (DEG). An alternative approach is proposed whereby responsibility for frequency regulation is shared by the DEG and a network of autonomous distributed secondary loads (DSLs) consisting of electric thermal storage (ETS) devices. This allows surplus wind to be distributed to residential consumers (as space heat) without the need for a centralized communication network. Numerical modeling of system dynamics with active DSLs is conducted using a SIMULINK® wind-diesel hybrid test bed model. The effects of controller gain, installed capacity, switching time and unit coordination timing on frequency and voltage regulation is explored. It is shown that the DSLs can improve frequency regulation in wind-diesel mode while providing storable thermal energy to distributed consumers.

Index Terms

Diesel driven generators, Load management, Frequency control, Power system dynamic stability, Wind energy

5.2 Introduction

Providing clean, reliable, and cost-effective electricity to isolated communities is a current power industry challenge. Without a substantial network of generation and transmission systems,

[3] Janssen, N.T., R.W. Wies, and R.A. Peterson. "Frequency regulation by distributed secondary loads on islanded wind-powered microgrids." *IEEE Transactions on Sustainable Energy* 7.3 (2016): 1028-1035. Funding provided by the U.S. Department of Energy, Office of Science, Basic Energy Sciences, under Award # DE-SC0004903.

frequency regulation and stability become a demanding task [1,2]. This is especially true when additional energy sources, such as wind power, are combined with existing diesel generation. Systems that make use of both wind and diesel power called wind-diesel hybrid systems [3] are particularly susceptible to frequency regulation problems.

Controlling AC frequency in an electrical grid requires the establishment of an instantaneous balance of real power generation and consumption [4]. Transients in wind generation and dynamics in the consumer load disturb this balance and upset the angular velocity of the synchronous generator. This results in undesirable frequency and voltage transients.

Regulation of frequency in a wind-diesel hybrid system is specific to the mode of operation. Wind-diesel systems may operate in any of three distinct modes as illustrated in the example energy balance in Figure 5.1 [5]. If wind is not present, the consumer load is provided exclusively by the Diesel Electric Generator (DEG). This is considered *diesel only* mode. The responsibility for both frequency and voltage regulation are with the DEG (Table 5.1). The diesel engine governor ensures a constant angular velocity by making appropriate adjustments to the fuel rack position.

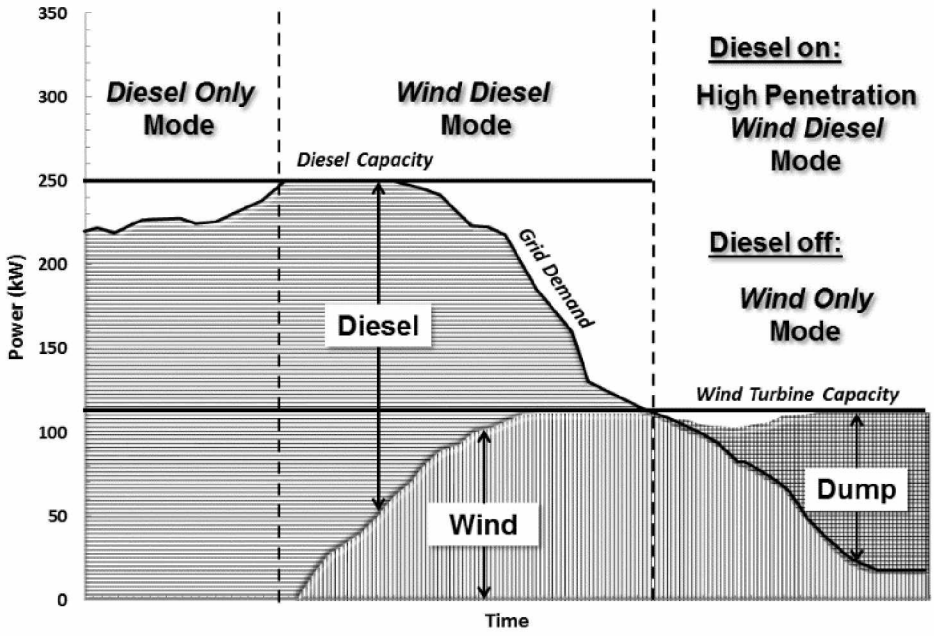

Figure. 5.1. Typical energy balance for a hybrid wind-diesel system [5].

Table 5.1. Control responsibilities for no-storage wind-diesel system.

Mode	*Frequency*	*Voltage*
Diesel only	DEG	DEG (AVR)
Wind-diesel	DEG*	DEG (AVR)
Wind only	Secondary Load	Varies

*Classically, this is the DEG. This paper proposes shared responsibility between the DEG and an autonomous distributed secondary load.

If wind turbines are connected and begin producing power, current will flow into the grid from both the DEG and the wind generator(s). The system is now in *wind-diesel* mode. In a classical system, the DEG regulates frequency and voltage, but its contribution is reduced. Wind generation may continue to increase to a point at which the DEG becomes scarcely loaded, or even motored (back-driven). This situation is to be avoided or the diesel will incur maintenance costs and/or reduced life [6]. Two options exist to prevent this. If wind generation approaches current

grid demand, either wind power can be trimmed using pitch control [7-8], or the additional power can be directed to a secondary load. (It is economically favorable to use this excess energy.) This is a special case of *wind-diesel* mode referred to as "high wind penetration" [9].

Finally, if instantaneous wind generation exceeds grid demand, it may be possible to disconnect the DEG and supply the entire load with wind power, as successfully demonstrated in [10]. Such a plant is said to be capable of *wind only* mode, which remains the highest level of technical complexity among wind-diesel hybrid systems. Depending on the situation, voltage control may be either conducted by the DEG's Automatic Voltage Regulator (AVR), a synchronous condenser, or some type of power electronic converter. Furthermore, frequency control can no longer be performed by the DEG. Thus, a switched secondary load and/or energy storage system must be employed as a power sink. Advanced storage technologies, such as flywheels [9] and battery banks [11], require a DC bus and are outside the scope of this study.

Secondary loads are a vital part of any high penetration no-storage wind-diesel system. Their purpose is to match power consumption with generation in order to ensure an instantaneous energy balance on the grid, thus regulating frequency. Secondary loads must be fast-switching, controlled, and ideally provide some benefit to the community. Use of an energy storage system (such as a battery) minimizes the loss of available work and has been shown to be economical in [12]. However, these systems are complex and often overwhelm the limited maintenance infrastructure of typical off-grid communities, resulting in continued use of the relatively reliable DEG. Electric boilers are useful secondary loads in cold climates (if a district heating loop can be directed to a proximate consumer) as demonstrated in [13], though the plant itself is often the sole benefactor of such a device. Many remote wind-powered plants use a fast-switching air-cooled load and wholly dispel otherwise usable energy, as in [14].

Electric thermal storage (ETS) devices are another useful application for excess wind energy [15-16]. ETS devices use resistive heating elements to charge a ceramic core or hydronic storage mass for subsequent thermostatic discharge. An array of ETS units placed in households as distributed secondary loads (DSLs) could provide clean, affordable, domestic space heat or hot water while playing a part in frequency regulation.

Such a network of DSLs would require some form of communication or alternative coordination method. Units must know when to activate or deactivate based on the needs of the grid. Either a microgrid central controller (MGCC) [17-19], or a dedicated distribution circuit centrally tied to the power plant, would be needed. For remote communities, either solution adds prohibitive cost and/or needless complexity.

So called "intelligent loads" have been proposed for frequency support on large grids in [20-22] whereby the idea of two-way communication between the load and the plant is abandoned. Loads instead react directly to changes in the grid frequency error. The concept is extended to microgrids in [23], though voltage error is used as an indicator of load deficit. The present work proposes a novel concept for coordination of distributed secondary loads in an islanded microgrid without the need for an MGCC or dedicated distribution circuit through the use of frequency-responding ETS devices.

This study provides the groundwork for a future vision of the isolated wind-powered microgrid in which secondary loads are distributed throughout the community, coordinated only by grid frequency error (without the need for a communication infrastructure). Two methods for simulating the collective electro-mechanical dynamics of such DSLs are proposed and tested in MATLAB® SIMULINK®. Frequency and voltage regulation are compared with that of a typical system solely under the control of the DEG. The focus of this study is on the responsibility for

frequency regulation shared by the distributed loads (ETS units) and the isochronous prime mover (DEG) at a low to moderate level of wind power penetration.

5.3 Mathematical Model

A dynamic MATLAB® SIMULINK® model of a wind-diesel hybrid system was used as developed in [5] and modified for accuracy. The self-sensing distributed ETS unit individual and collective network models are introduced here.

5.3.1 Wind-Diesel Hybrid System

The major components of the wind-diesel hybrid system model include the DEG, the wind turbine generator (WTG) and the load. An additional block representing the DSL was developed and added to the model. These components are connected via a common 480 Vac bus. A phasor solution at 60 Hz is calculated using the ode23tb solver.

The DEG model consists of three main subsystems: the diesel engine, the synchronous generator, and the exciter/AVR. The engine is modeled as a simple time delay (mean cylinder firing time) with a PID speed controller and second order actuator model from [24]. The mechanical torque (T_m) developed by the engine is transmitted through the shaft and opposed by the electrical torque (T_e) of the wye-connected salient-pole synchronous generator. The resulting angular frequency (ω) of the rotating shaft is expressed as a function of the inertia constant (H), the friction factor (F), and the difference between these torques in the "swing equation" [4].

$$\frac{d\omega}{dt} = \frac{1}{2H} \cdot (T_e - T_m - F\omega) \tag{5.1}$$

The DC exciter used in [5] was replaced with an IEEE type AC5A exciter [25] representing the rotating rectifier used for the exciter on the DEG for improved accuracy.

The mechanical model of the wind turbine's AC squirrel cage induction generator is

exactly that of the synchronous generator (1), though the electrical models are distinct [26]. The inertia constant includes the mass of the turbine rotor, shaft (assumed infinitely stiff), and generator rotor. The power transmitted through the shaft is a function of the rotor performance, air density, swept area, and wind speed [27].

The wind signal supplied to the WTG is synthesized one-second Shinozuka turbulence, as discussed in [28], with an average wind speed of 10 m/s, a standard deviation of 0.15 m/s and a Von Karman target spectrum. This method is shown to be accurate for short, dynamic time scales in [29].

A simple resistive-inductive load with a 0.80 lagging power factor was used to represent the consumer load. A three-phase breaker is activated to add and remove a fixed quantity of consumer load for further perturbation of the system.

5.3.2 Individual ETS Unit Response

The DSL modeled in this study is an ETS unit that can activate up to n resistive heating elements, depending on the severity of the wind excursion or load loss event. A commercially available ETS device, as tested in [30], can be equipped with a similar controller. Individual elements are activated in a fashion proportional to the frequency error until all are on. The frequency at which all elements activate (f_a) is directly related to the reciprocal of the controller proportional gain, P. The response of three distinct values of f_a is shown in Figure 5.2 ($n = 4$). Note that below 60 Hz the units cannot inject current into the system and may only unload in response to frequency dips if elements are already active. A cluster of such ETS units reacting in aggregate is modelled hereafter.

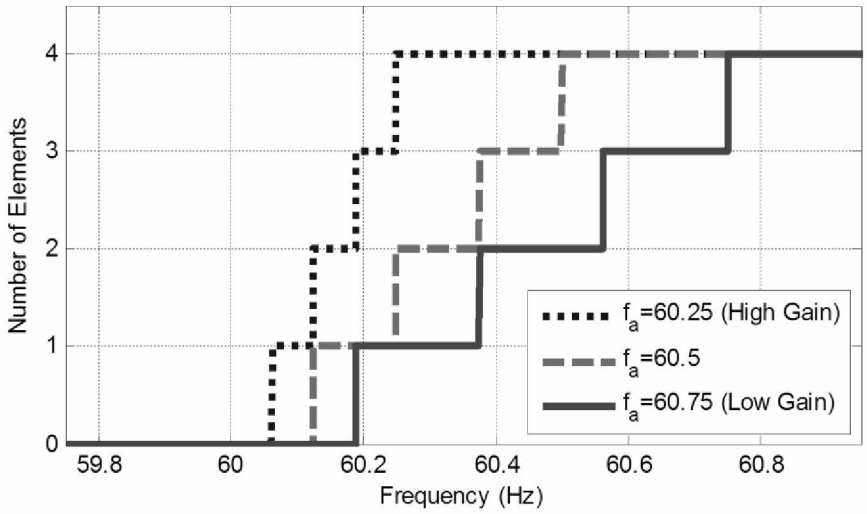

Figure 5.2. Individual ETS unit response to grid frequency deviations. A system with four heating elements ($n = 4$) is used in this study.

5.3.3 Aggregate DSL Response

The DSL block connects directly to the 3-phase 480 Vac bus with the other model components. Because unit synchronization among devices is of interest, two coordination modes are proposed that represent opposing ends of a spectrum: synchronized and staggered switching (Figure 5.3). For both of these modes, the DSL block is a calculator that resolves and applies the instantaneous, aggregate resistive load evenly over the three phases of the bus. A typical DSL block output (for both modes) is compared with the controller response to frequency error in Figure 5.4. The controller output signal (bold line) representing the instantaneous call for secondary load (kW) based on this error is shown. The responses each track this signal, but are limited by switching and synchronization intervals. The two coordination modes for the DSL are discussed in further detail as follows.

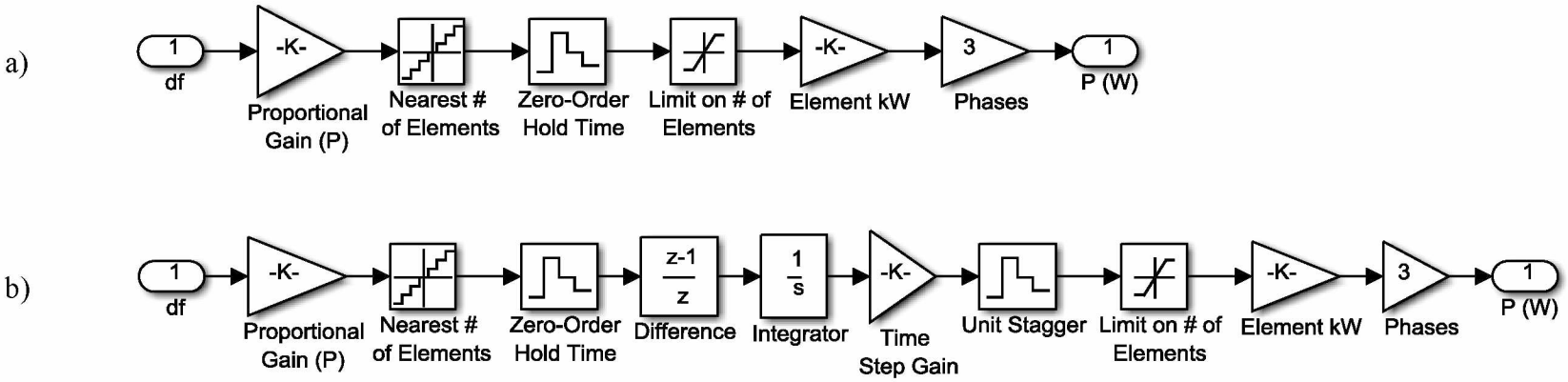

Figure 5.3. Sub-systems for a) **synchronized** coordination of DSLs and b) **staggered** coordination of DSLs.

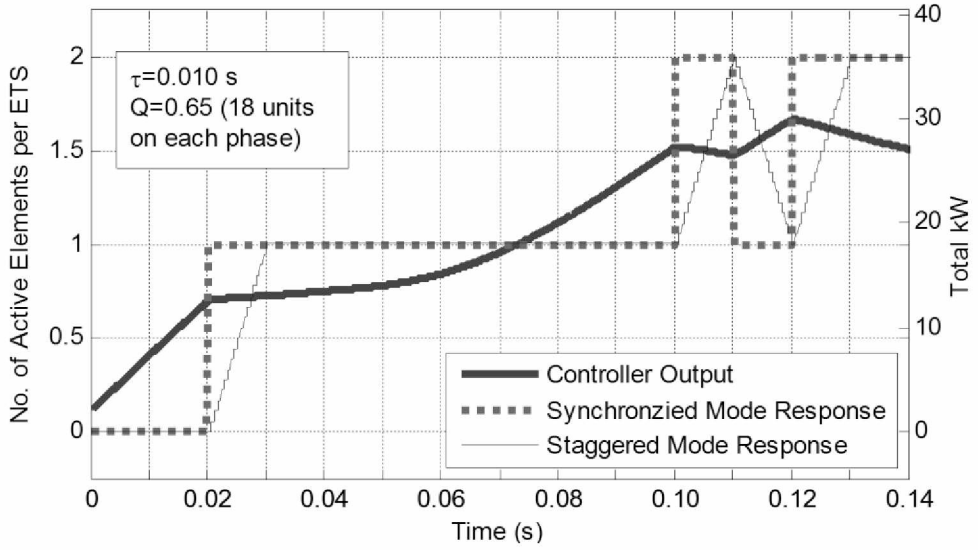

Figure 5.4. Aggregate response to frequency error (example). Up to two elements per device can be seen activating.

5.3.3.1 Synchronized DSL Switching

In *synchronized* mode (Figure 5.3a) a distributed group of ETS units switch simultaneously. This may represent an effort to coordinate the units (using a power line carrier signal, for instance) or a case where units naturally establish an approximately synchronous switching behavior.

As seen in Figure 5.3a, the product of the number of ETS units in the network, the number of elements the units are activating, and the kW rating of each element yield the cumulative load. The resulting load is continuously placed on the grid and switched in a similar fashion every τ seconds, where τ refers to the zero-order hold time. Saturation limits and quantizing blocks ensure calculations performed by the model result in a discrete number of elements between zero and n. This mode represents a system of distributed self-regulating loads that switch synchronously.

The only control signal input to the DSL block is grid frequency error (pu). Hence, the resolution of the applied collective load is limited by the number of elements in any single unit.

Furthermore, when the frequency changes, all units in the network switch states at precisely the same time. The proportional gain (P) is related to the full activation frequency (f_a) in a 60 Hz system as

$$P = \frac{n}{f_a / 60 - 1} \tag{5.2}$$

where n is the number of heating elements in the typical unit.

5.3.3.2 Staggered DSL Switching

As an alternative to *synchronized* unit coordination, a *staggered* switching method was considered (Figure 5.3b). Units in the network are each biased, such that they activate several milliseconds after a synchronized load switch. This may represent one of two things: 1) a concerted effort to bias the switching time of units in order to avoid large steps in load at switching intervals, or 2) the natural tendency for units to acquire distinct, uncoordinated switching times. An ideal case of this would be an even distribution of ETS units activating between zero-order hold times. The resulting control response can be seen in comparison with *synchronized* mode in Figure 5.4.

The natural behavior of the aggregate DSL will likely fall between the two cases presented. Some, but not all units will switch simultaneously. Analysis will be conducted in order to determine what these cases each look like in the time domain.

5.4 Analysis

Numerous 30-sec simulations were run with varying set points in order to ascertain the response of the system to perturbations in wind power and consumer load. (Trends in the resulting dynamics were shown to mature at such durations.) The behavior of the DSLs are evaluated with respect to a system only under the control of the DEG with no DSL, but subject to the same inputs

(represented by subscript 0). The DSLs may perform better or worse than this case.

5.4.1 Invariant Model Inputs (Machine Parameters)

The mathematical model described in 5.3 includes numerous machine parameters, including synchronous generator d and q axis reactances, induction generator friction and inertia coefficients, and many others. These will not be discussed, though select parameters are shown in Table 5.2.

Table 5.2. Invariant system parameters.

DEG Parameters		
DEG generating capacity	320	kVA
Nominal frequency	60	Hz
Nominal voltage	480	V_{RMS} L-L
Consumer Load Parameters		
Base consumer load	250	kW
Switched consumer load	20	kW
Load power factor	0.80	lagging
WTG Parameters		
Number of WTGs	1	
Wind turbine capacity	111	kW
ETS Network Parameters		
Number of elements per unit	4	
ETS Unit kW	1.33	kW

The ETS devices simulated in the present work represent four-element, 1.33 kW, 120 Vac ETS units. A consumer load perturbation of 20 kW is switched in and out of the primary load every five seconds during each simulation.

5.4.2 Variable Model Inputs

The behavior of the DSL network is governed by unit switching time, controller settings, the total capacity of the aggregate DSL and the timing between units. The following variables represent these properties.

5.4.2.1 Zero-order Hold Time (τ)

The time between which ETS unit relays can switch elements forces a hold value in the device's impedance. This time is measured in milliseconds (ms) and given the variable τ. Typical ranges of interest include values from 8 to 90 ms. This range is limited by practical factors, including the ability of a solid state relay to switch states, the capability of the controller to detect voltage zero crossings, and the efficacy of the controller, which is diminished at high values of τ.

5.4.2.2 Full Activation Frequency (f_a)

The full activation frequency is the grid frequency at which all ETS elements activate (Figure 5.2), drawing full capacity. The number of elements in the unit (n) is related to the controller proportional gain (P) in a 60-Hz system per (2). The range of relevant values of f_a is bounded at the high end (~62 Hz) by negligible controller effectiveness and at the low end (~60.1 Hz) by a proportional gain approaching infinity.

5.4.2.3 DSL Capacity (Q)

The size of the DSL can be thought of in terms of the total number of ETS units (assumed to be balanced by phase) or by its per-unit power consumption capacity at full load, measured as a fraction of wind turbine generating capacity. Q is then:

$$Q = \frac{Capacity_{DSL}[kW]}{Capacity_{WTG}[kW]} \tag{5.3}$$

As the present analysis is focused on the behavior of systems in *wind-diesel* mode, an upper limit of $Q \approx 1$ confines the capacity of the network to 100 kW (about one WTG at full output). An important justification for sweeping this variable is the potential for ETS units to reach their full charge capacity and lose their ability to participate in frequency regulation.

5.4.2.4 Unit Coordination Timing

The behavior of both coordination modes discussed in section 5.3.3 were tested. These include *synchronized* and *staggered* unit coordination.

5.4.3 Model Outputs

Of primary interest is the degree by which the DSL reduces the variability in grid *frequency* without disrupting *RMS voltage*. The time series voltage and frequency responses of a typical 20-second simulation are shown in Figure 5.5.

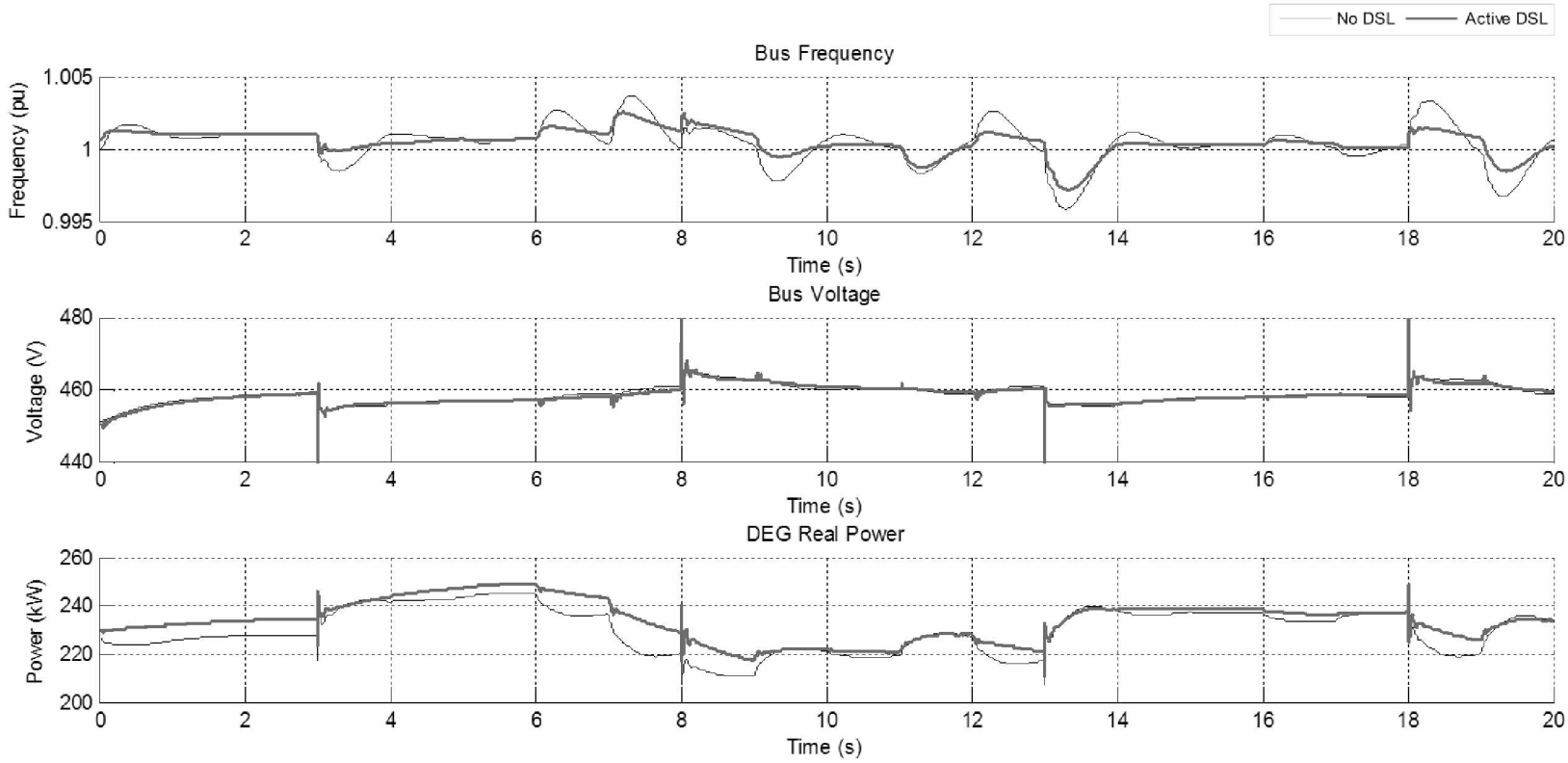

Figure 5.5. Time series *f*, *V*, and P_{DEG} without and with an active DSL. Perturbations include variable wind and a 20 kW load, switched every 5 sec.

The parameter sweeps in section 5.5 show the relative variability of the frequency and voltage signals by introducing two quantities: σ_f and σ_V, respectively. The numerators in (5.4) and (5.5) represent the mean square error of the f and V signals, respectively (from their own statistical mean), when an active DSL is connected. The denominators represent the error of a system with no DSL, but subject to the same input conditions. Thus, a quantitative comparison can be made between the variability of a system with and without an active DSL.

$$\sigma_f = \sqrt{\frac{\int \left(f(t) - \overline{f}\right)^2_{DSL} \cdot dt}{\int \left(f(t) - \overline{f}\right)^2_{0} \cdot dt}} \tag{5.4}$$

$$\sigma_V = \sqrt{\frac{\int \left(V(t) - \overline{V}\right)^2_{DSL} \cdot dt}{\int \left(V(t) - \overline{V}\right)^2_{0} \cdot dt}} \tag{5.5}$$

Values of $\sigma = 0$ indicate an invariant frequency or voltage signal with no departure from the mean value. A value of one indicates parity with a system with no active DSL. A value greater than one indicates detrimental performance of the DSL, as compared to a typical system. For example, a particular DSL configuration allows for a reduction in frequency variation as shown in Figure 5.5, represented by a value of $\sigma_f = 0.49$—a 51% reduction in frequency variability.

A difference in the DEG power with and without the presence of the DSL can also be seen in Figure 5.5. This exists because, in the former case, power is being absorbed by the ETS units in the DSL. This charging power is referred to hereafter as P_{DSL}. P_{DSL} is generally found to be under 10 kW (for this 320 kVA system) and cannot be negative, as the ETS loads are unable to feed current back into the bus.

Table 5.3 summarizes these input and output variables.

Table 5.3. DSL parameters and simulation metrics.

Variable	*Unit*	*Sim. Range*	*Description*
DSL System Parameters (Inputs)			
τ	[ms]	8 to 90	Zero-order hold time
f_a	[Hz]	60.1 to 62.0	Full activation frequency
Q	[pu]	0 to 1	DSL aggregate capacity
Simulation Metrics (Outputs)			
σ_f	[pu]	0 to 1+	Frequency variability
σ_V	[pu]	0 to 1+	Voltage variability
P_{DSL}	[kW]	0 to 10 kW	Power absorbed by DSL

5.5 Results and Discussion

Sweeps of the relevant parameters (as discussed in section 5.4) show regions of operation within which the frequency and/or voltage regulation is improved with the presence of a DSL ($\sigma_f < 1$ or $\sigma_V < 1$). Likewise there are regions for which the DSL has a negative effect on frequency or voltage regulation. These effects are outlined here in further detail for a picture of the interaction between the DEG and the distributed secondary loads in *wind-diesel* mode.

5.5.1 Synchronized Switching

The behavior of the ETS units responding to frequency changes in a synchronous fashion can be seen in Figure 5.6. σ_f, σ_V, and P_{DSL} are plotted against f_a and Q for three values of τ. Regions for which $\sigma_f = 1$, $\sigma_V = 1$ or $P_{DSL} = 0$ (medium grey, in Figures 5.6 and 5.7) represent comparable performance to a system solely under the control of the DEG prime mover (no DSL). Regions detrimental to such a base case are black, while light grey represents superior performance. Several key observations can be made.

First, there are large regions in this mode for which the improvement in frequency

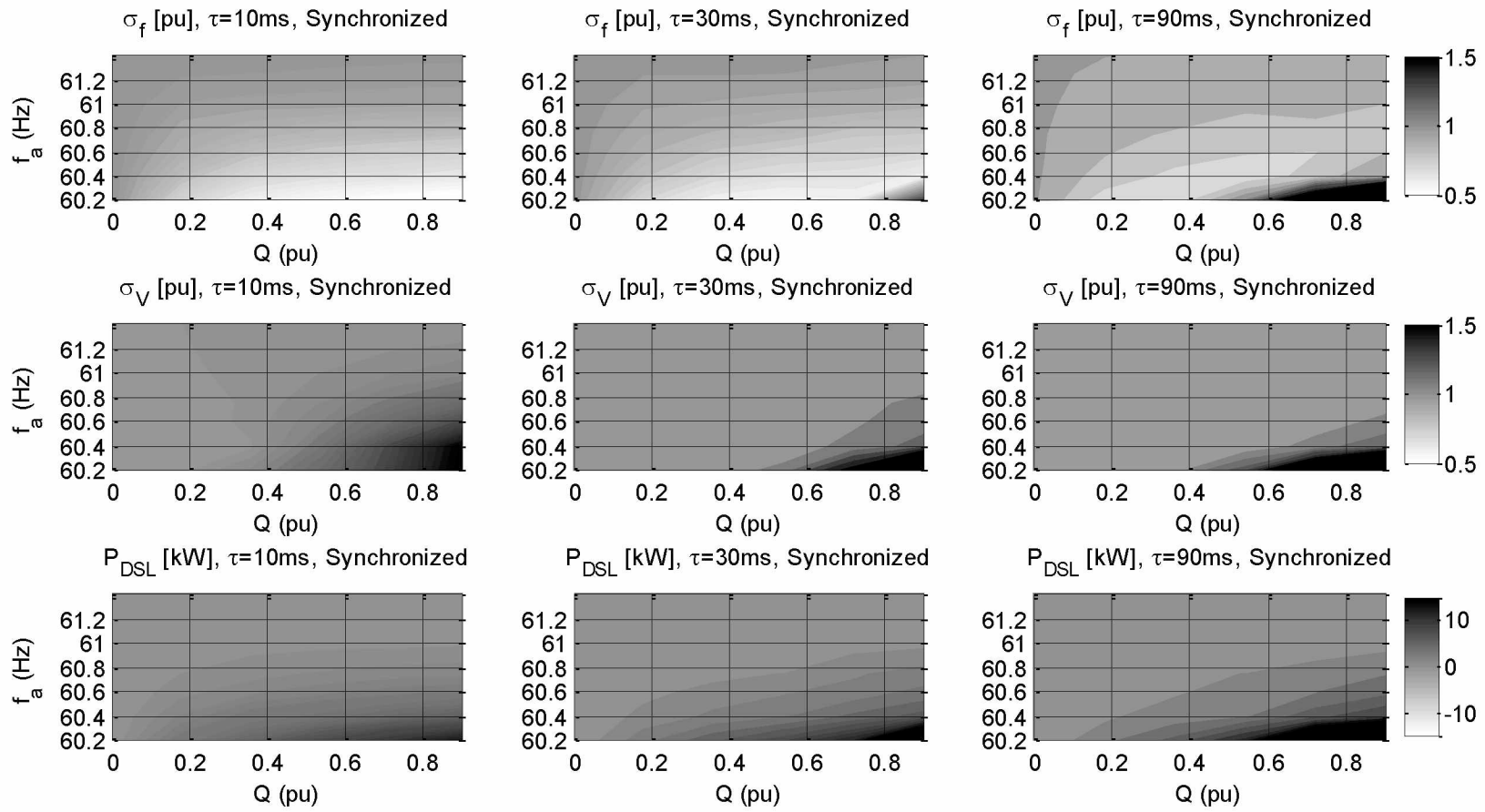

Figure 5.6. Contour plots of σ_f, σ_V and P_{DSL} for synchronous switching of ETS units at three values of τ. Regions: black ($\sigma_f > 1$, $\sigma_V > 1$, and $P_{DSL} > 0$) denotes detrimental performance, light grey ($\sigma_f < 1$, $\sigma_V < 1$, and $P_{DSL} < 0$) superior performance, and medium grey is comparable to no DSL.

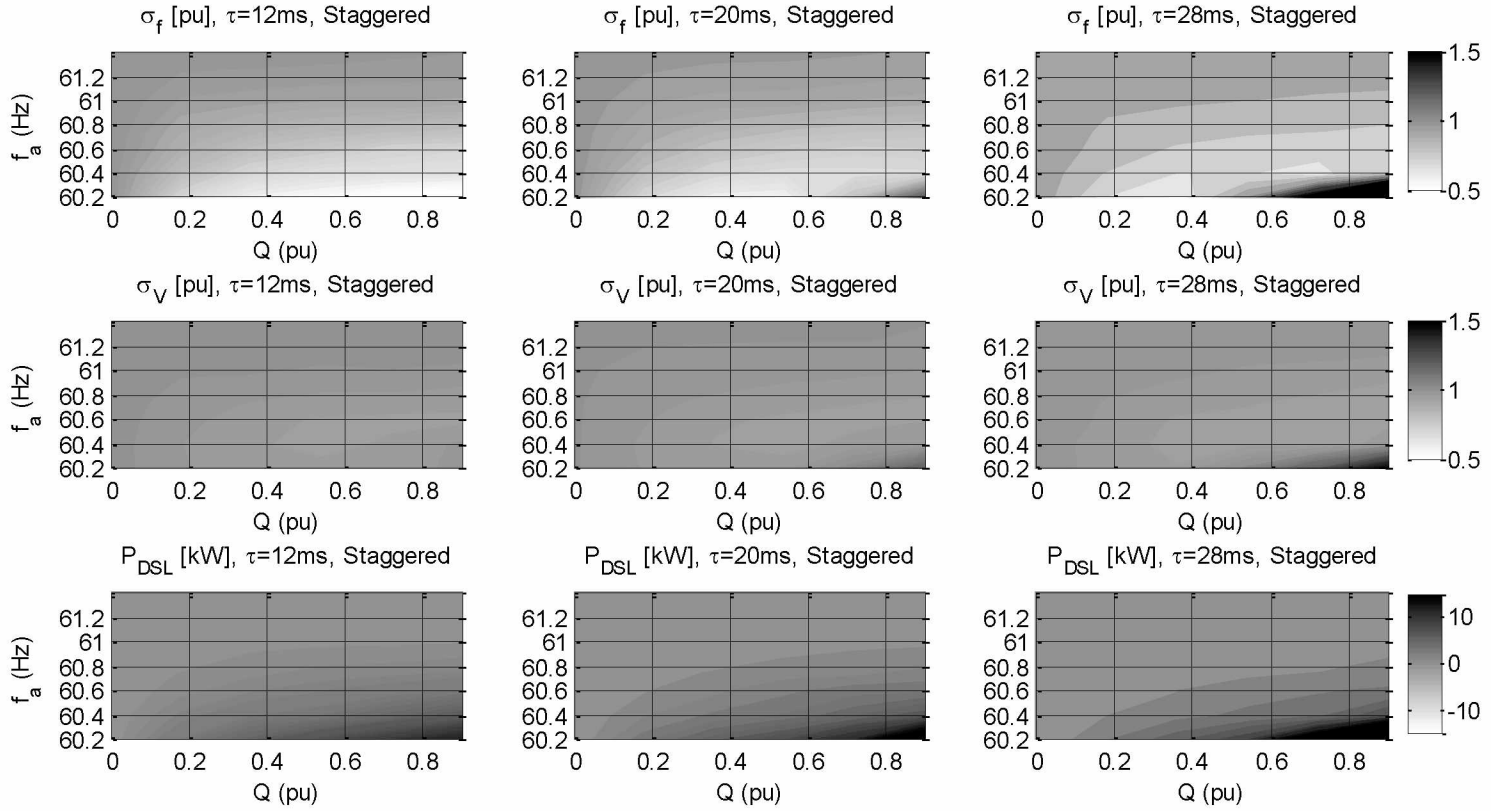

Figure 5.7. Contour plots of σ_f, σ_V and P_{DSL} for staggered switching of ETS units at three values of τ. Regions: black ($\sigma_f > 1$, $\sigma_V > 1$, and $P_{DSL} > 0$) denotes detrimental performance, light grey ($\sigma_f < 1$, $\sigma_V < 1$, and $P_{DSL} < 0$) superior performance, and medium grey is comparable to no DSL.

regulation is nearly 50%. These generally correspond to low f_a (high gain) and high Q (sufficient secondary load capacity). However, if the switching time is too slow (high τ) this region is replaced by a section of instability (Figure 5.6, 3rd column, black area), where frequency regulation is deficient. Fast-switching relays on the ETS units would ensure that this region is avoided by keeping τ low.

Second, visible in Figure 5.6 are the effects on voltage regulation. If τ is too low, voltage performance suffers due to an excessive number of small synchronized load steps. High values of τ also result in poor voltage regulation due to larger, but less frequent synchronized load steps. While the majority of the parameter space is benign ($\sigma_V \approx 1$), there are regions that represent voltage fluctuations several times more severe than a system solely under the control of the DEG.

Third, the ETS loads begin to draw measurable power (P_{DSL}) when the gain of each controller is set high ($f_a < 60.5$ Hz). This power is necessary to allow the DSL to trim frequency fluctuations, resulting in improved grid frequency regulation. Should wind power overtake grid demand (high wind penetration), this power will represent clean, wind-powered heat delivered to the DSL. However, in wind-diesel mode, this amounts to storing and delivering heat with diesel energy and is not economically favorable. Thus, a minimum value should be sought, which creates a compromise between frequency regulation and heating economics.

Finally, the effect of ETS units saturating and becoming unavailable for absorbing power can be seen in Figures 5.6 and 5.7 by tracing a horizontal line through the parameter space from right to left. In all cases, the system tends to behave more like an unassisted grid as ETS units reach their full charge—never worse. In *wind-diesel* mode, this is a positive fact since the DEG is always available to support frequency regulation.

5.5.2 Staggered Switching

When device switching is staggered, only one ETS unit in the network switches states at a time. (This could be achieved by pre-programming a small, unique time bias into the controller of each device.) It is clear upon inspection of Figure 5.7 that the performance characteristics of the staggered system are similar to that of the synchronized mode, from the standpoint of frequency regulation. However, voltage regulation problems in synchronized mode are mitigated by minimization of the DSL load step magnitudes via temporal spacing. Though no improvement is seen (or expected) over a system without an active DSL, values of $\sigma_V \approx 1$ are common to most of the parameter space–large spikes are scarcely present. DSL load is present in about the same quantities and locations as it is in synchronized mode.

5.5.3 Additional Observations and Discussion

Furthermore, varying the number of elements (not illustrated) significantly affects the individual unit response, and thus, frequency regulation. As the number of elements (n) are reduced (to two, for example), the less favorable the system's response is to frequency fluctuations. Adding elements results in an expansion of the positive parameter space, but with diminishing benefit above $n = 4$. In no case was the magnitude of the benefit improved past $\sigma_f \approx 0.5$.

A relationship between frequency variability (σ_f) and P_{DSL} can be seen in Figs. 5.6 and 5.7. The low points in σ_f (generally the lower right corners) correspond to the high points in P_{DSL}. As stated above, this is expected. When the data are plotted against these two variables, irrespective of their position in the parameter space, an indirect relationship is observed (Figure 5.8). If the relay switching time of the DSL is too high, a minimum occurs, whereby the application of additional secondary load (whether by gain tuning or increase in fleet size) will actually tend to

intensify frequency transients in the system.

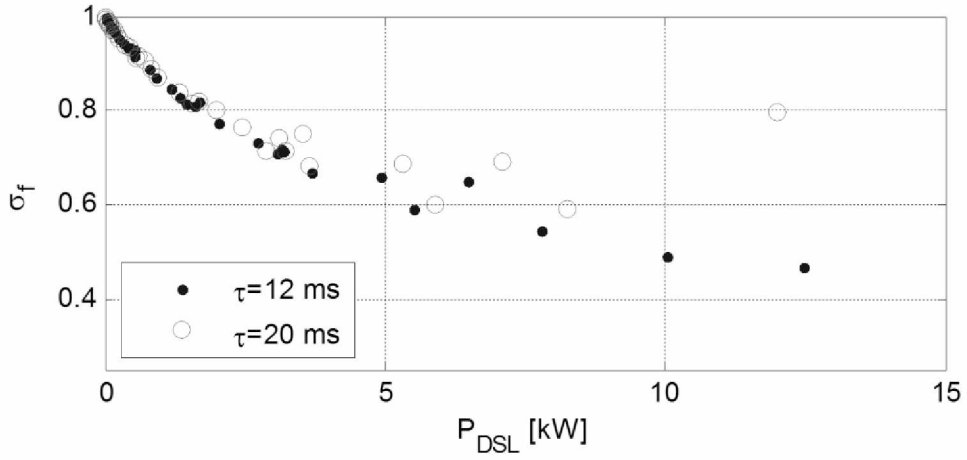

Figure 5.8. Relationship between frequency variability (σ_f) and P_{DSL} for two values of τ in staggered switching mode.

Optimizing the design of a network of autonomous ETS units is thus a problem specific to the circumstance. The performance requisites of the system may call for a particular Q, though different values may be favorable from a dynamics standpoint. Optimizing for frequency regulation may be a compromise on voltage regulation. Optimizing for either frequency or voltage regulation will result in high amounts of undesirable diesel-fed ETS charging power.

5.6 Conclusions and Future Work

Classical use of secondary loads in islanded wind-diesel microgrids does not allow for effective delivery of excess wind energy to distributed residences. The present study proposes the use of self-sensing distributed secondary loads with no centralized controller or communication network to assist in grid frequency regulation while providing supplemental domestic space heating with ETS devices. Through dynamic modeling, it is shown that DSLs can assist with frequency regulation of microgrids (given proper gain settings, switching times and fleet size) subject to variable wind power and dynamic consumer load in *wind-diesel* mode.

Conversely, it is possible that such a network of autonomous secondary loads causes disruptions to frequency and/or voltage greater than those observed in a system solely under the control of the DEG (in certain cases). By design, the DSL introduces a series of step perturbations, which, if uncontrolled, are a cause for the very fluctuations sought to be corrected. The present work demonstrates two methods for minimizing these perturbations: staggered switching of units and proper selection of network parameters (i.e., τ, Q and f_a).

Staggered unit switching (with a unique sub-cycle time delay) significantly minimizes the magnitude of DSL load steps by spacing them out in time. This delivers sound benefit to frequency regulation, while mitigating the negative impacts on voltage. However, improper selection of network parameters may increase the magnitude of step perturbations, resulting in poor voltage and frequency regulation. The present study demonstrates how a combination of slow switching times ($\tau > 25$ ms), high controller gain, and too many active DSLs may cause disruptions. Such combinations lead to an oversensitive, unstable secondary load, itself capable of disturbances larger than that of the consumer load. These situations should be entirely avoidable in practice.

The results also illustrate the effects of ETS units becoming saturated and unavailable for use as secondary loads. Favorably, there is no case where the loss of active units (from a stable operating point) results in frequency regulation worse than a system without an active DSL. As units saturate, the DEG will simply play a larger role in frequency regulation until it is the sole regulator. Nonetheless, the size of the aggregate DSL network is still an important design consideration, from a performance and economic standpoint.

The interaction between the DSLs and the DEG also shows that a fast-acting network of switching loads is more effective at frequency regulation when a portion of the distributed load (P_{DSL}) remains active and prepared for either frequency dips or swells. The primary reason this can

be seen in the simulations is due to the steady state error resulting from a lack of controller integral gain. Consequently, secondary loads in *wind-diesel* mode are fed with undesirable charging current from the DEG, rather than from cleaner wind.

As a goal of the present work is to increase the value of secondary loads on islanded wind-powered microgrids, future work must demonstrate the ability for a network of DSLs to function as a sole frequency regulator in high penetration *wind-diesel* mode. Moreover, a smooth transfer of frequency control responsibility from the DEG to the DSLs must be confirmed. Thus, it may be necessary to improve the frequency sensing, controller topology and load switching technology of the ETS units. Changes to the design, such as varying the impedance of the elements to a binary scheme would allow for more load resolution. Implementation of a PID type controller may also be a necessary advancement. Nonetheless, the goal of a significant reduction in frequency transients is achievable using distributed ETS units in *wind-diesel* mode.

5.7 References

[1] Stavrakakis, G. S. and G. N. Kariniotakis. "A general simulation algorithm for the accurate assessment of isolated diesel-wind turbines systems interaction. I. A general multimachine power system model." *IEEE Transactions on Energy Conversion* 10.3 (1995): 577-583.

[2] Hasanien, H. M., S. M. Muyeen, and J. Tamura. "Frequency control of isolated network with wind and diesel generators by using fuzzy logic controller." *IEEE 2009 International Conference on Electrical Machines and Systems (ICEMS 2009)*. IEEE, 2009.

[3] Sebastián, R. "Smooth transition from wind only to wind diesel mode in an autonomous wind diesel system with a battery-based energy storage system." *Renewable Energy* 33.3 (2008): 454-466.

[4] Glover, J. D, M. S. Sarma, and T. J. Overbye. *Power Systems Analysis and Design 5th ed.* Stamford, CT. Cengage Learning (2012): 590-634.

[5] Janssen, N. T., R. A. Peterson, and R. W. Wies. "Development of a Full-Scale-Lab-Validated Dynamic Simulink© Model for a Stand-Alone Wind-Powered Microgrid." *ASME 2014 Power Conference*. ASME, 2014.

[6] Nayar, C.V. et al. "Novel wind/diesel/battery hybrid energy system." *Solar Energy* 51.1 (1993): 65-78.

[7] Gampa, S. R. and D. Das. "Real power and frequency control of a small isolated power system." *International Journal of Electrical Power & Energy Systems* 64 (2015): 221-232.

[8] Bhatti, T. S., A. A. F. Al-Ademi, and N. K. Bansal. "Load frequency control of isolated wind diesel hybrid power systems." *Energy Conversion and Management* 38.9 (1997): 829-837.

[9] Sebastián, R. and R. Peña-Alzola. "Control and simulation of a flywheel energy storage for a wind diesel power system." *International Journal of Electrical Power & Energy Systems* 64 (2015): 1049-1056.

[10] US DOE. NREL. Systems Performance Analysis of Alaska Wind-Diesel Projects: St. Paul, Alaska. City: Apr, 2009. [Online]. Available http://apps2.eere.energy.gov/wind/windexchange/pdfs/wpa/2009/wind_diesel_ak_saint_paul.pdf

[11] Kim, Y. S., E. S. Kim, and S. I. Moon. "Frequency and Voltage Control Strategy of Standalone Microgrids with High Penetration of Intermittent Renewable Generation Systems." *IEEE Transactions on Power Systems* 31.1 (2016): 718-728.

[12] Isherwood, W. et al. "Remote power systems with advanced storage technologies for Alaskan villages." *Energy* 25.10 (2000): 1005-1020.

[13] Drouilhet, S. M. and M. Shirazi. "Wales, Alaska high-penetration wind-diesel hybrid power system: theory of operation." National Renewable Energy Laboratory (2002).

[14] Miller, M. "Sand Point Wind-Diesel Project Secondary Loads: Performance and Lessons Learned." (2013) [Online]. Available <http://alaskarenewableenergy.org/>

[15] Gomez, E. "A physically based load model of residential electric thermal storage: Application to LM programs." *International Journal of Power and Energy Systems* 24.1 (2004): 24-31.

[16] Sateriale, M. E. "Modeling and analysis of masonry electro-thermal heating and storage for optimal integration with remote stand-alone wind-diesel systems." Master of Science Thesis, University of Alaska-Fairbanks, 2013.

[17] Madureira, A., C. Moreira, and J. Peças Lopes. "Secondary load-frequency control for microgrids in islanded operation." *International Conference on Renewable Energy Power Quality* (2005).

[18] Lopes, J. A., L. Moreira, and A. G. Madureira, "Defining control strategies for microgrids islanded operation." *IEEE Transaction on Power Systems* 21.2 (2006): 916-924.

[19] Shafiee, O., J. M. Guerrero, and J. C. Vasquez. "Distributed secondary control for islanded microgrids—A novel approach." *IEEE Transactions on Power Electronics* 29.2 (2014): 1018-1031.

[20] Lu, N. and D. J. Hammerstrom. "Design considerations for frequency responsive grid friendly TM appliances." *IEEE 2006 Transmission and Distribution Conference and Exhibition (IEEE PES 2006)*. IEEE, 2006.

[21] Trudnowski, D., M. Donnelly, and E. Lightner. "Power-system frequency and stability control using decentralized intelligent loads." *IEEE 2006 Transmission and Distribution Conference and Exhibition (IEEE PES 2006)*. IEEE, 2006.

[22] Short, J. A., D. G. Infield, and L. L. Freris. "Stabilization of grid frequency through dynamic demand control." IEEE Transactions on Power Systems 22.3 (2007): 1284-1293.

[23] Vandoorn, T. L. et al. "Active Load Control in Islanded Microgrids Based on the Grid Voltage." *IEEE Transactions on Smart Grid* 2.1 (2011).

[24] Yaiger, K. E. and J. R. Willis. "Modeling of Emergency Diesel Generator in an 800 MW Nuclear Power Plant." *IEEE Transactions on Energy Conversion* 8.3 (1993).

[25] "Recommended Practice for Excitation System Models for Power System Stability Studies." IEEE Standard 421.5 (1992). IEEE.

[26] Krause, P. C., O. Wasynczuk, and S. D. Sudhoff. *Analysis of Electric Machinery and Drive Systems.* IEEE Press (2002): 109-190.

[27] Heier, S. *Grid Integration of Wind Energy Conversion Systems.* John Wiley & Sons Ltd (1998).

[28] Manwell, J. F., J. G. McGowan, and A. L. Rogers. *Wind Energy Explained: Theory, Design, and Application (Second Edition)*. West Sussex, United Kingdom: Wiley, (2009): 673.

[29] Kaminsky, F. C. "A Comparison of Alternative Approaches for the Synthetic Generation of a Wind Speed Time Series." *Journal of Solar Energy Engineering* 113.4 (1991): 280–289.

[30] Wies, R. W. and N. T. Janssen. "Review and Testing of Steffes Electric Thermal Storage Unit with Grid-Interactive Frequency Regulation." Intelligent Energy Systems Llc, Anchorage, AK, Technical Report (2013).

Chapter 6. Modeling Integration Strategies for Autonomous Distributed Secondary Loads on High Penetration Wind-Diesel Microgrids

6.1 Abstract

Remote islanded microgrids are frequently powered by a combination of diesel power and wind. Excess wind power is a common commodity that is often wasted or poorly utilized. In cold climates, this energy can be used to provide space heat or domestic hot water. However, storage and distribution of this renewable heat is a technical challenge. Use of Electric Thermal Storage (ETS) devices provides a means for conversion of electrical energy to heat, a storage medium for on-demand discharge, and a method of distribution throughout the residences of the community. The present research explores a means of using autonomous distributed ETS units to inherit frequency control responsibility from the diesel generator while keeping the diesel engine at its minimal optimal loading.

6.2 Introduction

Remote communities often struggle to obtain clean, affordable electrical power. Historically, diesel electric generators have been the mainstay of islanded microgrids due to availability for remote power applications and relatively low cost of operation. However, in recent years fuel prices in such locations have become exorbitant [1], resulting in crippling operating costs. Renewable resources, such as wind and solar power, present an opportunity to offset diesel fuel with a cleaner and more economical alternative.

At high latitudes, wind is often a more annually regular source of renewable energy than solar power [2], as the sun can disappear below the horizon for close to twenty four hours (during winter days). It is common practice to add an excessive amount of wind power capacity to such

diesel grids in order to provide a higher fraction of renewable power even when the wind farm may be operating well below its capacity [3, 4]. This causes an energy imbalance on the grid, which can be dealt with in one of several ways.

First, wind power generation can be regulated by the wind turbines (curtailment), as shown in [5]. However, it is economically undesirable to avoid capture of usable energy when the infrastructure exists to utilize it. Some systems may use a resistive load bank [6] or electric boiler [4] to generate heat. If this heat is used at all, the application is confined to heat loads within piping distance of the plant.

Storage is a competitive option and has been demonstrated on paper [7] and in practice [8]. Lead acid (or, more recently, lithium ion) batteries are the most common way of storing high amounts of electrical power for later consumption (load levelling). The addition of energy storage, however, immediately necessitates the use of a DC bus and power electronic rectifier/inverter for conversion between AC and DC forms. For many rural villages, this technology can be expensive and/or difficult to maintain.

What is needed is a way to take the typical fast-switching resistive secondary load, break it up into a fleet of smaller, useful loads, distribute them throughout a community of residences, and maintain functionality with little to no control infrastructure. In Alaska and other polar regions, heat is a useful application for this excess wind energy, but systems must be kept simple and cost effective to ensure sustainability [9]. Since the demand for domestic space heat in polar regions is present six to nine months out of the year, using excess wind power to provide clean domestic space heat to the residences of a remote community is a more economical use for energy that would otherwise be wasted [10]. However, the electrical energy must be immediately expended, regardless of the instantaneous demand for heat. Electric Thermal Storage (ETS) devices can be

used to convert electrical energy to heat and store it for subsequent thermostatic discharge. Thus, excess wind energy can be used to charge a fleet of ETS units [11] and later discharged when the heat is needed. However, controlling a family of these distributed units with little to no communication infrastructure can be a complicated undertaking.

The present work proposes a design for a high-penetration hybrid wind-diesel electrical system with self-regulating distributed secondary ETS loads. Individual units are able to measure and respond to changes in frequency and absorb the appropriate amount of energy, holding responsibility for grid frequency regulation. (The concept of decentralized intelligent loads is introduced in [12] and [13] for large, "infinite" grids, and in [14] for islanded microgrids.) A dynamic phasor model is used to show steady operation across a full range of potential conditions, including the mechanical decoupling of the diesel engine from the synchronous generator.

6.3 Model

6.3.1 System Requirements

The objective of the isolated microgrid is to supply the primary load with stable electrical power, on demand, in the cleanest and most economical way possible. This means providing consistent frequency and voltage regulation with optimal use of renewable energy sources (wind, in this case).

In addition to frequency regulation, the system must also meet the following requirements to ensure safe and stable operation.

1. Rotating mass must be maintained for transient stability [15]. Though some microgrids may make use of virtual inertia [16] from a DC power source, this no-battery system must have adequate rotational inertia at all times.

2. The distributed secondary loads are isolated and have no communication with the plant. Thus, they can respond only to the frequency or voltage of the grid. (Voltage will vary significantly by location and with changing conditions. Frequency will effectively be the same at all locations within a small grid and more accurately reflects the balance of real power on the system.)
3. The diesel must not be run below its minimum optimal loading (MOL). Extended operation below the MOL may result in NOx production, pre-mature wear of piston rings, and various other problems [17].

6.3.2 System Components

Hybrid wind-diesel microgrids consist of diesel and wind generation serving a primary load. Those that are also capable of a high level of wind power penetration require a fast-switching controlled secondary load [18]. Figure 6.1 illustrates these components and their connections.

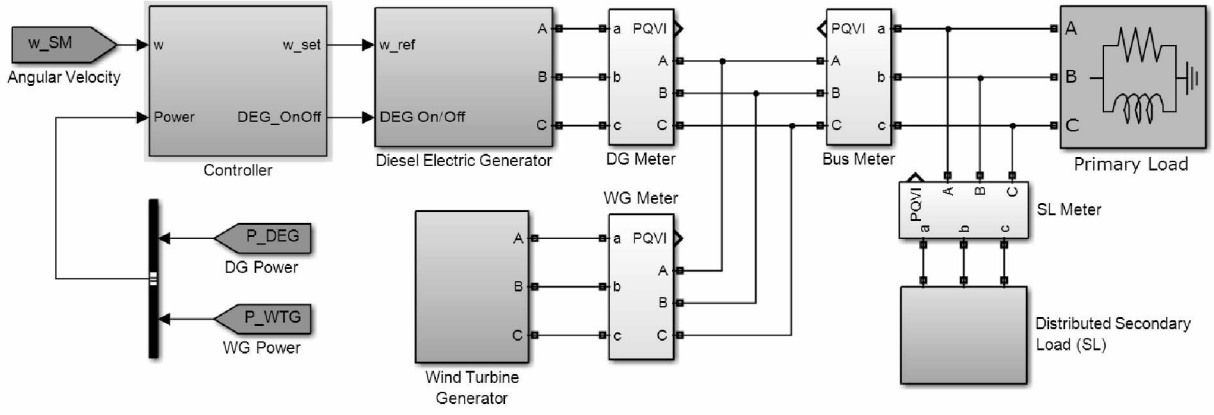

Figure 6.1. Proposed system layout with primary components shown.

The primary components of the proposed no-battery system can be categorized as shown in Table 6.1 (controlled and uncontrolled energy sources and sinks). The diesel generator acts as the controlled source of real power. Wind power is an unpredictable source that requires more

complex controls to regulate power output such as pitch, yaw, and rotor brake control. The primary consumer load and secondary load are energy sinks, though only the latter can be controlled without disrupting service to consumers. The intent of the proposed system is to make use of the controlled sources and sinks to establish a balance of real power on the system and maintain frequency regulation over a wide range of varying and uncontrollable situations.

Table 6.1. Primary grid components, categorized.

	Controlled	**Uncontrolled**
Energy Sources	Diesel Generation	Wind Generation
Energy Sinks	Distributed Secondary Loads	Primary Load

These components have been mathematically modelled and integrated to form a dynamic phasor type model of their electromechanical interactions in MATLAB® Simulink®. Validation of this model was conducted in a laboratory at the University of Alaska Fairbanks Power Systems Integration Lab (ACEP credit) [19]. The major system components are modelled as follows.

6.3.2.1 Diesel Generator

The diesel generator is comprised of a diesel engine directly coupled to a synchronous generator. The diesel generator model was introduced by [20] and verified in [19]. During operation, the error between measured shaft speed ω and the speed set-point is amplified, maneuvering the electronic actuator. (The actuator is represented by the two transfer functions shown in Figure 6.2.) A transport delay represents the mean firing time of the cylinder and the resulting delay in torque development.

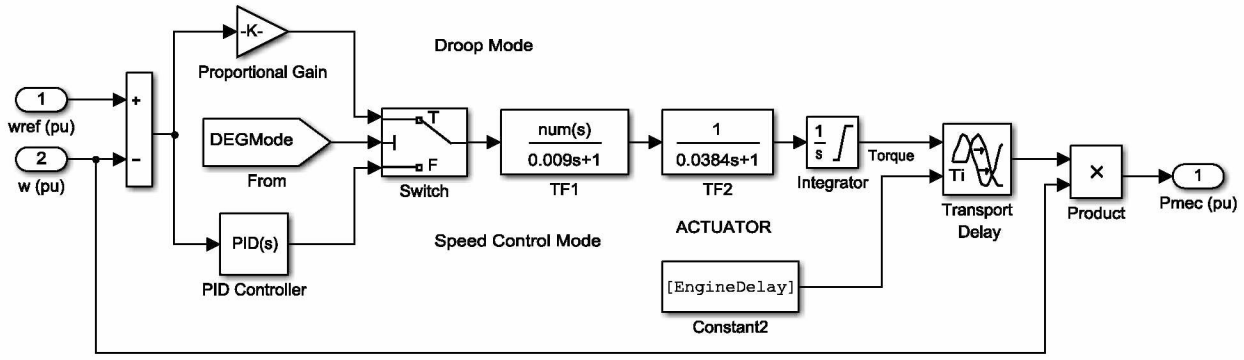

Figure 6.2. Block diagram of diesel engine.

The generator is a wye-connected salient-pole synchronous machine, modelled electrically in [21]. The mechanical model relates the balance of electrical and mechanical torque (T_e and T_m, respectively) with the inertia of the machine (H), the friction (F) and the resulting angular velocity ω in the "swing equation." [15]

$$\frac{d\omega}{dt} = \frac{1}{2H} \cdot \left(T_e - T_m - F\omega\right) \tag{6.1}$$

For the diesel generator in this system, a *droop mode* has been added so that the machine may control either speed (during normal "isochronous" operation) or power output, by altering the speed set-point. The steady state error corrected by the presence of integral gain in the speed control loop normally renders droop mode impossible. Thus, droop mode consists of a proportional gain alone. This mode will be important for keeping the diesel at or above its MOL during periods of high wind or low load.

Additionally, a clutch is placed between the diesel engine and the synchronous generator blocks (Figure 6.3). This allows the diesel engine to disconnect from the system when there is sufficient wind to support the primary load. Such a system was modelled and demonstrated by Sebastian et al [22]. When the command is given, the clutch opens, resulting in isolation of the

synchronous machine. The automatic voltage regulator and the inertia of the synchronous machine remain connected and serve to regulate voltage and stabilize the grid, respectively.

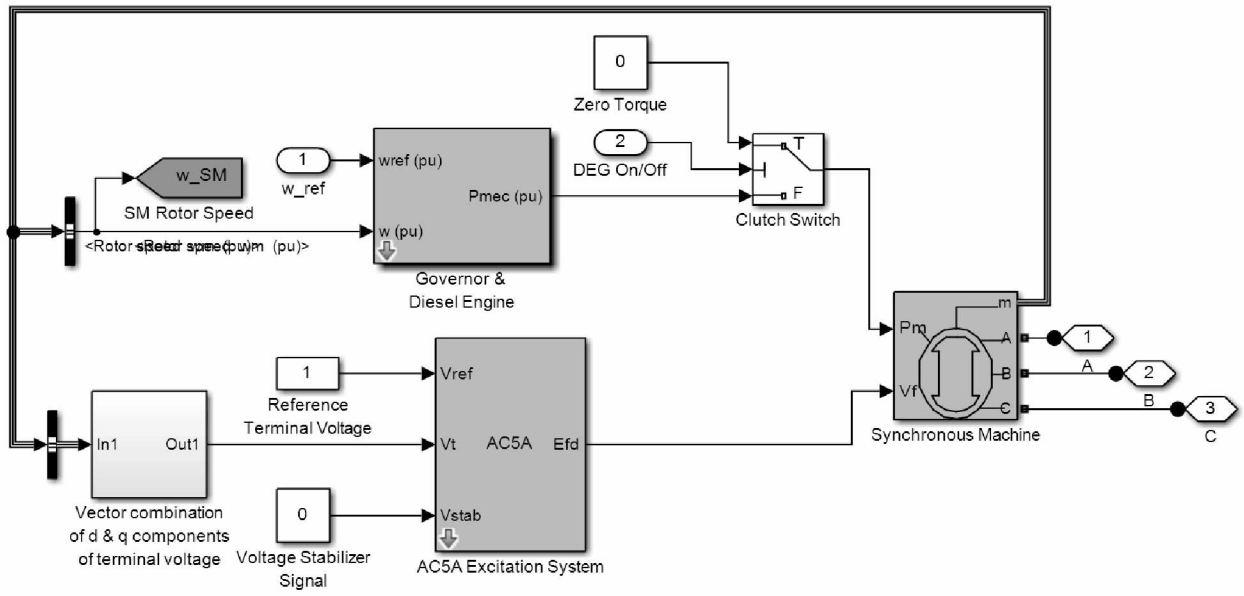

Figure 6.3. Diesel generator block with clutch shown between engine and synchronous machine.

6.3.2.2 Wind Generation

The wind generation block is formed by a rotor that transfers all captured power to a 150 HP induction generator, modelled in the rotating d-q reference frame. The input to the block is wind speed (in m/s) and the output is a balanced source of leading current. [14, 19] The relationship between electrical torque, mechanical torque, inertia, friction, and angular velocity is also accurately depicted by the same "swing equation" (Eq. 1) shown in 6.3.2.1.

6.3.2.3 Primary Load

The primary load is a three-phase balanced 480 VAC, 60 Hz resistive-inductive impedance with a power factor of 0.80 lagging.

6.3.2.4 Secondary Load

When the diesel is in droop mode or disconnected from the system entirely, the secondary loads are responsible for regulating frequency by absorbing the excess wind power. These loads are modelled as eight-element resistive loads with fast-switching solid state relays. Since all units on the grid respond to the same frequency error, they are aggregated into the following block diagram (Figure 6.4) and placed on the bus, near the primary load (see Figure 6.1).

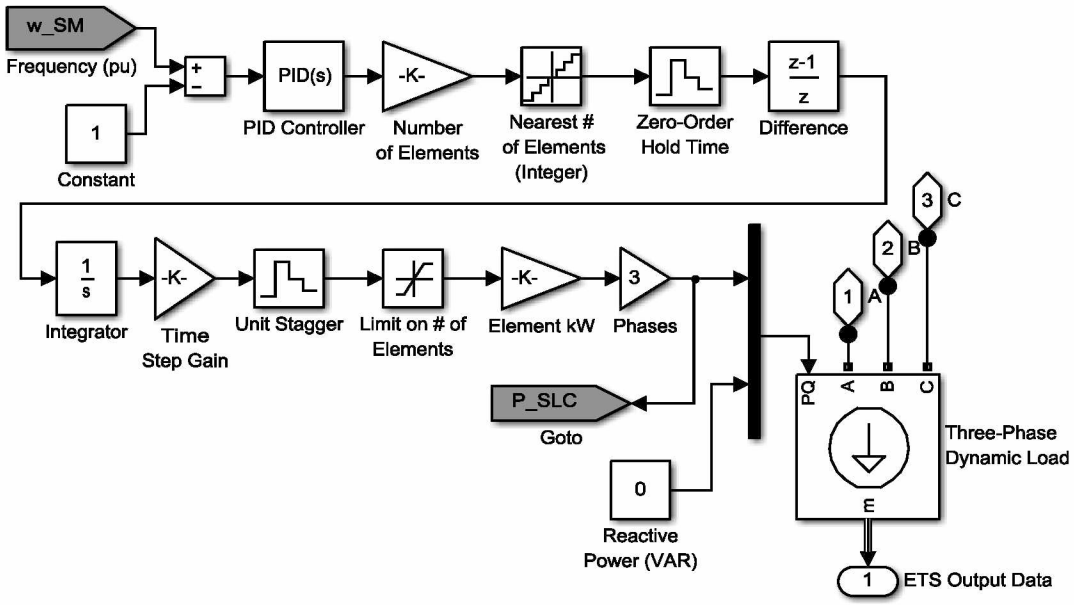

Figure 6.4. Distributed secondary load block diagram.

The impedance of the elements follow an eight bit arrangement, allowing for 2^8 (256) possible impedance values. The autonomous secondary loads monitor the grid frequency error and amplify the result using a PID controller, which then activates the appropriate elements to achieve

the desired charging impedance. The aggregate behavior of distributed ETS units was categorized in [14] by the degree to which units switch in synchrony. The present model uses a staggered unit switching model, as it can be shown that a more favorable voltage response is achieved when the units are not switching their elements at the same time. The zero order hold time [14] (20 ms in this case) represents the fastest possible switching time as limited by the solid state relays in the ETS controller.

6.3.3 Control Strategy

Frequency regulation is achieved based on the relative balance of wind power and total load on the system. Power meters are placed on the incoming bus from the wind farm and on the outgoing bus from the diesel generator. Since the secondary load is distributed throughout the primary load, there is no way for the central plant to measure its magnitude with respect to the total load. This creates a control challenge, which can be addressed as prescribed herein.

First, there are several distinct modes of system operation, defined as follows, in Table 6.2. When no wind is present, the diesel takes 100% of the primary and secondary load. The secondary loads only switch on to assist with frequency regulation, should a sudden change in load affect the frequency before the diesel can correct for it. The system is said to be in 'Diesel Only' mode.

Table 6.2. Grid control modes.

	Conditions		*Control Responsibilities*			*Settings*		
System Mode	**Wind Power (kW)**	**Diesel Power (kW)**	**Voltage Control**	**Frequency (Primary)**	**Frequency (Backup)**	**Clutch**	**Diesel Speed Setting (pu)**	**Diesel Mode**
Diesel Only	$P_{wind} = 0$	Any	AVR	Diesel	Distributed SLs	Closed	1.00	Isochronous
WD-Low	$P_{wind} > 0$	DG > MOL	AVR	Diesel	Distributed SLs	Closed	1.00	Isochronous
WD-High	$P_{wind} > 0$	DG ≤ MOL	AVR	Distributed SLs	-	Closed	Droop	Droop
Wind Only	$P_{wind} >$ MOL	Any	AVR	Distributed SLs	-	Open	0.30	Off

As wind generation cuts in, the diesel reduces its contribution, while still maintaining a steady synchronous speed. If the output power of the diesel is above its MOL, the system is in Wind Diesel-Low (WD-Low) mode. Still, the clutch is closed and the diesel maintains synchronous speed as the primary source of frequency regulation. In both 'Diesel Only' and 'WD-Low', the diesel is operating in an "isochronous" mode.

When the power meters sense that the diesel has reached its MOL, the system switches to 'WD-High' mode and the diesel is now in droop mode. The speed set-point is proportioned based on the error between the diesel MOL and its measured output power. It is still controlling its speed, but the presence of steady state error in the proportional only controller means that it will never reach the speed set-point. Instead, its output power will settle at the desired MOL set-point while the distributed SLs take responsibility for frequency regulation.

At this point, should wind continue to increase (or load decrease), the distributed secondary loads continue to maintain frequency regulation and a decision can be made about whether or not to disconnect the diesel by opening the clutch. This decision will depend on factors such as the consistency of the wind power, the startup time of the diesel engine, and the average allowable diesel starts and stops per day. A diesel speed set-point of 0.3 per unit is used in order to simplify the simulation of the diesel cranking process during the transition [14].

In the present model, the clutch is opened (decoupling the diesel engine from the synchronous generator) whenever there is sufficient wind to carry the primary load. (Note that there is a 16 kW buffer, which represents the real power drawn by the synchronous machine when the clutch is disengaged. This value will be condition and system specific.) Generally, the decision to decouple the diesel from the system will be much more intricate than this, as there are many complicating factors. Factors include but are not limited to wind power availability, acceptable

diesel start/stop frequency, and battery state of charge (should one be used). Here, it is simply meant to demonstrate the effectiveness of the transition and the resulting electro-mechanical dynamics. This transition will be simulated in the following section.

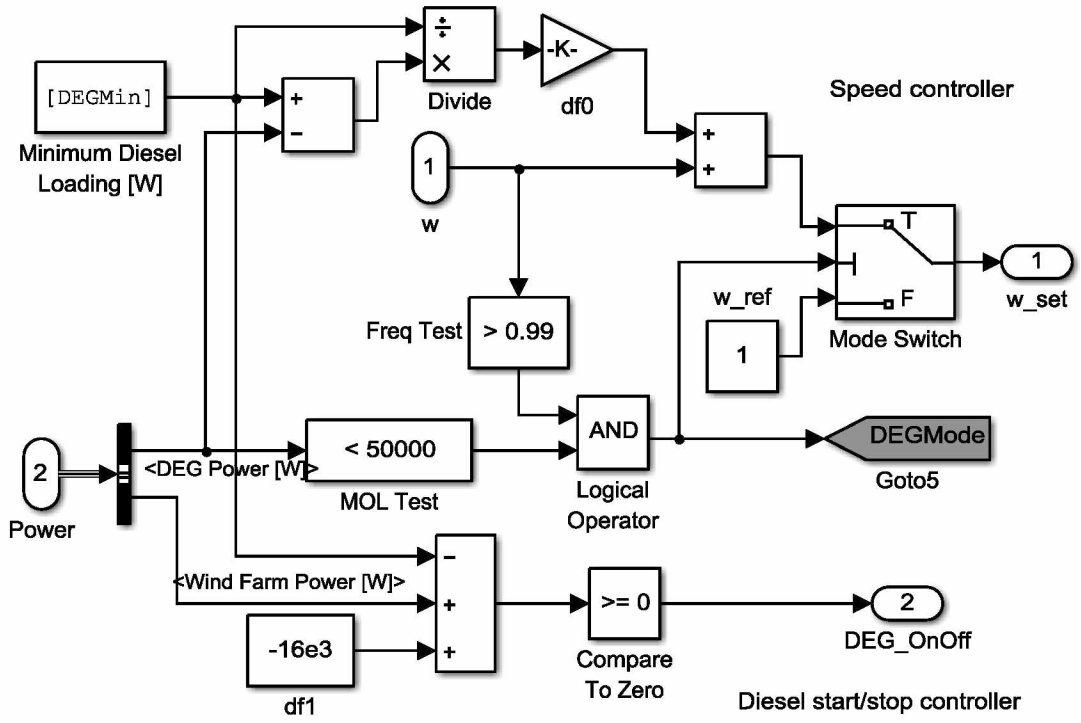

Figure 6.5. Block diagram of proposed diesel engine controller.

6.4 Results and Discussion

Two simulation routines are presented in this section. The first includes a steady ramp-up and ramp-down of wind speed in order to illustrate the system's response to a full range of conditions. The second utilizes synthesized wind speeds in a more realistic scenario of highly variable conditions.

6.4.1 Ramp Simulation

For the system to effectively control both voltage and frequency over a full range of conditions, it must be able to advance through a complete wind ramp-up and ramp-down cycle. The following ninety-second routine (Table 6.3) is simulated with results shown in Figure 6.6. (Note that mode changes are initiated by the controller's response to the given set of input conditions.)

Table 6.3. Simulated wind ramp-up/ramp-down cycle and associated control modes.

From (Time [s])	To (Time [s])	System Mode	Notes
0.00	10.00	Diesel Only	75 kW of load established, 25 kW of load removed at 10 s
10.00	21.21	WD-Low	Wind ramps up, diesel enters droop mode
21.21	37.7	WD-High	Wind ramps up, clutch is opened
37.7	53.22	Wind Only	Wind ramps down, clutch is closed
53.22	70.93	WD-High	Wind ramps down, diesel exits droop mode
70.93	80.00	WD-Low	Wind power disappears, 75 kW of load maintained by diesel
80.00	90.00	Diesel Only	25 kW of load added, diesel absorbs the addition

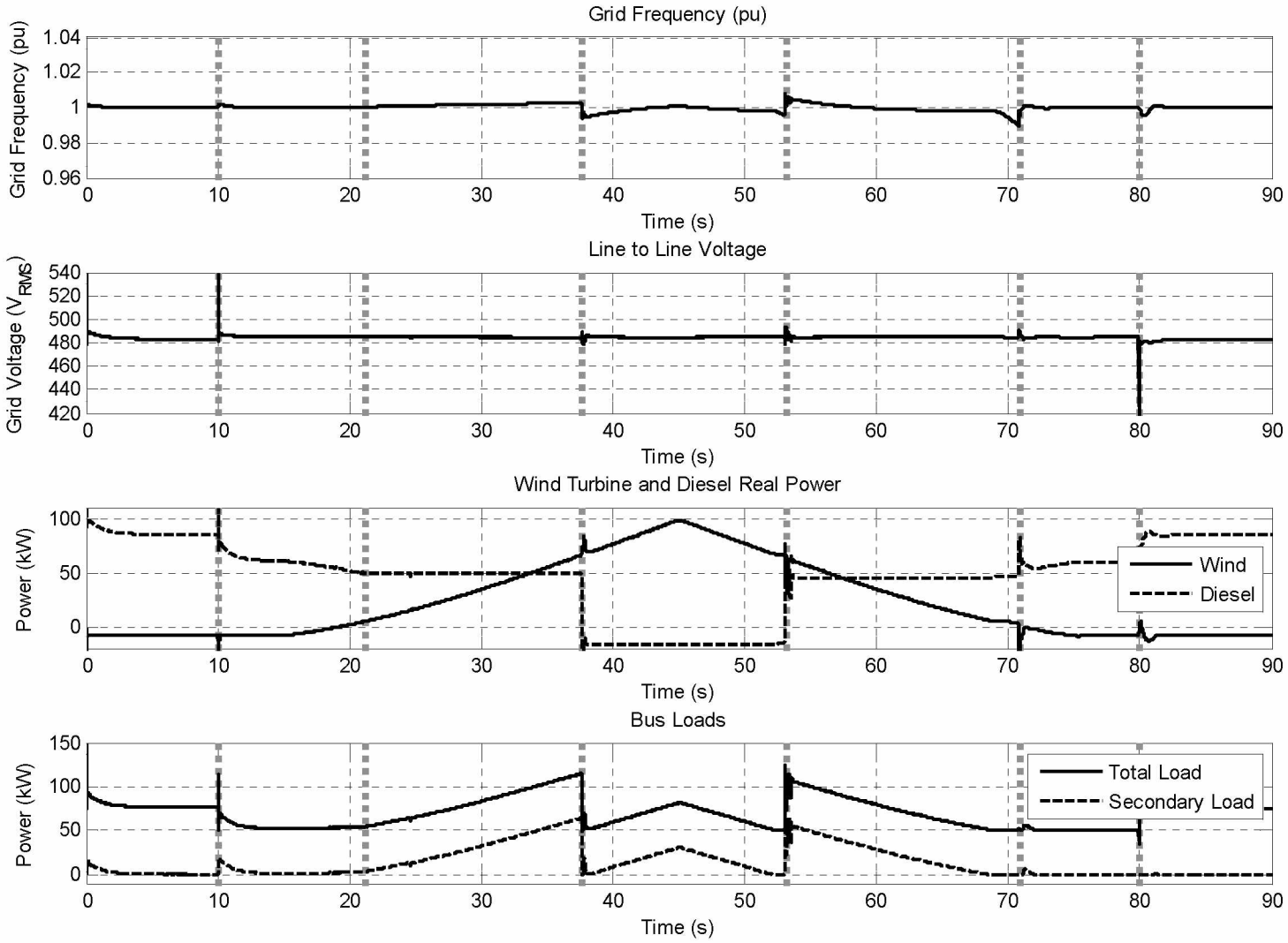

Figure 6.6. System (a) frequency, (b) voltage, (c) power generation, and (d) load consumption for a wind ramp up and ramp down.

The results in Figure 6.6 show (a) frequency (per unit), (b) line to line RMS voltage, (c) wind and diesel generation, and (d) the total bus load in Watts (bus meter, Figure 6.1) and secondary load (SL meter, Figure 6.1). (Note that only the total bus meter is a practical field measurement, whereas the SL meter is an abstract concept, only present in the model. When the secondary loads are distributed throughout the grid, there is no way to measure their penetration to the overall bus load in the absence of communication.) Also note that, throughout the duration of the simulation, the AVR on the diesel is functioning and regulating voltage. Sudden changes in load or generation cause transient spikes in the voltage, which are quickly controlled.

For the first ten seconds of the simulation, no wind power is present and the primary load is reduced from 75 kW to 50 kW. The change is entirely managed by the diesel and frequency is kept stable. This is representative of grid operation in 'Diesel Only' mode. Then, wind power is slowly introduced until the diesel reaches its MOL. Until this point, the diesel is still controlling frequency and voltage, but its contributions offset by the corresponding increase in wind power. This is termed 'WD-Low' mode.

When the power meter on the diesel measures an output less than the MOL (50 kW, in this case), the mode is changed to 'WD-High' and the diesel is now in droop mode. The speed set-point is slowly increased from 1.00 pu to allow the diesel to maintain its power output at the MOL while wind power continues to rise. Frequency regulation is now the responsibility of the distributed SLs. The SL power can be seen to begin ramping up to offset the increase in wind power at about 21 seconds (Figure 6.6d) while DG power is maintained at the 50 kW MOL.

Once the power balance between the wind and diesel differs by a set amount (16 kW in this case), the clutch is disengaged and the system is in 'Wind Only' mode. (The offset value represents the power consumed by the synchronous machine when it is still connected and

operating as a synchronous condenser.) The distributed SLs continue to maintain frequency regulation, but the diesel engine is mechanically decoupled from the synchronous machine. At this point, if the supervisory control deems it prudent, the diesel engine can be turned off and the system supported by wind only. This is a significant risk if a steady buffer of wind power cannot be ensured, as there is no storage system to provide quick backup. Forecasting and decision making of this type are beyond the scope of this study.

The above steps are then reversed as the system smoothly transitions from 'Wind Only' to 'Diesel Only' mode in the last 37 seconds of the simulation.

6.4.2 Representative Simulation

Realistically, the microgrid will not be subject to such an idealized ramped wind condition. Actual wind speeds will introduce a significant amount of variability, which the controller must address. Here, a three-minute synthesized Shinozuka wind speed profile has been generated based on [23] and introduced to the system under a steady load of 60 kW (Figure 6.7). At t = 30 sec, the average wind speed increases at a rate of 1/20 m/s^2 until wind speeds produce an abundance of energy. The system is allowed to transition from 'WD-Low' to 'Wind Only' using the distributed secondary loads for frequency control during and after the transition.

Until the clutch first closes (t = 85s) the diesel can freely switch between isochronous and droop modes as the amount of wind power varies. Once the clutch is locked (t = 114 s) the distributed secondary loads are responsible for frequency regulation and the diesel is isolated from the system. However, there is a transition period between these events that shows how the clutch will flicker open and closed if an appropriate programming mechanism is not implemented. This can be seen in Figure 6.7a with the control mode fluctuating between WD-High and Wind-Only.

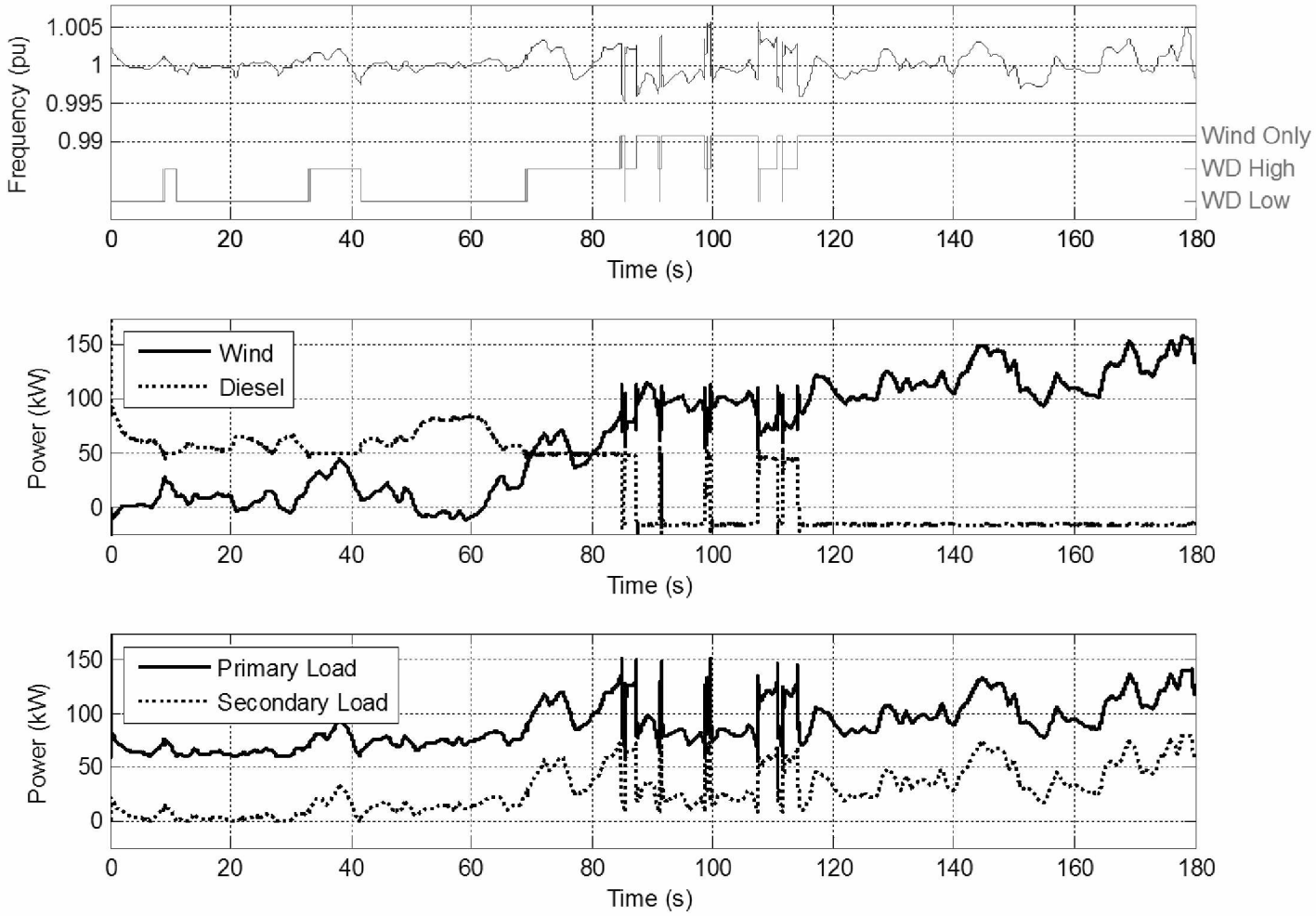

Figure 6.7. Simulation response to a realistic wind event. Frequency (pu) and control mode are illustrated in (a), wind and diesel power in (b), and primary and secondary load in (c). The transition to Wind-Only is managed by the distributed secondary loads.

An evaluation of frequency regulation efficacy illustrates the relative ability for the DEG and the ETS to maintain frequency at its 1.00 pu set point. Considering average wind speeds from 8 m/s to 11 m/s, the response of the system and its controller to four five-minute periods of synthesized Shinozuka turbulence can be seen in Figure 6.8. At lower wind speeds (Figure 6.8a) the system is primarily operating in WD-Low mode with the DEG entering droop 33% of the time (see Table 6.4). Frequency variance in WD-Low mode is lower than that in WD-High, as the DEG is responsible for providing frequency regulation. As the average wind speed increases from 8 m/s to 9 m/s, the system spends a much larger proportion of time in WD-High mode, with the ETS units regulating frequency for much of the five-minute period. Frequency variance tends to increase, but remains within a range of 0.995 to 1.005 pu.

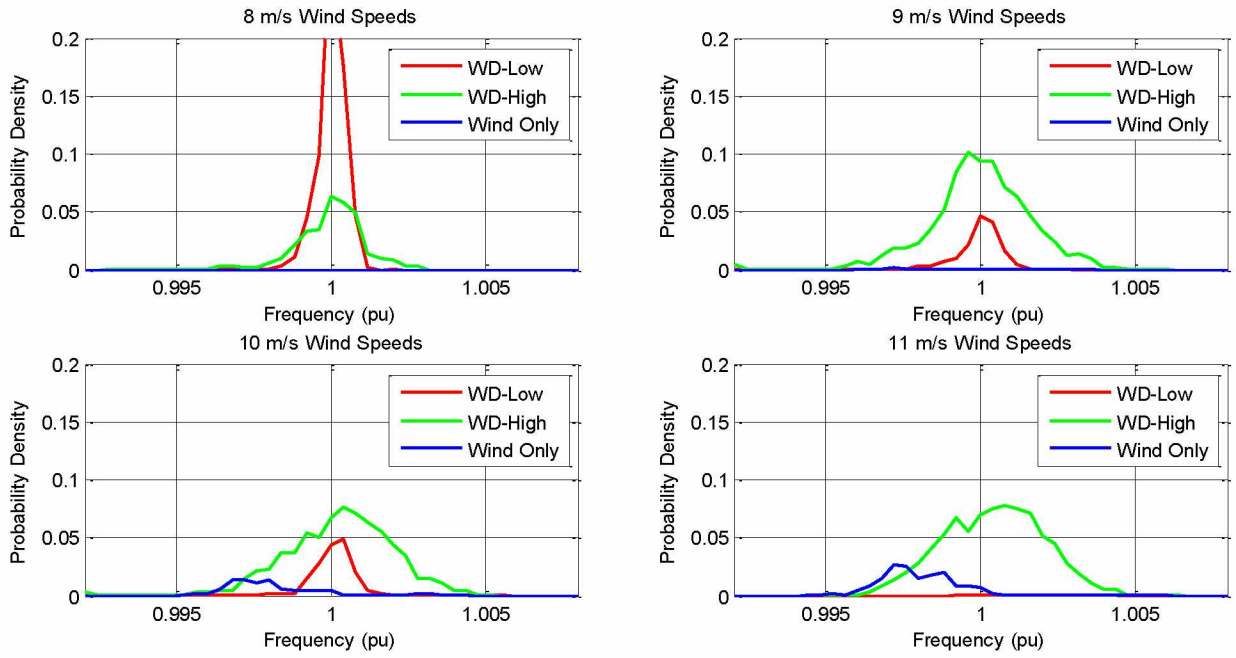

Figure 6.8. Probability density of pu frequency by mode for a) 8 m/s, b) 9 m/s, c) 10 m/s, and d) 11 m/s average wind speeds.

Table 6.4 Frequency variance at four five-minute periods of steady, turbulent wind speeds.

Avg Wind Speed (m/s)	Frequency Variance (pu^2)			Fraction of Time in Mode		
	WD-Low	WD-High	Wind Only	WD-Low	WD-High	Wind Only
8	2.16E-07	1.40E-06	-	67.13%	32.87%	0.00%
9	6.09E-07	3.01E-06	9.13E-07	15.47%	83.85%	0.68%
10	1.14E-06	3.36E-06	3.06E-06	17.77%	72.64%	9.58%
11	1.46E-06	2.67E-06	1.41E-06	0.28%	82.81%	16.91%

At 10 m/s, the system now spends nearly 10% of its time in Wind Only mode, with the diesel engine mechanically decoupled from the synchronous machine by an open clutch (see Figure 6.8c). Another increase in wind speed yields even more diesel-off time with the system almost never operating in WD-Low. At these wind speeds, system frequency is no longer under the control of the diesel engine and is maintained by the ETS units. Recall from Table 6.2 that WD-Low mode is the responsibility of the DEG and WD-High and Wind Only modes are the responsibility of the ETS units. Though it is clear from Figure 6.8 that the DEG is better at regulating frequency (WD-Low mode), the ETS units are still able to regulate the system frequency to within acceptable limits of service in all system control modes [24].

6.4.3 Design Considerations

The present control scheme does depend upon the ability of the distributed secondary loads to be plugged in, turned on, and able to absorb the full capacity of the excess wind load. This is not a realistic expectation 100% of the time, since it is possible for units to saturate or become otherwise inoperative. (If the secondary loads are ETS devices, the units can be considered to be inactive outside of the heating season.) In this case, it would be wise to have a backup secondary load bank co-located with the plant, which may operate at a slightly higher frequency set-point. This would allow for emergency backup frequency regulation in cases where the full fleet of distributed secondary loads cannot collectively fulfill its responsibility.

It is also worth noting that the use of the clutch for 'Wind Only' mode is not a necessary part of the proposed design. Use of the diesel droop controller only, in conjunction with the distributed secondary loads, would be an effective way to keep the diesel from extended operation below its MOL while utilizing the associated excess energy to charge a distributed network of ETS units. Though this is an inefficient way of providing domestic space heat, it is economically preferable to wasting the heat generated by the secondary load.

6.5 Conclusions

An integration strategy for a high-penetration wind-diesel system with switched distributed secondary loads has been proposed. The proposed grid consists of a diesel generator, a wind farm, and a primary load (typical technology), as well as a distributed network of autonomous secondary loads (emerging technology). Normally, a centralized secondary load (such as an electric boiler, or other resistance device) would be utilized to match load to generation.

The distributed secondary loads discussed in the present work are electric thermal storage devices with fast-switching solid state relays and eight heating elements in a binary impedance arrangement. The loads sense the grid frequency error and are used to absorb excess power (normally the function of the secondary load) while providing residences with stored thermal energy for on-demand domestic space heat. The ETS devices are also autonomous—centralized control and communication are not required.

The diesel generator is equipped with a clutch, which can decouple the engine and the synchronous machine. When sufficient wind power exists, the clutch can be opened and frequency regulation becomes the responsibility of the distributed secondary loads. The diesel is also equipped with a power meter and a droop controller, which prevents it from dropping below its

minimum optimal load. Voltage control throughout all modes is achieved by the AVR on the synchronous machine, which stays connected at all times.

The system has been modelled and tested in MATLAB® Simulink® to show a complete wind ramp-up / ramp-down cycle and a three minute period of turbulent wind. Results indicate that frequency and voltage regulation remain stable as the responsibility for frequency control is passed between the diesel and the distributed secondary loads without help from a centralized controller. Thus, secondary load is not wasted or consumed solely at the plant, but distributed to a series of useful loads throughout the grid.

Implementation of a system such as the one described herein could provide many benefits to a community, given proper design considerations. Heating oil consumption can be replaced by cheaper (or cost free) wind power. Additional wind generation capacity could be installed, if sufficient ETS capacity exists to moderate it, and existing distribution infrastructure can carry the surplus electrical current. Finally, since the ETS units are capable of autonomous frequency regulation (given sufficient wind power), reliance on the diesel engine can be eliminated. This allows diesel-off technologies the opportunity to maximize energy savings without simply dumping energy to a secondary load.

The present work has demonstrated that isolated communities, or microgrids capable of islanded operation, can make use of distributed secondary loads to provide frequency regulation when renewable sources (such as wind) are in abundance.

6.6 Acknowledgements

This work was supported by the U.S. Department of Energy, Office of Science, Basic Energy Sciences, under Award # DE-SC0004903.

6.7 References

[1] Devine, M. et al. "Wind-diesel hybrid options for remote villages in Alaska." Available from: US Department of Energy's Wind Powering America Program, 2000.

[2] Isherwood, W. et al. "Remote power systems with advanced storage technologies for Alaskan villages." *Energy* 25.10 (2000): 1005-1020.

[3] US. DOE. NREL. "Systems Performance Analyses of Alaska Wind-Diesel Projects." Wind Powering America, n.d. Web. 13 Sept. 2016, [Online]. Available: <http://apps2.eere.energy.gov/wind/windexchange/pdfs/wpa/2009/wind_diesel_ak_saint_paul.pdf>.

[4] Drouilhet, S. M. and M. Shirazi. "Wales, Alaska high-penetration wind-diesel hybrid power system: theory of operation." National Renewable Energy Laboratory, 2002.

[5] Bhatti, T. S., A. A. F. Al-Ademi, and N. K. Bansal. "Load frequency control of isolated wind diesel hybrid power systems." *Energy Conversion and Management* 38.9 (1997): 829-837.

[6] Miller, M. "Sand Point Wind-Diesel Project Secondary Loads: Performance and Lessons Learned." [Online]. Available: <http://alaskarenewableenergy.org/>

[7] Sebastián, R. "Application of a battery energy storage for frequency regulation and peak shaving in a wind diesel power system." *IET Generation, Transmission & Distribution* 10.3 (2016): 764-770.

[8] Lyons, J. "Kokhanok Wind-Diesel System – Update". Alaska Wind Diesel Workshop, 14 February 2013, AVTEC, Seward, AK, http://alaskarenewableenergy.org/wp-content/uploads/2010/09/Kokhanok-Update_JohnLyons_2013.pdf

[9] Weis, T. M., A. Ilinca, and J. P. Pinard. "Stakeholders' perspectives on barriers to remote wind–diesel power plants in Canada." *Energy Policy* 36.5 (2008): 1611-1621.

[10] Sateriale, M. E. "Modeling and analysis of masonry electro-thermal heating and storage for optimal integration with remote stand-alone wind-diesel systems." Master of Science Thesis, University of Alaska-Fairbanks, 2013.

[11] Johnson, C. et al. "Design and modeling of dispatchable heat storage in remote wind/diesel systems." *2002 World Wind Energy Conference* (2002).

[12] Lu, N. and D. J. Hammerstrom. "Design considerations for frequency responsive grid friendly TM appliances." *IEEE 2006 Transmission and Distribution Conference and Exhibition (2006 IEEE PES)*. IEEE, 2006.

[13] Trudnowski, D., M. Donnelly, and E. Lightner. "Power-system frequency and stability control using decentralized intelligent loads." *IEEE 2006 Transmission and Distribution Conference and Exhibition (2006 IEEE PES)*. IEEE, 2006.

[14] Janssen, N. T., R. W. Wies, and R. A. Peterson. "Frequency Regulation by Distributed Secondary Loads on Islanded Wind-Powered Microgrids." *IEEE Transactions on Sustainable Energy*. 7.3 (2016): 1028–1035.

[15] Glover, J. D. et al. *Power System Analysis and Design, 5th ed.* Stamford, CT: Cengage Learning (2012): 679-728.

[16] Soni, N., S. Doolla, and M. C. Chandorkar. "Improvement of transient response in microgrids using virtual inertia." *IEEE Transactions on Power Delivery* 28.3 (2013): 1830-1838.

[17] Tufte, E. D. "Impacts of Low Load Operation of Modern Four-Stroke Diesel Engines in Generator Configuration." Norwegian University of Science and Technology, 2014, pp. 87-90, http://www.diva-portal.org/smash/get/diva2:744089/FULLTEXT01.pdf

[18] Hunter, R. and G. Elliot. *Wind-diesel systems: a guide to the technology and its implementation*. Cambridge University Press, 1994.

[19] Janssen, N. T., R. A. Peterson, and R. W. Wies. "Development of a Full-Scale-Lab-Validated Dynamic Simulink© Model for a Stand-Alone Wind-Powered Microgrid." *ASME 2014 Power Conference* Volume 2 (2014). ASME, 2014.

[20] Yeager, K. E., and J. R. Willis. "Modeling of emergency diesel generators in an 800 megawatt nuclear power plant." *IEEE Transactions on Energy Conversion* 8.3 (1993): 433-441.

[21] Rezkallah, M., A. Chandra, and B. Singh. "Three-leg four-wire voltage source inverters for hybrid standalone system feeding unbalanced load." *IEEE 2013 International Conference of the Industrial Electronics Society (IECON 2013)*. IEEE, 2013.

[22] Sebastián, R. "Smooth transition from wind only to wind diesel mode in an autonomous wind diesel system with a battery-based energy storage system." *Renewable Energy* 33.4 (2008): 454-466.

[23] Kaminsky, F. C. "A Comparison of Alternative Approaches for the Synthetic Generation of a Wind Speed Time Series." *Journal of Solar Energy Engineering* 113.4 (1991): 280–289.

[24] "IEEE Guide for Design, Operation, and Integration of Distributed Resource Island Systems with Electric Power Systems." IEEE Standard 1547, 2011. IEEE, 2011.

Chapter 7. Results and Observations

The general results and observations of the research described in the papers of Chapters 3-6 are discussed and summarized here.

7.1 Results and Observations of Chapter 3

A numerical heat transfer study was conducted to investigate the effects of various ETS heater core parameters on the charge and discharge characteristics of the stove. A generalized charge/discharge model was presented, which could be used to predict the stove core's state-of-charge at a given time after a set of known conditions and input parameters.

Electrical charging was shown to be a simple matter of electrical resistive heat flux within the stove core. However, forced air discharging became a more complicated scenario which demanded the application of the numerical heat transfer study conducted. For this study, core material properties such as density, thermal conductivity, and specific heat were considered, as well as bulk air flow velocity and core geometry (brick height). As shown in Section 3.5, these parameters determine the behavior of the stove core's output, which can be modeled as a simple exponential discharge parameterized by a single time constant, τ. Additional accuracy can be obtained with a second quadratic term, but results were presented in terms of the simpler one-parameter model.

Recall that the three parameters driving the discharge behavior of the core can be represented in a single dimensionless quantity, presently referred to as the "modified Graetz number." This modified Graetz number (Gz*) is the product of several quantities, including the Reynolds number (Re), the Prandtl number (Pr) and the quantity L/D_H, but it reduces to a function of three key variables: u (bulk air flow velocity), L (ratio of simulation region volume to surface

area), and α (thermal diffusivity). (Note that the thermal diffusivity is itself a reduction of the relevant thermal properties ρ, c_p, and k.) This modified Graetz number was used as the independent variable of the parameter sweeps conducted in Chapter 3.

The study dependent variable was the time constant, τ, which described the exponential output of the stove core. τ is a function of the convective heat transfer coefficient, mass, specific heat, and heat transfer surface area of the simulation region. However, the results were found to be presented more generally in terms of the Biot number (Bi), which contains the convective heat transfer coefficient, h. From h, it is possible to obtain the time constant, τ. Figure 7.1 shows how it is possible to obtain τ from the given input parameters and the correlation equation presented in Chapter 3 of this thesis.

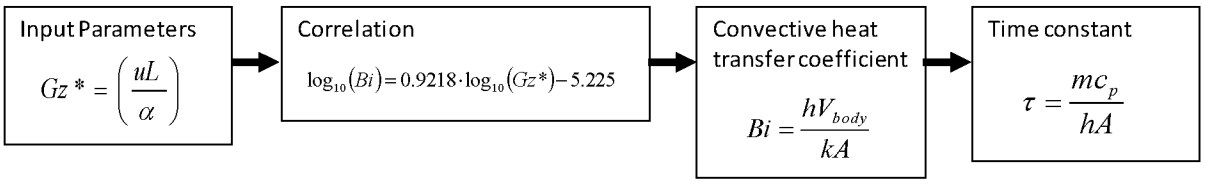

Figure 7.1. Flow chart showing the steps necessary to obtain the time constant from a given set of ETS stove core input parameters.

In 3.5.2 it was shown that improvement of the single-parameter model can be obtained through the addition of a second parameter. The discharge of the heater core then takes on a pattern of the form

$$SOC = SOC_0 e^{at^2+bt} \tag{7.1}$$

where a and b are the two parameters that describe the fit and SOC is the "state of charge".

Finally, putting the charge and discharge models together, instructions for the development of a realistic ETS charge/discharge performance study were presented in terms of a core energy

balance. Given a known set of input conditions and core parameters, the state of charge of the ETS core can be predicted at a given time, *t*, if the charge and discharge signals are known.

7.2 Results and Observations of Chapter 4

The foundation of the electromechanical portion of this study was the MATLAB® SIMULINK® model used to represent a hybrid wind-diesel system as it interacted with a family of autonomous ETS devices using a proportional frequency response controller. This model was tested and validated by measurements made on a full-scale laboratory test bed at the Alaska Center for Energy and Power (ACEP) Power Systems Integration (PSI) laboratory. Diesel-only and wind-diesel modes were both explored, with frequency and voltage measurement samples taken at a rate of 6000 Hz. The results of the model development, lab validation, and model tuning formed the basis of Chapter 4.

Measured results showed frequency responses to perturbations falling into three distinct categories, based on the step size seen by the diesel electric generator. The largest steps (up and down) were considered "type 1" responses and exhibited a distinct frequency recovery pattern. (See 4.5) Moderate steps displayed a unique 2.3 Hz undamped oscillation lasting approximately three seconds, referred to presently as a "type 2" response. Finally, a third frequency response pattern was identified for small steps, both up and down. These were referred to as "type 3" responses.

Efforts to accurately predict the results observed on the test bed with the developed model were of mixed success. Model parameters were chosen to provide the best results over the range of inputs tested without significant deviation from nominal values. Fortunately, the most commonly seen frequency excursions (those of the smallest magnitude) appeared to be well-

predicted by the model. The simulation results of type 1 and 2 perturbations differed in shape, but not magnitude, from those measured on the test bed. In fact, agreement between model and laboratory frequency excursion magnitudes were within 1.1%. However, the model significantly overestimated the settling time for medium to large steps down in load.

Results were later improved with the use of an AC5A type exciter model block, which was unavailable at the time of publication. Use of this exciter block dramatically improved the correlation of the model with the laboratory measurements and was applied to the studies conducted in Chapters 5 and 6.

7.3 Results and Observations of Chapter 5

Chapter 5 used the electromechanical hybrid wind-diesel model to explore the interactions of a distributed network of autonomous ETS devices on an isolated hybrid wind-diesel microgrid. In Chapter 5, these are generally referred to as distributed secondary loads (DSLs). The DSLs were used to assist with frequency regulation in wind-diesel mode and absorb surplus wind power for charging. The effects of switching time, unit coordination, network size, and controller proportional gain were all considered. Frequency regulation was of primary interest, with voltage regulation not to drop below existing levels.

Extensive parameter sweeps showed regions of operation whereby frequency regulation is improved with the presence of a DSL network. Improvements of up to 50% were observed under certain circumstances, including high controller gain, sufficient secondary load capacity (number of units), and fast relay switching times. However, these same regions, when replaced with high switching times (slow relays), became largely unstable and represented an overall detriment to the performance of the system.

While most of the parameter space was shown to be neutral to voltage control, there were regions that represented voltage fluctuations several times more severe than a system solely under the control of the DEG. If switching times were too low, voltage regulation significantly suffered. As the system power balance changed, the longer the DSLs waited to react to such a change (by switching their elements), the larger the magnitude of the required switching load. This resulted in severe disruptions to voltage regulation, which were avoided with faster switching times.

Additionally, it was shown that the optimal frequency regulation parameter space corresponded to regions of high DSL network power consumption. This power was shown to be necessary to allow the DSL to trim frequency fluctuations, resulting in improved grid frequency regulation. Should wind power overtake grid demand (illustrated in Chapter 6), this power would come from clean, wind-powered heat delivered to the DSL. However, in wind-diesel mode, this would amount to storing and delivering heat with diesel energy; a strategy that is generally economically unfavorable.

Chapter 5 also considered the effect of ETS units saturating and becoming unavailable for absorbing power. In all cases simulated, the system tended to behave more like an unassisted grid as ETS units reached their full charge and never worse. In *wind-diesel* mode, this is a good thing since the DEG is always available to support frequency regulation.

The effects of unit coordination were also considered as a primary factor in system frequency and voltage regulation. Results showed a significant reduction in voltage fluctuation when each unit was given a unique, sub-second delay. This ensured that no two units would change their states at precisely the same time.

A change to the number and impedance of heating elements in ETS units were tested as well. Typical ETS units have four elements of equal impedance. It was found that increasing the

number of heating elements (while keeping the capacity of the network the same) provided improved frequency regulation with no negative effects on voltage. Furthermore, varying the element size to a binary arrangement would allow for markedly improved performance. For example, an ETS unit with 8 elements in a binary impedance fashion would have 256 energy states between "on" and "off".

Finally, an indirect relationship between frequency variability and ETS network power consumption was seen. If the relay switching time of the DSL network was too slow, a performance maximum occurred, whereby the application of additional secondary load (whether by gain tuning or increase in fleet size) would actually tend to intensify frequency transients in the system. However, the presence of the DSL network was observed to have an overall positive effect on frequency regulation for nearly all representative scenarios.

7.4 Results and Observations of Chapter 6

In Chapter 6, the idea of the autonomous network of DSLs was taken a step further and the hybrid wind-diesel system was simulated in wind-only mode. For this study, when enough wind power was present to service the load, a clutch was used to mechanically disconnect the diesel engine from the system and the DSLs assumed responsibility for frequency control with no signal from the microgrid central controller. Additionally, a protective minimum load was kept on the diesel engine using a droop controller so as to ensure it did not operate outside of its optimal range. The results of two simulations were presented: 1) a ramp simulation and 2) a realistic/representative simulation using synthetic wind speed data.

The ramp simulation took the entire system through a swell in wind power from zero to full wind farm capacity and back down again in order to clearly illustrate the transitions between

control modes. Frequency control responsibility was handed off from the diesel to the DSLs and back to the diesel again; the transition was entirely managed by the individual components and their responses to the changing grid frequency. Resulting frequency, voltage, and component power balances confirm a smooth transition with a minimum protective load present on the diesel. Opening of the mechanical clutch between the diesel engine and the synchronous machine could be seen as a sudden drop-off in diesel generation and a corresponding increase in the amount of power drawn by the DSLs which became responsible for frequency regulation. These results are presented in section 6.3.1 and illustrated in Figure 6.6.

As a further validation of the proposed control strategy, a realistic scenario was run whereby three minutes of synthesized Shinozuka wind speeds were fed into the simulation to test the effects of variable wind speeds. Frequency control was verified by the simulation results, but with two key observations. First, the clutch had a tendency to flicker between its opened and closed states, causing minor frequency disturbances and potentially major health problems for the mechanical integrity of the clutch. These could be avoided with strategic programming changes made specifically for the situation. (This was a general study.) Second, a comparison was made between the frequency regulation ability of the diesel and the frequency regulation ability of the DSLs. Frequency regulation by the diesel was measured to be 41% better than frequency regulation by the DSLs. However, the variability of frequency using the diesel or the DSLs was well within acceptable limits. (Less than 0.3% variation.)

Between the studies presented in Chapter 5 and 6, the concept of autonomous frequency control by distributed secondary loads on an isolated wind-diesel grid was fully illustrated. The tools to design such a system, from ETS thermal performance, to the design of the autonomous ETS controller, were simulated and validated.

Chapter 8. Conclusions

The following conclusions can be drawn from the preceding chapters:

8.1 Conclusions for Generalized Heat Flow Model of a Forced Air Electric Thermal Storage (ETS) Heater Core

A number of conclusions can be drawn from the results of the numerical heat flow analysis. These conclusions illustrate the concepts needed to model the energy balance of an ETS heater core subject to a realistic set of conditions.

- Numerical model results showed that bulk air velocity, core dimensions, and material properties have a strong impact on the discharge characteristics of the electric thermal storage heater core.
- Air velocity profile and heat gradients within the storage media were shown to have little effect on the discharge curve for typical operation of the core.
- The discharge characteristics can be modeled as an exponential decay in State of Charge (SOC) with a single parameter (time constant) or, for more accuracy, a two-parameter exponential decay curve.
- Time constants were calculated (and expressed in terms of their Biot numbers) for a wide range of parameters and summarized against a single non-dimensional modified Graetz number. Plotted on a log-log scale, the Biot number varies linearly with this Graetz number.
- A simple energy balance equation was given and can be used to establish the energy balance of a wide range of ETS heater cores subject to a given set of conditions.

The results presented in this section could be used to facilitate the typical performance analysis involving the application of ETS units in a hybrid wind-diesel system.

8.2 Conclusions for Development of a Full-Scale-Lab-Validated Dynamic Simulink© Model for a Stand-Alone Wind-Powered Microgrid

The following conclusions were formed as a result of the model development presented in Chapter 4.

- The dynamics of a full-scale hybrid wind-diesel test bed were measured and found to fit into three distinct categories (based on their frequency response size and shape) when the system was subject to a series of various load and wind perturbations.
    - Type 1: Large steps in load resulting in an intentional drop in voltage to allow frequency recovery
    - Type 2: Oscillatory/underamped frequency response
    - Type 3: Small perturbations/critically-damped frequency response
- A mathematical model was developed and tuned to match the actual system with good agreement in the results at medium to high levels of diesel loading and relatively small perturbations.
- The highly simplified exciter model used was found to be in need of updating for improvement in the accuracy of results.
- Implementation of a "discontinuous" type exciter model was recommended. For this type of exciter the automatic voltage regulator (AVR) driving the exciter boosts the level of field current following a fault, thus increasing terminal voltage and air gap power.

Confidence in the use of the model developed in this section was established through full-scale laboratory measurement and verification. This model was then used for the research presented in both Chapter 5 and Chapter 6.

8.3 Conclusions for Frequency Regulation by Distributed Secondary Loads (DSLs) on Islanded Wind-Powered Microgrids

Many conclusions can be drawn based on the results and observations of Chapter 5, whereby the model developed in Chapter 4 was used to simulate the interaction of a distributed network of secondary loads with an isolated hybrid wind-diesel (HWD) system. These conclusions are summarized as follows.

- Self-sensing DSLs (with no centralized controller) can be used to assist a HWD system with grid frequency regulation in wind-diesel mode. This allows for the distribution of secondary load to consumers throughout the grid.
- Controller gain settings, switching times, and fleet size were shown to be important variables impacting the performance of the autonomous secondary loads on the grid.
- ETS devices can be equipped with autonomous frequency-response capability and used to store domestic space heat when an excess of wind power exists.
- A family of autonomous DSLs may cause disruptions to frequency and/or voltage greater than those in a system solely under the control of the DEG for certain conditions. A combination of slow switching times ($\tau > 25$ ms), high controller gain, and too many active DSLs may result in an oversensitive, unstable secondary load, itself capable of disturbances larger than that of the consumer load.
- Two methods for unit synchronization were explored: staggered switching and synchronized switching. Staggered switching was shown to have less of an effect on voltage regulation. As such, it was recommended that each individual ETS device be given a unique time delay in its response based on a fraction of the switching time to ensure a staggered switching scheme.
- When units become saturated or otherwise unavailable for use, the frequency regulation

benefits of the family of units are reduced, but are never made worse than a system solely under the control of the diesel.

- Since the DSLs can only absorb power (they cannot inject it back into the grid), they do a better job with frequency regulation when a fraction of unit elements remain loaded in preparation for a sudden lack of generation. However, this results in secondary loads fed with undesirable diesel-fed charging current when the system is in wind-diesel mode.
- Suggestions for improvements to the system included the use of a PID type controller for each DSL for better response to frequency changes and a change to the impedance of electrical charging elements in the ETS devices. (Rather than have 4 elements of like size, it would make sense to use a 4 bit [or higher] arrangement for better frequency resolution.)

The results of this study formed the basis of the work conducted in Chapter 6 of this thesis.

8.4 Conclusions for Modeling Integration Strategies for Autonomous Distributed Secondary Loads on High Penetration Wind-Diesel Microgrids

The final study of this thesis (presented in Chapter 6) generated several important conclusions regarding the application of autonomous DSLs to higher penetration wind-diesel systems as follows.

- Fast-switching 8-bit ETS devices can be used to regulate frequency on a wind-diesel microgrid when the diesel electric generator is either in droop mode or disconnected from the system entirely.
- A clutch placed between the diesel engine and the synchronous machine allows the diesel engine to shut down while the automatic voltage regulator (AVR) on the synchronous machine continues to regulate voltage. Frequency regulation can be performed by a distributed family

of secondary loads. This was confirmed through the use of the dynamic model developed in Chapter 4.

- Modeling also confirmed that the diesel electric generator can remain in droop mode in order to maintain operation at or above its minimum optimal loading (MOL) while the DSLs assume responsibility for frequency regulation.
- The loading scheme for the ETS devices could be redesigned to improve frequency control. The number of elements were increased from four to eight and a PID controller was added. The impedance of the elements was also diversified into an 8-bit arrangement for improved resolution in frequency control.
- No communication signals are needed for the DSLs—they can be operated based on measured grid frequency error alone.
- Voltage control can be performed at all times by the AVR on the synchronous generator, as long as it remains electrically connected to the system. When disconnected from the diesel engine with a clutch the synchronous machine acts as a synchronous condenser.
- The clutch can only be opened when sufficient wind power exists or the grid will collapse. A clutch system was modelled to show autonomous operation in diesel-off mode. However, any diesel-off technology could make use of such a strategy.
- Benefits of the prescribed system include reduction in heating oil consumption and possible expansion of wind generation capacity.

The successful demonstration of the control strategy presented in this section opens the door for new modes of operation and economic distribution of available secondary load as clean, domestic space heat on isolated wind-diesel systems.

8.5 Suggestions for Future Research

Hybrid wind-diesel power technology is rapidly being developed and deployed in rural Alaska and other remote, cold-climate locations. As installed wind generation capacity climbs, excess power will become increasingly available. It is imperative, for the economic success of these projects, that this excess wind energy be utilized to the fullest extent possible. The most cost-effective technologies will be those that can deliver this surplus to the local consumer without the need for a centralized microgrid controller or secondary distribution circuit.

A significant amount of work has been presented in this thesis to demonstrate how ETS devices can be used to autonomously regulate frequency on hybrid wind-diesel microgrids. Such technology is gaining traction in industry, but additional research is needed to address the following issues.

- Use of storage technologies is also gaining popularity in the field. Integrating autonomous DSLs with battery/inverter systems would be a highly useful area of study.
- Further study of various diesel-off options is needed. There are very few examples of high penetration wind-diesel systems that can successfully disconnect the diesel engine from the system without energy storage.
- The present work has proposed several redesigns of the commercially-available ETS device. (Increase in number of elements, 8-bit impedance arrangement, and the use of a PID controller.) Lab testing must be used to verify the operation of such a prototype device.
- An investigation needs to be conducted on how these ETS units and other types of secondary loads can be used in hybrid wind-diesel microgrids for other system stability services such as phase balancing.

Studies that address these issues by modeling, lab research, prototyping, and field testing will propel this technology into a successful future where excess wind energy can be widely used to provide domestic space heat to the local consumer in a clean, economic, and sustainable manner.

8.6 Overall Conclusions

ETS devices are a promising application for excess wind energy in isolated hybrid wind-diesel microgrids. A family of such devices can be made to respond to changes in grid frequency and assist with or autonomously perform frequency regulation. Changing the design of the typical commercially-available stove from four equally-sized elements to eight elements (arranged in a binary fashion) as well as implementation of a PID type frequency-response controller, would improve their performance in such a role. Also, DEGs equipped with a droop mode would allow the diesel engines to sustain a minimum amount of load before relinquishing frequency control responsibility to an autonomous family of ETS units. This excess load can be used to charge the ETS as the wind resource continues to increase, maximizing distribution of available electrical energy. At this point, mechanical isolation of the diesel could be achieved through deactivation of a mechanical clutch between the engine and the synchronous machine. Thus, the technical feasibility of a hybrid wind-diesel system with distributed autonomous frequency-response loads has been explored and validated through mathematical modeling. (Models used for this study were validated by field measurements on a full-scale laboratory test bed, as discussed in Chapter 4.)

Additionally, system sizing and performance evaluation strategies have been developed through numerical thermal modeling. Sizing and economic performance can be predicted based on the known core material properties, geometry, and air flow characteristics summarized in this

thesis. These strategies can be used to drive system design and sizing studies prior to the installation of ETS devices in any applicable system.

Moreover, the usefulness of the control strategies presented in this thesis are not limited to arctic regions, where domestic space heat is in high demand. Additional applications may exist within the following fields.

- Alternative secondary load applications in warmer climates, where air conditioning, refrigeration loads, and "cold storage" applications are of high value and wind is readily available
- Distributed secondary loads on larger, more interconnected grids, with high levels of renewable energy (not limited to wind) and an *internet-of-things* architecture
- Diversification of energy sources for military applications, i.e. remote outposts, which may possess unreliable fuel supply chains
- Use of electric vehicles as distributed secondary loads capable of charging during off-peak wind events

Overall, it has been shown that electric thermal storage is a promising strategy for assistance with frequency regulation and for the optimization of secondary loads on isolated wind-diesel microgrids. With advancements in wireless communications and switching converter technologies, these types of smart secondary loads combined with storage could provide a multitude of stability and dispatch services in hybrid microgrids where excess renewable energy and energy storage are of significant value.

8.7 Acknowledgements

The author would like to acknowledge contributions to this work from Dr. Richard W. Wies and Dr. Rorik A. Peterson from the UAF College of Engineering and Mines (CEM). Judicious review and valuable commentary was also provided by committee members Dr. Marc Mueller-Stoffels, from the Alaska Center for Energy and Power (ACEP), Dr. Yujiang Xiang, from the UAF CEM Department of Mechanical Engineering, and Dr. Sean Topkok, from the UAF School of Education. Funding for this research was largely provided by the U.S. Department of Energy, Office of Science, Basic Energy Sciences, under Award # DE-SC0004903.